UNIVERSITY OF WEST ATTICA
SCHOOL OF ENGINEERING
DEPARTMENT OF NAVAL ARCHITECTURE

Diploma Thesis

Μελέτη δυναμικής συμπεριφοράς πλοίου σε θαλάσσιους κυματισμούς με χρήση κωδίκων συνοριακών στοιχείων

Seakeeping study using Boundary Element Method

Author:

ANGELIKI D. LYSIKATOU

A.M.: 18393067

Supervisor: Theodoros Gerostathis

Egaleo, 2024

UNIVERSITY OF WEST ATTICA
SCHOOL OF ENGINEERING
DEPARTMENT OF NAVAL ARCHITECTURE

Διπλωματική εργασία

Μελέτη δυναμικής συμπεριφοράς πλοίου σε θαλάσσιους κυματισμούς με χρήση κωδίκων συνοριακών στοιχείων

Συγγραφέας

Αγγελική Δ. Λυσικάτου (Α.Μ.: 18393067)

Επιβλέπων

THEODOROS GEROSTATHIS Digitally signed by THEODOROS GEROSTATHIS Date: 2024.07.17 11:59:32 +03'00'

Θεόδωρος Γεροστάθης,

Αναπλ. Καθηγητής ΠΑ.Δ.Α.

Ημερομηνία εξέτασης

02/07/2024

Εξεταστική Επιτροπή

THEODOROS GEROSTATHIS Digitally signed by THEODOROS GEROSTATHIS Date: 2024.07.17 12:00:20 +03'00'

Θεόδωρος Γεροστάθης,

Αναπλ. Καθηγητής ΠΑ.Δ.Α.

Konstantinos Politis Digitally signed by Konstantinos Politis Date: 2024.07.18 11:35:50 +03'00'

Κωνσταντίνος Πολίτης,

Καθηγητής ΠΑ.Δ.Α.

ALEXANDROS THEODOULIDIS Digitally signed by ALEXANDROS THEODOULIDIS Date: 2024.07.17 21:12:42 +03'00'

Αλέξανδρος Θεοδουλίδης,

Επικ. Καθηγητής ΠΑ.Δ.Α.

ΔΗΛΩΣΗ ΣΥΓΓΡΑΦΕΑ ΔΙΠΛΩΜΑΤΙΚΗΣ ΕΡΓΑΣΙΑΣ

Η κάτωθι υπογεγραμμένη Αγγελική Λυσικάτου του Δημητρίου με αριθμό μητρώου 18393067 φοιτήτρια του Πανεπιστημίου Δυτικής Αττικής της Σχολής Μηχανικών του Τμήματος Ναυπηγών Μηχανικών, δηλώνω υπεύθυνα ότι:

«Είμαι συγγραφέας αυτής της διπλωματικής εργασίας και ότι κάθε βοήθεια την οποία είχα για την προετοιμασία της είναι πλήρως αναγνωρισμένη και αναφέρεται στην εργασία. Επίσης, οι όποιες πηγές από τις οποίες έκανα χρήση δεδομένων, ιδεών ή λέξεων, είτε ακριβώς είτε παραφρασμένες, αναφέρονται στο σύνολό τους, με πλήρη αναφορά στους συγγραφείς, τον εκδοτικό οίκο ή το περιοδικό, συμπεριλαμβανομένων και των πηγών που ενδεχομένως χρησιμοποιήθηκαν από το διαδίκτυο. Επίσης, βεβαιώνω ότι αυτή η εργασία έχει συγγραφεί από μένα αποκλειστικά και αποτελεί προϊόν πνευματικής ιδιοκτησίας τόσο δικής μου, όσο και του Ιδρύματος.

Παράβαση της ανωτέρω ακαδημαϊκής μου ευθύνης αποτελεί ουσιώδη λόγο για την ανάκληση του διπλώματός μου».

Η Δηλούσα

Αγγελική Λυσικάτου

Acknowledgements

Concluding my undergraduate studies in Naval Architecture and Marine Engineering, I would like to extend my gratitude to all those who have supported me throughout this journey. I wish to express my appreciation to all my professors for their dedication to their students. I would especially like to thank my advisor and the supervisor of this thesis, Associate Professor Gerostathis, who provided invaluable expertise, assistance, and guidance, even under challenging circumstances. Additionally, I am grateful to the team at the Danaos Research Center, where I completed my internship, for their support. It would be a significant omission not to mention my family, to whom I am eternally grateful for their dedication and continuous endorsement. Lastly, to my dear friends, thank you for always being there for me and for your endless encouragement.

Περίληψη

Στην παρούσα διπλωματική εργασία μελετάται η δυναμική συμπεριφορά πλοίου εμπορευματοκιβωτίων σε θαλάσσιους κυματισμούς, με τη χρήση της μεθόδου συνοριακών στοιχείων. Πρωτίστως, γίνεται μία εισαγωγή στο πρόβλημα της δυναμικής συμπεριφοράς πλοίου σε κυματισμούς, τα κριτήρια λειτουργίας, τους κανονισμούς και τις μεθοδολογίες, συμπεριλαμβανομένων των πειραματικών και αριθμητικών μεθόδων. Έπειτα, παρουσιάζεται η μαθηματική διατύπωση του προβλήματος, ενώ εισάγεται η μέθοδος συνοριακών στοιχείων και το σχετικό λογισμικό προσομοιώσεων και υπολογισμών που εφαρμόστηκε. Στη συνέχεια, παρουσιάζεται το κύριο μέρος της εργασίας, στο οποίο μελετώνται, αναλύονται και υπολογίζονται οι αποκρίσεις πλοίου εμπορευματοκιβωτίων, τόσο σε αρμονικούς κυματισμούς για τον υπολογισμό των αντίστοιχων τελεστών απόκρισης (*Response Amplitude Operators - RAOS*), όσο και σε τυχαίους κυματισμούς, προσομοιώνοντας συγκεκριμένες καταστάσεις θάλασσας. Ακόμη, ελέγχονται τα κριτήρια λειτουργίας του πλοίου σε κυματισμούς και γίνεται σύγκριση δύο μεθόδων υπολογισμού (υπολογισμός στο πεδίο συχνοτήτων και στο πεδίο του χρόνου), μέσω ανάλυσης λειτουργικότητας του πλοίου (*operability analysis*) σε τυχαίους κυματισμούς. Τέλος, καταγράφονται συμπεράσματα και προτάσεις, όπως προέκυψαν από τα αποτελέσματα της συγκεκριμένης εργασίας.

Λέξεις κλειδιά: δυναμική συμπεριφορά πλοίου, υδροδυναμική πλοίου, κριτήρια δυναμική συμπεριφοράς πλοίου, μέθοδος συνοριακών στοιχείων, κινήσεις πλοίου, τελεστές αποκρίσεων πλοίου, DTC γάστρα, αρμονικοί κυματισμοί, τυχαίοι κυματισμοί, ανάλυση λειτουργικότητας πλοίου.

Abstract

In this diploma thesis, the seakeeping performance of a containership in ocean waves is studied, using the Boundary Element Method. Firstly, an introduction of the seakeeping problem is provided, including an overview of seakeeping operational criteria, regulations, and methodologies, encompassing both experimental and numerical methods. Subsequently, the mathematical formulation of the problem is presented, along with an introduction on the Boundary Element Method and the software employed for calculations and simulations. The main part of the thesis focuses on the study, analysis and calculation of the responses of the containership hull, in both regular waves, for the calculation of the Response Amplitude Operators (RAOs), and in irregular waves, simulating specific sea conditions. Furthermore, the seakeeping operational criteria of the ship in waves are evaluated, and a comparison of two methods (frequency and time domain) is conducted through operability analysis of the ship in irregular waves. Finally, conclusions and recommendations based on the results of this study, are documented.

Key words: *seakeeping, ship hydrodynamics, seakeeping criteria, Boundary Element Method, ship motions, RAOs, DTC hull, regular waves, irregular waves, operability analysis*

Contents

List of figures

List of Tables

Chapter 1 Seakeeping criteria, regulations and methodologies

In this chapter, the general problem of seakeeping is introduced. Specifically, the seakeeping criteria that ships must adhere to, as well as regulations of classification societies, are mentioned. Additionally, the range of methodologies followed for seakeeping calculations and their fundamental theoretical background are presented.

1.1 The seakeeping problem

Seakeeping is one of the noteworthy facets in Naval Architecture and Marine Engineering, representing in broadest sense, the dynamic behavior of a ship in waves or, as is more commonly known, in seakeeping terms, the vessel's ability to withstand (resist) adverse sea conditions. A more specific and accurate definition is:

Seakeeping is the study of responses (motions, velocities and accelerations), required propulsion power, and events such as wetness and slamming of vessels or floating structures, when subjected to rough wave loads, encompassing the results imposed on humans, the system itself and its capabilities, while emphasizing its resilience and performance (Judge, 2019).

The properties of seakeeping may have been historically considered of secondary importance for ship's performance, portraying it in a more scientific domain. However, in contemporary maritime engineering, as endeavors intensify towards reducing fuel consumption, and consequently mitigating greenhouse gas emissions, combined with refinements in numerical methods and their tools, seakeeping is poised to emerge as a promising part of Naval Architecture. Delving into the seakeeping characteristics of vessels, provides insights for their responses to adverse sea conditions, directly influencing their overall performance.

Generally, understanding and calculating ship's motions and accelerations are noteworthy for assessing cargo and equipment loads, as well as ensuring safe working environment for crew. Furthermore, in challenging sea conditions, the relative motion between ship and water takes on significance, as it affects the risks of phenomena such as "green water" on deck, propeller emergence, bottom slamming, bow flare slamming and grounding in shallow waters (Molland, 2008).

Concluding, seakeeping is integral to Naval Architecture, reserving/promising transformation from a traditionally scientific sector to a promising one, addressing challenges and improving maritime performance and safety.

1.2 Seakeeping criteria and regulations

1.2.1 Criteria

Evaluating whether a hull design is successful regarding seakeeping performance or not, criteria have been established and thorough analysis is required to be conducted. Basic seakeeping criteria contain ship motions and ship-motion related phenomena, while addressing wave loads and dynamic stability (Tan, 1995).

Seakeeping performance for commercial ocean-going vessels is primarily evaluated in terms of (Svensen, n.d.) :

- Habitability, referring to the ship's ability to complete a mission with the least amount of discomfort.
- Operability, referring to the ship's ability to carry out a mission under all possible weather conditions.
- Survivability, being satisfied by classification rules, load line and stability regulations compliance.

The distinctions between habitability and operability are often ambiguous and the two of them will always be considered together. Limiting values for distinctive performance criteria have emerged from full-scale operational experience. These encompass design limits, which are absolute threshold values that must not be exceeded during operation, and operational limits, standing for limiting values beyond of which performance demotion and damages to vessel or cargo may occur.

These operational limits are assumed to be crucial for voluntary speed reduction or alternation of course in service, as they are exceptional subjective actions taken by the captain of a ship, when habitability or operability are deteriorated (Ghaemi & Olszewski, 2017). The operability limits are presented based on one or some of the following seakeeping criteria and standards:

i. Motion Induced Interruptions (MII) (Baitis et al., 1995). Motion induced interruption is defined as an occurrence where ship motions become adequately large to affect a person's balance and capability to work in an upright position.
ii. Motion Sickness Incidence (MSI) (O'Hanlon & McCauley, 1974). Motion sickness incidence points out the percentage of experiencing vomiting due to frequency and amplitude of linear acceleration.

iii. The North Atlantic Treaty Organization Standard Agreement 4154 (NATO, 1997, 2018). NATO STANAG 4154 is an agreement containing criteria for human performance at sea, addressed to crew (military) and technical/warfare/launching equipment, applied in naval vessels, mostly for operability and safety aspects.

iv. U.S Navy and U.S Coast Guard Cutter Certification Plan (Sheinberg et al., 2003; Stevens & Parsons, 2002). USCGC is an agreement for 47, 82 and 100 feet US Coast Guard Cutters, for operability.

v. NORDFORSK 1987 (Nordforsk, 1987) is an agreement for operability reasons addressed to crew, transit passengers, hull, cargo and technical equipment, applied in merchant, naval, fishing, offshore vessels and fast small crafts.

vi. ISO 2361/3-1985 (ISO, 1997) (in relation to vertical acceleration) is an agreement addressed to crew and passengers, applied to monohull vessels, for habitability reasons.

vii. Tasaki et al. and Cruikshank and Landsberg are mentioned in publications of (Ghaemi & Olszewski, 2017; Pipchenko, 2011) for operability reasons, without having known direct source in literature.

Seakeeping performance quantification and evaluation can be addressed by the following ship operability limitation criteria regarding:

1. **Heave motion.** Heave signifies the vertical displacement of the ship along its vertical axis.
2. **Pitch motion.** Pitch denotes the rotational movement of the ship around its transverse axis.
3. **Roll motion.** Roll corresponds to the rotational movement of the ship around its longitudinal axis.
4. **Lateral and vertical accelerations.** Lateral acceleration, or sway acceleration, designates the acceleration encountered by the ship in the sideward direction, perpendicular to its longitudinal axis. On the other hand, vertical acceleration relates to accelerations along the vertical axis.
5. **Displacement (mainly vertical displacement)**, is the ship's vertical motion relative to the water surface.
6. **Local relative motion,** is the movement and impact experienced by a ship in relation to its motion relative to the waves it encounters.
7. **Slamming.** Slamming is the abrupt impact of the ship's bottom on the free surface of sea when the bow rises from the water due to intense waves and subsequently strikes

forcefully against the sea, causing potentially hazardous loads. There are three types of slamming: bottom, bow flare, and stern.

8. **Deck wetness.** Deck wetness refers to the seawater that washes over the deck) due to forward deck relative motion to the wave surface.
9. **Propeller emergence.** Propeller emergence is the phenomenon where the ship's propeller, due to its movements, emerges from the water, significantly reducing its thrust.

In the Table 1.1 below, the complete set of standards and agreements for seakeeping criteria is presented. Additionally, the threshold values of the phenomena are recorded, above of which the operability, habitability, and safety aspects of seakeeping are not satisfied, according to each agreement and for the respective types of vessels to which they apply.

Table 1.1: General operability limiting criteria for ships (Pipchenko, 2011).

Ref. Criterion	NATO STANAG 4154	U.S. Coast Guard Cutter Certification Plan	Tasaki et al. (Japan)	NORDFORSK 1987			Cruikshank & L.andsberg (USA)
				Merchant ships	Naval vessels	Fast small craft	
Vertical acceleration at forward perpendicular	0.2g RMS[1]	0.4g SSA[2]	0.80g @ P=0.001	0.275g (L≤ 100m) or 0.05g (L≥330m)	0.275g	0.65g	0.25g
				0.20g for light manual work 0.15g for heavy manual work 0.10g for intellectual work 0.05g for transit passengers 0.02g for cruise liner			
Vertical acceleration at bridge	0.1g RMS	0.2g SSA		0.15g	0.2g	0.275g	0.20g
Lateral acceleration at bridge	0.1g RMS	0.2g SSA	0.60g @ P=0.001	0.12g	0.1g	0.1g	
				0.10g for light manual work 0.07g for heavy manual work 0.05g for intellectual work 0.04g for transit passengers 0.03g for cruise liner			
Motion Sickness Incidence (MSI)	20% of crew in 4 hours	5% in a 30 minute exposure					
Motion Induced Interruption (MII)	1 tip per minute	2.1 tip per minute					
Roll amplitude	4.0° RMS	8.0° SSA	25.0° @ P=0.001	6.0°	4.0°	4.0°	15.0°
				6.0° for light manual work 4.0° for heavy manual work 3.0° for intellectual work 2.5° for transit passengers 2.0° for cruise liner			
Pitch amplitude	1.5° RMS	3.0° SSA					
Slamming (probability)			0.01	0.03 (L≤ 100m) or 0.01 (L≥300m)	0.03	0.03	0.06
Deck wetness (probability)			0.01	0.05	0.05	0.05	0.07
Propeller Emergence (probability)			0.1				0.25

[1] RMS: Root Mean Square value (Equation 2.23)

[2] SSA: Significant Single Amplitude (Equation 2.24)

One of the several worth mentioning research papers and studies that supported and influenced the current thesis is the recent scientific research work by (Pennino et al., 2020). In this study, an adaptive weather routing model is developed based on seakeeping analysis for an S175 containership traveling in the North Atlantic Ocean. Specifically, the selection of the optimal route, for maximum performance, is achieved by combining limiting seakeeping criteria and weather forecast maps. To assess the criteria, the Seakeeping Performance Index (SPI) is formulated, which aggregates determinant criteria and depends, according to the study, on the type of vessel and the route. The SPI index formulation has emerged, which constitutes an optimization function for seakeeping performance based on the criteria of NATO STANAG 4154 and NORDFORSK 1987. Specifically, it implements the five criteria for pitch amplitude, relative vertical acceleration at the forward perpendicular, probability of slamming, probability of green water on deck and the MSI. The results of this work are significant, however, they remain to be validated through simulations under real conditions, routes, and data.

1.2.2 Regulations

The design and construction of ships must adhere to stringent regulations defined by classification societies or international maritime organizations to ensure the safety, stability and performance of vessels. Consequently, an increasing number of regulations has been and continues to be established, to which ships must comply. Concerning seakeeping, aside from the criteria already mentioned, there are no dedicated and specific regulations. However, the study and analysis of seakeeping and ship motions in waves play a significant or even decisive role in complying with critical regulations governing ship stability, fatigue, maneuvering and other fields.

Indicatively, some of the significant contributions of seakeeping analysis pertain to the following requirements and guidelines:

- Guidelines for defining the minimum propulsion power to maintain the maneuverability of ships in adverse weather conditions. It is well-known that maneuvering and seakeeping are directly interconnected domains, more specifically in this case, seakeeping is utilized to determine the added resistance due to waves (ABS, 2006).
- Guidelines for slamming phenomenon. The slamming strength assessment procedure includes slamming load prediction and strength assessment. In the part of slamming load prediction, once the loading condition and the slamming-affected region are determined, environmental data are obtained, and an analysis of vessel motions is

performed to calculate the Response Amplitude Operators (RAOs) for relative vertical velocity and relative vertical motion. Statistical analysis of these results is then conducted to compute the design slamming pressure (ABS, 2021).

- Guidelines for whipping assessment phenomenon. Whipping is the rapid vibration of hull girder, as a consequence of severe slamming. Using a similar methodology as in the case of slamming, after determining the loading conditions and weather data, vessel motion analysis is performed. The results are utilized for the calculation of impact and wave loads and the determination of bending moment and fatigue damage due to whipping (ABS, 2014).
- Guidelines for dynamic loading analysis. This method determines the dynamic loads, the results of which are utilized as a basis to increase scantlings where necessary. However, this optimization is conducted without allowing decrease in the scantlings from those defined by the regulations of classification societies. Therefore, following the determination of loading conditions and wave data, a hydrodynamic numerical model is created and the Response Amplitude Operators (RAOs), extreme values, non-linear ship motions, and wave loads are analyzed. Subsequently, the external pressure, motion-induced loads for cargo and ballast tanks, and ultimately, the structural analysis are calculated. The results of the structural analysis are then assessed against established acceptance criteria (ABS, 2018).

1.3 Methodologies

The predominantly used methodologies for seakeeping analysis are divided into experimental and numerical approaches. Each complements the other, ensuring the precision and accuracy of results. Importantly, due to latest technological advancements, both experimental and numerical methods can simulate real-world conditions and response effects to an exceptional degree.

1.3.1 Experimental methodologies

In the second half of the 19th century, William Froude proposed to the British Admiralty the construction of, what is now known as, a model experiment tank in Torquay, England. Froude had already developed his methodology for calculating the resistance of smaller-scale ships, the models, and needed the tank to conduct experiments with these models. Froude's proposal was accepted, and in 1872, the first professional experimental method was conducted in a tank

measuring $85 \times 11 \times 3$ meters (RINA, 2024). Thus, starting with resistance experiments, the study and analysis of seakeeping in experimental tanks were subsequently established.

The experimental approach involves simulating various sea conditions in conventional long, narrow ship tanks or basins to calculate and assess the model's behavior (and resistance) in these conditions. Therefore, the primary purpose of experiments is to simulate real seakeeping conditions and issues. The essential equipment for experiments includes model-scale ships, regular and irregular wave generators and measurement tools to collect data on responses, velocities, accelerations, wave characteristics, and forces acting on the model (Rawson & Tupper, 2001).

Indicative methodologies employed in experimental procedures include:

1. Calculation of model responses in regular waves, measuring Response Amplitude Operators (RAOs) and utilizing them to estimate model's behavior in irregular waves, based on the theory of regular waves superposition. These experiments are usually conducted in moderate wave conditions and simple facilities, necessitating numerous runs to cover a wide range of speeds and wave lengths.
2. Calculation of model responses in irregular waves, analyzing results to estimate RAOs. Therefore, these experiments require an irregular wave generator and a large amount of runs for each speed, to enhance statistical analysis accuracy.
3. Transient wave testing, where the wave generator produces high-frequency waves, subsequently decreasing frequency until stopping. Starting from calm water, the model encounters all wave lengths within the required frequency range, providing a comprehensive picture of model responses in various wave conditions. A significant limitation is the avoidance of steep waves to prevent potential breaking and deterioration of the flow field due to reflection in the tank.
4. Simulation of irregular waves to calculate and assess responses, power, wetness, and other phenomena. Precisely simulating irregular wave conditions is challenging, but successful approximation of the wave spectrum allows the comparison of the behavior with existing statistical data, and the verification of the assumption of linear superposition theory.

1.3.2 Numerical methodologies

As mentioned earlier, experimental methodologies demand sophisticated facilities and equipment, along with time and cost to perform such experiments. Therefore, experimental

models for seakeeping performance assessment are primarily conducted to validate the accuracy and correctness of numerical methodologies. From the late 20th century to present, plethora of numerical methods has been developed and utilized, aligning with technological advancements and the availability of high computing power. These methods further enhance the representation and discretization of the flow field and the precision in computing seakeeping motions and other parameters (Molland, 2008).

Given the dynamic and stochastic nature of sea waves, it is expected that the influence of wave amplitude on the seakeeping of the vessel will develop nonlinearity. Hence, the exploration of vessel responses in linear wave conditions is of little significance, in extreme wave conditions. These non-linear cases signify the stochastic structure of the seakeeping problem, in which prevails the simulation of the time domain as tool for resolution through numerical methodologies.

However, if the nonlinearity of seaways is negligible or mild (moderate), then the seakeeping properties of a vessel can be computed by the superposition of responses in regular waves of different frequencies and directions. In such cases, precision can be improved by introducing some straightforward corrections to the purely linear calculations, such as considering the time-dependent changes in position and wetted surface of the vessel. Nevertheless, the time dependency remains harmonic, i.e. sinusoidal, due to the harmonic/regular wave oscillations.

The governing equations describing the phenomena of ship seakeeping are the Navier-Stokes equations, regarding conservation of momentum, and the continuity equation for conservation of mass respectively. Given that, we neither desire, nor can resolve every little turbulent fluctuation in the boundary layer and wake of the vessel, so we accept time intervals that are large for turbulent fluctuations and small for wave periods. This assumption introduces the Reynolds-Averaged Navier-Stokes (RANS) equations, the solution of which forms the basis for a significant part of numerical methods, specifically in Computational Fluid Dynamics (CDF). If viscosity is disregarded in the Navier-Stokes equations, we obtain the Euler equations, which do not solve the boundary layers due to the absence of viscosity, allowing coarser grids and shorter computational times (Molland, 2008).

In practice, widely used for seakeeping calculations and predictions are the Potential Flow solvers. In addition to the assumptions of Euler solvers, they introduce the assumption of irrotationality of the flow, which does not deviate significantly from the physical model, as rotation is created by water adherence to the hull, a parameter/case already neglected in the

Euler equations. Some differentiating features of Potential Flow solvers from the aforementioned numerical methods are:

1. For solving the potential flow, only a linear differential equation is used, as opposed to four non-linear coupled differential equations, making Potential Flow solvers to be faster than equivalent Euler or RANS solvers.
2. Potential Flow solvers discretize only the boundaries of the domain, not the entire fluid volume, as they rely on Boundary Element Methods (BEM), thus significantly reducing grid generation effort.
3. Potential Flow solvers require simple and continuous free surfaces and, therefore, cannot incorporate and compute flows implicating splashes and breaking waves.

Nevertheless, viscosity is a crucial parameter in seakeeping, especially in roll and yaw motions, where the boundary layer periodically detaches from the hull. In this case, certain assumptions and corrections are introduced, such as, for example, applying the Kutta condition (Crighton, 1985) to smooth the flow separation from the sharp edges of the ship's aftbody. The fundamental theory and boundary conditions of linear potential flow methods for seakeeping are thoroughly and extensively analyzed in the literature, e.g. (J. N. Newman, 1978)(Molland, 2008).

1.3.3 Boundary Element Method (BEM)

Among numerical methods, potential flow methods stand out in seakeeping. All types of potential flow methods share the common principle, in which the water fluid is idealized as incompressible, irrotational and inviscid. According to these methods, boundary fields are modeled based on the superposition of sources, dipoles, and vortices, while considering the local geometry of the vessel (not the main particulars). However, these methods entail various limitations.

Far field. (Maruo, 1960) introduced the first far-field approach, according to the conservation of momentum theory, estimating the added resistance in waves based on the potential of incident wave in relation to the reflected waves from the body. Subsequently, Mauro's formula was extended by (Longuet-Higgins & Selwyn, 1977) for finite water depth and by (Gerritsma & Beukelman, 1972) for more general types of vessels, delving into the approximation of radiated energy, where the drift force is related proportionally to the amplitude of the radiated waves in the far field.

Direct pressure integration. The direct pressure integration method, which delves into near-field approximations based on hull pressure integration, was first introduced by (Pinkster & Van Oortmerssen, 1977) and extended by to include arbitrary water shapes and forward speed. However, this method is applicable only to blunt bodies with vertical side walls and short waves, making it unsuitable for a range of vessels and wave conditions (Lagemann, 2019).

Strip theory. Strip theory is widely used for seakeeping calculations. According to this method, the ship is considered slender, meaning it is much longer compared to its height and width. Therefore, the flow is assumed to vary mainly in the cross-sectional plane, simplifying the three-dimensional (3D) problem into a set of two-dimensional (2D) boundary value problems. This assumption also requires simplification of the free surface conditions. This method was introduced in 1950 through the work of (Korvin-Kroukovsky & Jacobs, 1957), while the majority of strip theory methods used today are extensions of the methods presented by (Salvesen et al., 1970). Salvesen combined the far-field and strip theory methods, achieving improved results for both motions and added resistance due to waves. The calculations of the flow field and forces in the two-dimensional problem, i.e., for each cross-section, can be performed through analytical approximations. One approach is to implement conformal mapping for transforming semicircles into cross-sections resembling ship sections (Lewis sections) (Journée, 1992) or to use panel methods. Although this transformation entails several limitations and inaccuracies in areas of complex geometry (e.g., bulbous bow), this method outweighs performance comparable to other strip methods based on panel methods (closed-fit approach) for many types of vessels. The closed-fit method was introduced by (Bertram, 2000). In general, despite some theoretical shortcomings of the method, the strip method excels in terms of time efficiency and computational power, proving to be effective in addressing most problems (Lagemann, 2019).

Panel methods. Panel methods constitute a significant part of boundary element methods. In these methodologies, when computing the potential flow of incompressible fluids, such as water, the flow is considered as a superposition of elementary flows from point sources and vortices, satisfying the conservation of fluid volume, i.e., incompressibility. Consequently, the actual flow is accounted for through this superposition, satisfying the boundary conditions of the real problem, i.e., the actual flow. Specifically, the boundaries where the boundary conditions must be satisfied are discretized into a large number of small panels, which can be triangular, quadrilateral or curved. Typically, the boundary conditions are applied at or near the centers of the panels, while the elementary flows consist of constant-density sources in each

panel. To avoid or smooth out flow irregularities often present in boundary conditions, using continuous source density distributions, placing the source distribution outside the region of the modeled fluid, or employing point sources per panel outside the fluid and satisfying the boundary conditions on average for each panel (not pointwise) (Söding, 2010). The calculation of potential flow based on 3D numerical panel methods can be introduced through two methodologies:

1. Green function panel method: This approach relies on the frequency domain and employs the Green function (J. Newman, 1985), where the velocity potential of each panel satisfies the Laplace equation, the radiation condition and linearized the free-surface conditions. More specifically, the radiation condition implies that the body moves in a uniform flow field and is disturbed only by incident waves and the body itself. Therefore, the radiation condition is satisfied by the base flows, which are flows attributed to constant and pulsating sources. Furthermore, the strength of the sources is determined by the acceptance that there is no flow on the body's surface and thus the free-surface boundary conditions are also satisfied by the base flows. Consequently, only the condition on the body's surface, i.e., the wetted surface, needs to be numerically satisfied and covered by panels. There are various methods by (Ba, 1995) and (Iwashita, 1992).
2. Rankine panel methods. This approach is applicable in both frequency and time domains. Among methodologies pertaining to flow potential, Rankine panel methods stand out as particularly conducive to achieving heightened precision in seakeeping calculations. In addition to addressing boundary conditions on the body, they introduce the free-surface condition and radiation condition. This implies that both the ship’s hull and the free surface around it, need to be numerically computed and, thus, discretized into panels. Although this method has more unknowns than those in Green function panel method and is, therefore, more complex, it is prevalent. Nonetheless, this method also shares the limitations of other Boundary Element Methods (BEM) where viscous phenomena or breaking waves cannot be computed, and flow conditions must be known. Overview of these methods are provided by (Bertram & Yasukawa, 1996) and MIT, which developed time-domain SWAN code (end of 1990s) (Sclavounos, 2002).
3. Combined Green function and Rankine panel method. The combination of these two methods is employed to address the deficiencies inherent in each. The Green function panel method encounters limitations and difficulties in accurately approximating

natural phenomena when the steady flow deviates from uniform flow. Conversely, the Rankine panel method faces challenges in approximating the radiation condition. Thus, the hybrid method encompasses the distribution of Rankine sources in the inner domain and employs the Green function in the outer one (Molland, 2008).

1.3.4 Computational Fluid Dynamic (CFD)

Numerical methods that consider and solve the fluid volume and non-linear phenomena, utilizing Navier-Stokes equations, are referred to as Computational Fluid Dynamics (CFD) methods. CFD incorporates viscous phenomena into its calculations, as well as the non-linearities arising from the ship's motions in random waves and swells, hence requiring greater computational power compared to potential flow methods. CFD methods encompass a range from Reynolds-Averaged Navier-Stokes (RANS) methods, which estimate turbulent fluctuations over time, to Detached Eddy Simulation (DES) and Large Eddy Simulation (LES) methods, recognized for their higher accuracy (Bertram, 2012). DES meticulously resolves turbulent fluctuations, demanding a dense computational mesh in the flow field and finding practical application mainly in 2D simple problems. Similarly, the LES method is still under scrutiny as it necessitates substantial computational resources to become commercially viable. Therefore, the most prevalent and widely employed CFD methods in seakeeping are RANS methods (Lagemann, 2019).

Chapter 2 Seakeeping fundamentals

In this chapter, the fundamental mathematical relationships and equations, upon which the calculations of this thesis, are based will be presented.

The seakeeping problem can be divided into the following three parts:

1. the waves, including both regular and irregular, which constitute the input of the system
2. the characteristics of the ship, such as size and shape of the hull, which constitute the system
3. the ship motions, which constitute the output of the system

2.1 Waves

Regular waves

Regular waves are shaped like sinusoidal or cosinusoidal waves on the free surface of the sea. To define a regular wave, it is required to determine its amplitude ζ_α, wavelength λ, period T and the direction of propagation.

In linear theory, is required to assume that the waves are long (steepness and velocities in x, y and z axis are quite small), the fluid is incompressible and inviscid, as well as the flow is irrotational. Thus, the harmonic displacements, velocities and accelerations of water particles are linearly related to the water surface elevation.

The wave height H of a sinusoidal wave is described by the expression:

$$H = 2\zeta_\alpha \tag{2.1}$$

The wave period T is described by the equation:

$$T = \frac{1}{f} = \frac{2\pi}{\omega} \tag{2.2}$$

where f is the frequency and ω is the angular wave frequency.

The wave number k is the spatial frequency of the wave, known as repetency, and its expression is:

$$k = \frac{2\pi}{\lambda} \tag{2.3}$$

The relationship connecting the wave angular frequency ω, wave number k and water depth h is the **dispersion equation**:

$$\omega = kg\ tanh(kh) \tag{2.4}$$

Replacing equations (2.2) and (2.3) to the dispersion equation (2.4), arises the analytical expression for wavelength λ, which depends on the water depth, and is expressed by the general relationship:

$$\lambda = \frac{g}{2\pi} T^2 \tanh 2\pi \left(\frac{h}{\lambda}\right) \tag{2.5}$$

Waves evolve both in time and space, therefore, the equation of the free surface $\zeta(x,t)$ is described by the mathematical expression:

$$\zeta(x,t) = \zeta_\alpha \sin(kx - \omega t + \varepsilon)\,, \tag{2.6}$$

where t is the variable for time, x is the variable for space, ω is the wave angular frequency and ε is the phase angle.

The total energy per unit area of sea surface E is the sum of kinetic energy and potential energy, and it is given by the relationship:

$$E = \frac{1}{2}\rho g \zeta_\alpha^2 \tag{2.7}$$

Irregular waves

In real conditions, the free surface of the water appears and behaves highly irregular and random. Therefore, the analysis of seakeeping in actual sea states is based on stochastic phenomena. Thus, the simulation of an irregular sea state is conducted, as mentioned earlier, through the linear superposition of a series of simple regular waves, each one with its unique amplitude and frequency, but random phase. Consequently, the elevation of the free surface of the sea in irregular waves in the time domain, propagating in the longitudinal plane, can be expressed as the sum of many regular wave components in the frequency domain, as follows:

$$\zeta(t;x) = \sum_{n=1}^{\infty} \zeta_{\alpha_n} \cos\left(k_n x - \omega_n + \varepsilon_n\right) \tag{2.8}$$

where, for each index n, ζ_{α_n} is the wave amplitude (m) calculated through Fourier analysis, ω_n is the angular wave frequency (rad/s), $k_n$is the wave number (rad/m) calculated by dispersion equation and ε_n is the random angular phase (rad).

2.2 Ship motions/Ship's response in waves

The dynamic behavior of all floating bodies, including the ship, is described by a six degrees of freedom system, assigning one translation and one rotation to each of the three axes. Translations are determined with respect to the ship's center of gravity (CG) and rotations are with respect to the orthogonal axes through the center of gravity. These movements are defined as follows:

Surge (Translation along longitudinal axis): $x = z_1 \cos(\omega_e t + \varepsilon_x)$ (2.9)

Sway (Translation along transverse axis): $y = z_2 \cos(\omega_e t + \varepsilon_y)$ (2.10)

Heave (Translation along vertical axis): $z = z_3 \cos(\omega_e t + \varepsilon_z)$ (2.11)

Roll (Rotation around longitudinal axis): $\varphi = z_4 \cos(\omega_e t + \varepsilon_\varphi)$ (2.12)

Pitch (Rotation around transverse axis): $\theta = z_5 \cos(\omega_e t + \varepsilon_\theta)$ (2.13)

Yaw (Rotation around vertical axis): $\psi = z_6 \cos(\omega_e t + \varepsilon_\psi)$ (2.14)

In the above equations, $z_1, z_2, z_3, z_4, z_5, z_6$ represent the amplitudes of corresponding motion, and ω_e is the encounter frequency of the ship (rad/s), i.e., the frequency at which the the ship encounters wave and thus is the frequency of the excitation forces. The encounter frequency ω_e is given by the equation,

$$\omega_e = \omega - kU\cos\mu \tag{2.15}$$

It is evident that the encounter frequency ω_e depends on the wave frequency ω, the wave length k, the ship's speed U and the incident wave angle μ.

For deep water encounter frequency ω_e reduces to,

$$\omega_e = \omega - \frac{\omega^2 U}{g}\cos\mu \tag{2.16}$$

For shallow water encounter frequency ω_e reduces to,

$$\omega_e = \omega - \sqrt{\frac{\omega^2}{gh}}U\cos\mu \tag{2.17}$$

Having calculated the ship's motions at the center of gravity, using a body-fixed coordinate system, the motions can be analyzed at any other point of interest.

2.3 Wave energy spectrum

As mentioned in the paragraph regarding irregular waves, random wave states are considered to be a superposition of many regular waves, where the frequency characteristics of such a wave are analyzed using Fourier series. A record of free surface elevation can be statistically analyzed by taking N samples at equal time intervals Δt. Based on the Fourier assumption, each examined point repeats after a certain time period. The instantaneous wave elevation is expected to have a normal distribution with a mean value of zero.

The individual amplitudes of the waves ζ_{α_n} composing the irregular condition are calculated through Fourier analysis in that interval. However, for each minor change in time in the recording history, a new set of amplitudes ζ_{α_n} is observed, constituting the stochastic phenomenon. Therefore, the mean square value of the amplitudes $\overline{\zeta_{\alpha_n}^2}$ is calculated. The variance $Var(\zeta)$ of this interval is proven to be equal to:

$$Var(\zeta) = \sigma_\zeta^2 = \sum_{n=1}^{N} \frac{1}{2} \zeta_{\alpha_n}^2 \tag{2.18}$$

The distribution of wave amplitudes is thus expressed as a wave spectrum, known as the Energy Spectrum of waves $S_\zeta(\omega_n)$, representing the distribution of the energy of random waves at different frequencies and is related to the amplitudes by the equation:

$$S_\zeta(\omega_n)\Delta\omega \approx \frac{1}{2} \zeta_{\alpha_n}^2(\omega_n) \tag{2.19}$$

where $\Delta\omega = \omega_{n+1} - \omega_n$ is the difference between two successive wave frequencies.

In the condition when $\Delta\omega \to 0$, the wave energy spectrum is given by the expression:

$$S_\zeta(\omega_n)d\omega = \frac{1}{2} \zeta_{\alpha_n}^2 \tag{2.20}$$

The variance of the sea surface elevation is equal to the area under the spectrum:

$$\sigma_\zeta^2 = \int_0^\infty S_\zeta(\omega_n)d\omega \tag{2.21}$$

The total energy of the random wave is given by the equation:

$$E_{total} = \rho g \int_0^\infty S_\zeta(\omega_n)d\omega \tag{2.22}$$

2.4 Spectral parameters

Having the wave energy spectrum, its energy content can be described and analyzed through the spectral parameters that arise. Specifically, the moments $m_{n\zeta}$ of the spectrum, for various orders n, are given by the relation,

$$m_{n\zeta} = \int_0^\infty \omega^n S_\zeta(\omega) d\omega \,. \tag{2.23}$$

It reasonably follows that the zero-th moment $m_{0\zeta}$ is given by the expression,

$$m_{0\zeta} = \int_0^\infty \omega^0 S_\zeta(\omega) d\omega = \int_0^\infty S_\zeta(\omega) d\omega = Var(\zeta) = \sigma_\zeta^2. \tag{2.24}$$

and thus,

$$\sigma_\zeta = RMS = \sqrt{m_{0\zeta}}. \tag{2.25}$$

The significant wave height $H_{1/3}$ is defined as the mean value of one third of the highest heights of the free surface elevation ratio in irregular waves. The significant wave height can be measured both from statistical analysis and wave spectrums, while for narrow-banded wave spectrums is given by the following relationship:

$$H_{1/3} = 4\sqrt{m_{0\zeta}} \tag{2.26}$$

where narrow-banded wave spectrums indicating that the values of the bandwidth parameter are finite and small, meaning that the range of values of the spectrum around the mean frequency is small.

Through the centroids of the surface, mean period T_{01}, mean zero-crossing period T_{02}, peak period T_{24} and energy period T_{-10} are defined:

$$\bar{T} = 2\pi \frac{m_{0\zeta}}{m_{1\zeta}} \tag{2.27}$$

$$T_{02} = T_z = 2\pi \sqrt{\frac{m_{0\zeta}}{m_{2\zeta}}} \tag{2.28}$$

$$T_{24} = T_p = 2\pi \sqrt{\frac{m_{2\zeta}}{m_{4\zeta}}} \tag{2.29}$$

$$T_{-10} = T_E = 2\pi\sqrt{\frac{m_{-1\zeta}}{m_{0\zeta}}} \tag{2.30}$$

2.5 Wave spectral models

Today, while satellite systems and sensors become more advanced, there is available a vast amount of weather data, including information for both wind and waves. Regarding wave data, it is measured as time series of sea surface elevation in specific geographical areas that exhibit greater interest. Various empirical expressions for standardized spectra have been developed by analyzing this data. Currently, two types of wave spectral models are widely used, based on two parameters, significant wave height and the mean period of the waves. The general expression for these wave spectra is given by the relationship:

$$S_\zeta(\omega) = H_{1/3}^2 f(\omega, T) \tag{2.31}$$

2.5.1 Bretschneider wave spectral model

The Bretschneider spectrum, also known as the Modified Two-Parameter Pierson-Moskowitz spectrum, describes various sea states (mostly open sea states), is a unimodal spectrum and has been established as a standard one for seakeeping studies since the 2nd International Ship Structures Congress (ISSC) in 1967 and the 12th International Towing Tank Conference (ITTC) in 1969. The general expression for the Bretschneider two parameter spectra is given by the relationship:

$$S_\zeta(\omega) = \frac{A}{\omega^5} exp\left(\frac{-B}{\omega^4}\right) \tag{2.32}$$

where the two parameters are the characteristic wave height H_{char} and the average period $\bar{T}$:

$$A = 172.75\frac{\bar{H}_{char}^2}{\bar{T}^4} \;\; and \;\; B = \frac{691}{\bar{T}^4} \tag{2.33}$$

Through calculation of spectral moments it is proven that:

$$m_0 = \frac{A}{4B} \; and \; \bar{H}_{char} \approx 4\sqrt{m_0} \tag{2.34}$$

$$T_z = 0.92\bar{T} \;\; and \;\; T_p = 0.0 \tag{2.35}$$

Generally, Bretschneider wave spectrum is a broad-band spectrum ($\varepsilon = 1.0$), containing all wave frequencies (up to infinity). However, due to adjacent peaks with infinitesimally small

ripples, peak period T_p is zero, and the wave spectrum becomes narrow-banded, as high frequency ripples are neglected. Thus, the followings apply:

$$H_{1/3} \approx 4\sqrt{m_0} \quad hence \quad \bar{H}_{char} \approx H_{1/3} \tag{2.36}$$

2.5.2 JONSWAP spectral model

The JONSWAP wave spectrum emerged from the analysis of the Joint North Sea Wave Project in the North Sea. Due to its sharper spectrum, it can cover more sea states than the Bretschneider spectrum, as it is suitable for both deep-sea adverse conditions and shallow waters. This wave spectrum began to be used in seakeeping analysis after the 17th International Towing Tank Conference (ITTC) in 1984 and is described by the expression:

$$S_{JONSWAP\zeta}(\omega) = 0.658 S_{ITTC\zeta}(\omega) C(\omega) \tag{2.37}$$

In which expression:

$$\begin{gathered} C(\omega) = \gamma \, exp\left[\frac{-1}{2\sigma^2}\left(\frac{\omega}{\omega_0} - 1\right)^2\right] \\ \gamma = 3.3 \\ \omega_P = \frac{2\pi}{T_P} \\ \sigma = \begin{cases} 0.07, & \omega \le \omega_P \\ 0.09, & \omega > \omega_p \end{cases} \end{gathered} \tag{2.38}$$

2.5.3 DNV Spectrum

DNV spectrum is a general formulation used by DNV, including both Bretschneider spectrum (when γ is 1.0) and JONSWAP spectrum (when γ is 3.3). As mentioned below, the peak enhancement factor γ is defined by the significant wave height and modal period:

$$\begin{gathered} \gamma = 5.0, \qquad \frac{T_P}{\sqrt{H_{1/3}}} \le 3.6 \\ \gamma = \exp\left(5.75 - \frac{1.15 T_P}{\sqrt{H_{1/3}}}\right), \quad 3.6 < \frac{T_P}{\sqrt{H_{1/3}}} \le 5.0 \\ \gamma = 1.0, \qquad 5.0 < \frac{T_P}{\sqrt{H_{1/3}}} \end{gathered} \tag{2.39}$$

DNV spectrum is described by the expression:

$$S_{DNV\zeta}(\omega) = \frac{a}{\omega^5} exp\left(\frac{-\beta}{\omega^4}\right) \times \gamma \, exp\left[\frac{-1}{2\sigma^2}\left(\frac{\omega}{\omega_P} - 1\right)^2\right] \tag{2.40}$$

where:

$$\sigma = \begin{cases} 0.07, & \omega \leq \omega_P \\ 0.09, & \omega > \omega_P \end{cases}$$

$$a = 5\pi^4(1 - 0.287\ln(\gamma))\frac{H_{1/3}^2}{T_P^4} \quad and \quad \beta = \frac{20\pi^4}{T_P^4} \tag{2.41}$$

2.6 RAOs and linear-time invariant system (LTI)

In order to evaluate the specific sea state on the ship's motions, the calculation of the Response Amplitude Operators (RAOs) is needed. RAOs is as the ratio of the amplitude of the ship's response (e.g. motion, velocity, acceleration) to the amplitude of the wave. The RAO values are solely dimensionless in the three translations, while in the three rotations, they can be both dimensionless and dimensional. In the following relationships are indicated only the dimensionless expressions, in which k is the wave number:

$$\left|RAO_{surge}\right| = \frac{z_1}{\zeta_\alpha} \tag{2.42}$$

$$\left|RAO_{sway}\right| = \frac{z_2}{\zeta_\alpha} \tag{2.43}$$

$$\left|RAO_{heave}\right| = \frac{z_3}{\zeta_\alpha} \tag{2.44}$$

$$\left|RAO_{roll}\right| = \frac{z_4}{k\zeta_\alpha} \tag{2.45}$$

$$\left|RAO_{pitch}\right| = \frac{z_5}{k\zeta_\alpha} \tag{2.46}$$

$$\left|RAO_{yaw}\right| = \frac{z_6}{k\zeta_\alpha} \tag{2.47}$$

2.7 Response spectrum

According to linear theory, the spectra $S_{z_i}(\omega_\varepsilon)$ of a ship's motions z_i, is derived from the wave spectrum and the corresponding RAO_{z_i}, as described by the expression,

$$S_{z_i}(\omega_\varepsilon) = \left|RAO_{z_i}\right|^2 S_\zeta(\omega_\varepsilon) \tag{2.48}$$

Additionally, the spectra of velocities $S_{\dot{z}_i}(\omega_\varepsilon)$ and accelerations $S_{\ddot{z}_i}(\omega_\varepsilon)$ of motions are proven to be,

$$S_{\dot{z}_i}(\omega_\varepsilon) = \omega^2 S_{z_i}(\omega_\varepsilon) \tag{2.49}$$

$$S_{\ddot{z}_i}(\omega_\varepsilon) = \omega^4 S_{z_i}(\omega_\varepsilon) \tag{2.50}$$

With the response spectra calculated, spectral parameters can be obtained using procedures similar to those for wave spectra.

2.8 Seakeeping criteria

There are many seakeeping criteria (Table 1.1), the calculation of which is based on the RMS of ship's responses. The most important of them are:

- The RMS of pitch amplitude:

$$rms_p = \sqrt{\int_0^\infty \left|RAO_{pitch}(\omega_\varepsilon)\right|^2 S_\zeta(\omega_\varepsilon)} \tag{2.51}$$

  where RAO_{pitch} is the pitch motion transfer function as a speed-dependent parameter.

- The RMS of roll amplitude:

$$rms_r = \sqrt{\int_0^\infty |RAO_{roll}(\omega_\varepsilon)|^2 S_\zeta(\omega_\varepsilon)} \tag{2.52}$$

  where RAO_{roll} is the roll motion transfer function as a speed-dependent parameter.

- The RMS of vertical acceleration at forward perpendicular (FP):

$$rms_a = \sqrt{\int_0^\infty \left|RAO_{heave}(\omega_\varepsilon) - \bar{x}RAO_{pitch}(\omega_\varepsilon)\right|^2 {\omega_\varepsilon}^4 S_\zeta(\omega_\varepsilon)} \tag{2.53}$$

  where RAO_{heave} is the heave motion transfer function as a speed-dependent parameter and $\bar{x}$ is the longitudinal distance of the ship FP from its CG.

- The RMS of relative vertical acceleration at forward perpendicular (FP):

$$rms_{ra} = \sqrt{\int_0^\infty \left|RAO_{heave}(\omega_\varepsilon) - \bar{x}RAO_{pitch}(\omega_\varepsilon) - e^{-ik\bar{x}\cos\mu}\right|^2 {\omega_\varepsilon}^4 S_\zeta(\omega_\varepsilon)} \tag{2.54}$$

  where RAO_{heave} is the heave motion transfer function as a speed-dependent parameter and $\bar{x}$ is the longitudinal distance of the ship FP from its CG.

- The RMS of vertical acceleration at bridge:

$$rms_{vert,acc,b} = \sqrt{\int_0^{\infty} \left|RAO_{heave}(\omega_\varepsilon) + \bar{y}RAO_{roll}(\omega_\varepsilon) - \bar{x}RAO_{pitch}(\omega_\varepsilon)\right|^2 {\omega_\varepsilon}^4 S_\zeta(\omega_\varepsilon)} \quad (2.55)$$

where $RAO_{heave}, RAO_{roll}, RAO_{pitch}$ are the heave, roll and pitch motion transfer functions as a speed-dependent parameter and $\bar{x}$ and $\bar{y}$ are the longitudinal and the lateral distances of the ship bridge from its CG respectively.

- The RMS of lateral acceleration at bridge:

$$rms_{lat,acc,b} = \sqrt{\int_0^{\infty} \left|RAO_{pitch}(\omega_\varepsilon) + \bar{y}RAO_{roll}(\omega_\varepsilon) - \bar{z}RAO_{heave}(\omega_\varepsilon)\right|^2 {\omega_\varepsilon}^4 S_\zeta(\omega_\varepsilon)} \quad (2.56)$$

where $RAO_{heave}, RAO_{roll}, RAO_{pitch}$ are the heave, roll and pitch motion transfer functions as a speed-dependent parameter and z and $\bar{y}$ are the vertical and the lateral distances of the ship bridge from its CG respectively.

- The slamming probability, of ship's bottom to be out water and ship's relative velocity (to free surface) not to exceed the threshold velocity, is:

$$p_{sl}\left(|\zeta_{VR}| > d, \left|\dot{\zeta}_{VR}\right| > v_{cr}\right) = e^{-\left(\frac{v_{cr}^2}{2C_s^2 m_{2,r}} + \frac{d^2}{2C_s^2 m_{0,r}}\right)} \quad (2.57)$$

where the threshold velocity is $v_{cr} = 0.093\sqrt{gL}$, C_s is the swell up coefficient (equal to 1 for Froude values up to 0.30) and d is the ship draught at FP.

- The green water on deck probability, of ship's amplitude to exceed freeboard, is :

$$p_{wd}(|\zeta_{VR}| > f_b) = e^{-\left(\frac{f_b^2}{2C_s^2 m_{0,r}}\right)} \quad (2.58)$$

where f_b is the ship freeboard at FP.

- The MSI (Motion Sickness Incidence) is the percentage of people who vomit after exposure of specified time in motions:

$$MSI\ \% = 100\Phi(z_a)\Phi(z'_T) \quad (2.59)$$

where Φ is the standard normal cumulative distribution and the variables are determined by the following:

$$z_a = 2.128log_{10}\left(\frac{a_{MSI}}{g}\right) - 9.277log_{10}(f_m) - 5.809[log_{10}(f_m)]^2 - 1.851 \quad (2.60)$$

$$z'_T = 1.134 z_a - 1.989 log_{10}\left(\frac{T}{60}\right) - 2.904 \quad (2.61)$$

where T is the exposure time in sec, a_{MSI} is the RMS of ship's vertical acceleration and f_m is the mean frequency in Hz respectively.

From literature review was found a research study, in which an index named SPI was constructed for the assessment of seakeeping criteria (Pennino et al., 2020), implementing five fundamental criteria and formulated as follows:

$$SPI = max\left\{0; \left(1 - \frac{rms_p}{rms_{p,l}}\right) \cdot \left(1 - \frac{rms_a}{rms_{a,l}}\right) \cdot \left(1 - \frac{p_{sl}}{p_{sl,l}}\right) \cdot \left(1 - \frac{p_{wd}}{p_{wd,l}}\right) \cdot \left(1 - \frac{MSI}{MSI_l}\right)\right\} \quad (2.62)$$

where the values with index l are the limit values presented in Table 1.1and the rest of them are already listed above.

2.9 Ship Resistance

Although this study does not focus on ship resistance, some results will be presented for the sake of completeness and coherence. Therefore, the following formulas for calculating R_T (Total resistance), R_F (Friction resistance), R_{AW} (Added resistance), R_W (Wave resistance from pressure integration), R_C (Calm water resistance) and frictional resistance are provided below.

$$R_T = R_W + R_F \quad (2.63)$$

$$R_F = \frac{1}{2} S \rho V^2 c_F (1 + k) \quad (2.64)$$

where S is the wetted surface, ρ is the density of sea water, V is the velocity, c_F is the friction resistance coefficient and k is the form factor.

$$R_{AW} = R_T - R_C \quad (2.65)$$

$$R_{AW} = \rho g \left(\frac{h}{2}\right)^2 \frac{{B_{WL}}^2}{L_{PP}} c_{AW} \quad (2.66)$$

where h is the wave height, B_{WL} is the waterline beam and c_{AW} is the added resistance coefficient.

Chapter 3 Boundary Element Method for Seakeeping

In this chapter, the theory and assumptions underlying the SHIPFLOW software, utilized in this study, are presented.

3.1 Fully non-linear unsteady potential flow method

In this diploma thesis, regarding the study of the dynamic behavior of the ship in waves, the SHIPFLOW Motions software was used. This tool utilizes a fully non-linear unsteady potential flow solver, with time-dependent 3D panel method, both for the free surface of the sea and for the floating body or bodies, recording their responses at the six degrees of freedom (6DOF) (Flowtech International AB, n.d., 2022). This software package creates an unstructured grid on the body and free surface, automatically refined grid when altering the free surface, as well as it extracts time-series data and 3D visualizations.

3.1.1 Coordinate systems

The software SHIPFLOW Motions performs calculations taking into account five coordinate systems, for the use case of a ship.

Table 3.1: SHIPFLOW coordinate systems.

Coordinate system (c. s.)	Description	Usability
Earth-fixed Cartesian right-handed coordinate system O_{xyz}	The origin of this c.s. is at an arbitrary position of the free surface, when calm. The z-axis is pointing upwards and is perpendicular to the horizontal plane.	Creating the prime equations of incoming waves, free surface evolution and fluid flow.
Body-fixed coordinate system $O_b x_b y_b z_b$	The origin of this c.s. is at the center of gravity (CG) of the body. In cases when the initial position of the body is not given by user, the origin is placed at (x, y) = (0, 0) of the earth-fixed coordinate system.	Moving along with the floating body, for description of point responses with respect to the computational coordinate system.
Offset coordinate system $O_o x_o y_o z_o$	The origin of this c.s. is at the baseline and AP (aft perpendicular), with x_o-axis	Description of offset file.

	pointing towards the bow and z_o-axis upwards.	
Computational coordinate system $O_c x_c y_c z_c$	The origin of this c.s is on the horizontal plane (aligned to the body-fixed c. s), below or above CG in the z_c-axis and towards the bow in the x_c-axis.	Moving with respect to body velocity
Initial coordinate system $O_i x_i y_i z_i$	The origin of this c.s is at the water plane, x_i is at LPP/2 and all the axis have the same orientation as the offset c.s.	Description of free surface elevation.

3.1.2 Potential flow

Essential in potential flow theory is the assumption that endures a scalar quantity φ, portraying the motions of the fluid. Therefore, relevant to a fluid velocity $\vec{u}(x, y, z, t)$,

In the context of potential theory, the flow is considered:

- irrotational, meaning the circulation of the flow velocity $\vec{u}(x, y, z, t)$ is zero,

$$\nabla \times \boldsymbol{u} = 0 \tag{3.1}$$

- incompressible, meaning the density is constant,
- inviscid, meaning the viscosity is zero.

Based on the irrotationality assumption, the velocity potential can be expressed as the gradient of scalar valued function $\varphi(x, y, z, t)$, as follows:

$$\nabla\varphi = \left(\frac{\partial\varphi}{\partial x}, \frac{\partial\varphi}{\partial y}, \frac{\partial\varphi}{\partial z}\right) = (u, v, \omega) = \vec{u} \tag{3.2}$$

where u, v, ω are the velocity components of the fluid in the x, y, z axes of the earth-fixed coordinate system.

Combining the incompressible flow assumption and the continuity equation, the well-known linear partial differential equation Laplace is derived, representing the governing equation for the velocity potential:

$$\nabla \cdot \vec{u} = 0 \tag{3.3}$$

$$\nabla \cdot \nabla\varphi = 0 \tag{3.4}$$

3.1.3 Fluid domain

Concerning the fluid domain, the SHIPFLOW software, for the ship's seakeeping problem, defines an overall boundary domain S, which includes the free surface S_f, the wetted surface of the floating body S_b, and the bottom surface S_t.

3.1.4 Boundary conditions

In the context of potential theory, linearity is involved in the Laplace equation for the velocity potential and nonlinearity is introduced by the following boundary conditions:

Free surface boundary conditions

Kinematic free surface boundary condition. This condition expresses that the fluid particles of the free surface are located on it at any given time *t*, indicating that the surface does not 'break' or form holes and voids, common to a solid surface. Therefore, the velocities of the fluid elements at the free surface are equal to the velocity of the surface itself, as a geometric surface. The kinematic boundary condition is stated by:

$$\frac{D\vec{x}}{Dt} = \left(\frac{dx}{dt}, \frac{dy}{dt}, \frac{dz}{dt}\right) = (u, v, \omega) = \nabla\varphi \tag{3.5}$$

where $\vec{x} = (x, y, z)$ is fluid particle's position on the free surface.

Dynamic free surface boundary condition. This condition expresses that the manometric pressure at the free surface is zero, signifying that the (absolute) pressure there is constant and equal to the atmospheric one. The dynamic boundary condition is stated based on the Bernoulli equation, as follows:

$$\frac{D\varphi}{Dt} = -gz + \frac{1}{2}\nabla\varphi \cdot \nabla\varphi - \frac{p_a}{\rho} \tag{3.6}$$

where g is the gravitational acceleration, ρ is fluid density and p_a is the atmospheric pressure and z is the free surface elevation, while the material derivative is given by:

$$\frac{D}{Dt} \equiv \frac{\partial}{\partial t} + \nabla\varphi \cdot \nabla \tag{3.7}$$

Mixed free surface boundary condition. Combining the kinematic and dynamic conditions the mixed free surface condition is produced, given by:

$$\frac{\partial^2\varphi}{\partial t^2} + g\frac{\partial\varphi}{\partial z} = 0, z = n \tag{3.8}$$

Boundary condition on the body

This is a non-entrance condition, as it indicates the condition on the solid boundary. Thus, it entails that the fluid particles osculate the body, on the wetted surface, have perpendicular velocities with respect to it, which are equal to the fluid velocity in the normal direction of the body. This occurs because the fluid is inviscid and thus, there is no tangential velocity at the surface of the body. The boundary condition on the body is a Neumann type impermeability condition, as follows:

$$\nabla\varphi \cdot \vec{n} \equiv \frac{\partial\varphi}{\partial n} = \vec{n}\,(\vec{v} + \vec{\omega} \times \vec{r}) \tag{3.9}$$

where $\vec{n}$ is the unit normal vector heading to the fluid domain, $\vec{v}$ and $\vec{\omega}$ are the rigid's body translatory and angular velocities, respectively and $\vec{r}$ is the radius vector with respect to the center of rotation of the body.

Boundary condition on the bottom

This condition is also a non-entrance condition, as the fluid cannot infiltrate a solid boundary

$$\nabla\varphi \cdot \vec{n} = 0, \;\; z = -h(x, y)$$

and in the case of deep water (infinity condition) it is described by:

$$\|\nabla\varphi\| \to 0, \qquad response \to -\infty \tag{3.9}$$

Radiation boundary condition at infinity

An additional condition is required to determine the potential flow away from the body, in order to find a unique solution. The radiation boundary condition is given by:

$$\|\nabla\varphi\| \to 0, \quad R \to \infty \tag{3.10}$$

Chapter 4 Seakeeping use case: DTC containership

In this chapter, an introduction to the use case of this thesis is provided, which concerns the seakeeping analysis of a containership hull, specifically the benchmark DTC hull (ITTC, 2021).

4.1 Containerships

A container ship, sometimes known as a boxship, is a cargo type of ship that uses a method of containerization to carry all of its load in intermodal trucks-size containers. Most of seagoing non-bulk cargo, approximately the 90%, is currently transported by containerships, which are also a popular mode of commercial intermodal freight transportation.

Twenty-foot equivalent units are used to estimate the capacity of container ships (TEUs), while 20-foot (20ft - 1 TEU) and 40-foot (40ft – 1 FFE) ISO-standard containers are typically used for loading, with the latter being more common. There is a variety container types used in shipping besides dry containers. Containerships widely carry refrigerated containers, which consume energy to control their interior temperature, as well as special dimensioned containers, such as open-top containers, flat racks, platforms and tank containers (*Container Ship*, 2024).

Commonly to all types of vessels, containerships are also categorized based on their size and according to certain dimensional constraints, such as those imposed by the Panama and Suez Canals. Containerships are known for their high speeds due to their slender and hydrodynamically efficient geometry, characterized by long length, narrow beam and shallow draft. Therefore, the following table serves as an indicative representation of the size categories of containerships (*Evolution of Containerships | The Geography of Transport Systems*, 2023).

Table 4.1: Containership types (https://transportgeography.org/contents/chapter5/maritime-transportation/evolution-containerships-classes/).

Name	Capacity (TEUs)	Length overall (m)	Beam (m)	Draft (m)
Early containerships (1956-)	500-800	200	20	9
Fully Cellular (1970-)	1000-2500	215	20	10
Panamax (1980-)	3000-4000	250	32	12.5
Panamax Max (1985-)	3400-4500	290	32	12.5

Post Panamax I (1988-)	4000-6000	300	40	13
Post Panamax II (2000-)	6000-8500	340	43	14.5
VLCS (2006-)	11000-15000	397	56	15.5
New Panamax (2014-)	12500	366	49	15.2
ULCS (2013-)	18000-21000	400	59	16
MGX-24 (2019-)	21000-25000	400	61	16

4.2 DTC ship

After extensive literature review, several research papers and studies that supported and influenced the current thesis were mentioned. The research paper that this thesis was initially based on was by (Chirosca et al., 2023), in which the additional resistance due to waves of the DTC hull is calculated in regular heading waves, in both experimental and numerical methods, using the SHIPFLOW software for the later. More specifically, similarities were observed in the results of the resistance curves between the experimental and numerical methods, while limitations of the linear theory for calculating the additional resistance were identified, especially in waves with increased wave steepness, as well as with the occurrence of the double reasoning phenomenon.

In this case study, the DTC (Duisburg Test Case) hull was utilized. The design of the DTC hull has been exclusively developed for benchmarking and validation purposes, whereas representing a large category of existing containerships. Specifically, it is a modern Post-Panamax 14000 TEUs containership. Both its size characteristics and its special features, such as extensive stern with large overhang and bulbous bow, can have a significant impact on seakeeping analysis. Moreover, these unique features of the DTC hull are not found in other similar benchmark models, posing a challenge to numerical methods and thus contributing to considerable results in seakeeping software tools and prediction methods. In design loading condition, the draft of the DTC hull is $T = 14.5m$, while the wetted surface S_w refers to the bare hull, excluding appendages. The basic dimensions and elements of the full-scale DTC hull used in the study are presented in the table below (Chirosca et al., 2023; Liu et al., 2021).

Table 4.2: DTC hull characteristics.

Main dimensions			
Length between perpendiculars	L_{PP}	m	355
Waterline breadth	B_{WL}	m	51
Midship draft	T	m	14.5
Volume displacement	∇	m^3	173,467
Block coefficient	c_B	$-$	0.661
Wetted surface	S_w	m^2	22,032
Design speed	V	m/s	12.86
Longitudinal center of gravity (measured from aft perpendicular)	x_{CG}	m	174.059
Vertical center of gravity (measured from aft perpendicular)	z_{CG}	m	19.851
Radius of gyration	r_{yy}	m	87.3

The 3D model of the full-scale DTC hull is also presented below.

Figure 4.1: DTC hull profile design.

Figure 4.2: DTC hull 3D model.

4.3 Use case

The DTC hull was tested by the SHIPFLOW software in calm water condition, as well as in both regular and irregular waves. Specifically, simulating the behavior of the DTC ship in calm water was conducted so as to calculate its calm water resistance (R_C). Concerning the seakeeping simulation in regular waves, one speed was selected, specifically the operational speed of the vessel, at 10 wave frequencies, which are of interest for this hull and in 4 wave headings, maintaining the steepness (height to wavelength ratio) constant at a value of $h/\lambda = 0.031$.

Regular waves

The entire test matrix used in the simulation for regular waves is displayed in the Table 4.3.

Table 4.3: Regular waves characteristics.

Type	Speed	Wave Frequency	Wave Length	Wave Height	Wave Period
	$V(m/s)$	$\omega\ (rad/sec)$	$\lambda(m)$	$H_w\ (m)$	$T_w\ (sec)$
Calm water	12.86	-	-	-	-
Following sea (Wave heading 0°)	12.86	**0.20**	1541.0	47.8	31.4
	12.86	**0.30**	685.0	21.2	20.9
Quartering sea (Wave heading 30°)	12.86	**0.40**	385.2	11.9	15.7
	12.86	**0.45**	304.4	9.4	14.0
	12.86	**0.50**	246.6	7.6	12.6
Beam sea (Wave heading 90°)	12.86	**0.60**	171.2	5.3	10.5
	12.86	**0.70**	125.8	3.9	9.0
Heading sea (Wave heading 180°)	12.86	**0.80**	96.3	3.0	7.9
	12.86	**1.00**	61.6	1.9	6.3
	12.86	**1.20**	42.8	1.3	5.2

Some interesting points to be clarified are:

- The calm water simulation was conducted for a very small wave height, with the value of $H_W = 0.001m$, as the SHIPFLOW software has limitations and could not run a scenario with exactly zero wave height.
- The wave frequencies selected, for the seakeeping analysis of the vessel in regular waves, were determined after numerous trials for various frequencies. Thus, the most significant wave frequencies were investigated, in which the DTC hull exhibited interesting results and responses. Specifically, the software displayed limitations regarding the minimum wave frequency it could simulate. Therefore, the minimum frequency found was approximately $0.20\ rad/sec$, based on the selected steepness ratio, as the iterative solver of the software did not converge after a number of restarts. The maximum frequency was set at $1.20\ rad/sec$, at which the vessel's responses were extremely minimized. For frequencies above $1.20\ rad/sec$, the responses were nearly zero, thus, the information from these frequencies did not contribute to the problem and were neglected. The intermediate value of wave frequency at $0.45\ rad/sec$ was selected because from simulations at various frequencies, it was found that the highest/maximum added resistance due to waves occurred at the frequency of $0.40\ rad/sec$, as its wavelength approach the ship's length and could result in the resonance phenomenon, and thus an intermediate frequency was needed for accuracy purposes. Therefore, it was intentional to include this wave frequency and record its results accordingly.
- The value of wave steepness is based on literature reference (Chirosca et al., 2023), reflecting real experimental tank conditions for regular wave simulations of DTC hull. Also, the selected steepness value has been found from literature (Arena et al., 2010; Heineke & Verhagen, 2009; Mendes & Oliveira, 2021; Toffoli et al., 2010) to be an average one for irregular waves as well, which simulates several realistic sea conditions and ensures that breaking waves will not occur, as $h/\lambda . < 1/7$. For the selection of the wave characteristic, such as height and length, it is recommendable to use values of height and length that can be generated by the wave maker in the tank during the experimental process. However, because of the difficulty in finding these conditions, due to variations in the capabilities of wave makers and the dimensions of the tanks, an indicative steepness value was chosen from the already mentioned paper (Chirosca et al., 2023), to ensure that all waves adhere to a common principle. Lastly, the most

important note is that $h/\lambda = 0.031$ indicates small amplitude waves, approaching more precisely the linear theory.

- Four headings of regular waves were selected, covering the majority of the possible wave directions, in order to explore areas of interest and responses to these individual directions adequately and enable the proper analysis of the RAOs.

Before presenting the results, it is important to mention that numerous Python scripts were created to perform all calculations and generate all diagrams in this work, due to the large volume of data. Specifically, these scripts include:

- Batch process scripts for continuous running of SHIPFLOW, along with YAML input files.
- Scripts for collecting useful data from the software's output files and gathering them in CSV files, for further processing.
- Scripts for plotting diagrams (using spline interpolator) and time series.
- Scripts for spectral analysis in irregular waves (using the PyWafo library).
- Scripts for calculating RAOs (RAOs in points of interest other than CG and RAOs of relative responses).
- Scripts for operability analysis in both regular and irregular conditions, along with the creation of contour diagrams.
- Scripts for general handling of data (trials, data filtering, etc.).

Chapter 5 Responses in regular waves

In this chapter, the results of the simulations and the calculations of the time series of responses at the ship's center of gravity (CG), as well as the RAOs in regular waves, will be presented for the conditions addressed in Chapter 4.

5.1 Geometry verification

Before initiating the simulations of the ship responses to waves, it is mandatory to verify the correct input of its geometry into the SHIPFLOW software. For this purpose, the XMESH command of the software was used to simulate the geometry of the hull, exporting dimensionless results for the length, width, draft, wetted area, volume and block coefficient. Once these parameters were dimensioned, they were compared with those of the DTC hull, as presented in Table 4.2, revealing differences well below the 1% tolerance and almost negligible. Thus, it was confirmed that the vessel's geometry was accurately inputted into the software, validating the readiness to proceed with the simulations.

5.2 Description of computation

At the start of the computation, the hull panelization is generated, and the hull is positioned in calm water. If the longitudinal center of gravity (LCG) and mass of the hull are not specified in the configuration file, a hydrostatic calculation is performed to determine these parameters. Once established, the hull panelization remains constant throughout the computation (Flowtech International AB, 2022).

Next, a free surface mesh is created starting, while free surface panels that are entirely inside the hull are removed, and those intersecting the hull are divided into four smaller panels. This subdivision continues until the panels reach a certain size. To bridge the gap between the free surface and the hull, the panels closest to the hull are skewed.

The hull is then accelerated to the specified speed, which is maintained constant. As the computation continues, wave patterns begin to form, necessitating further refinement of the free surface panels based on the local curvature of the surface.

The free surface mesh is regenerated at each time step, adapting to the position of the hull and the wave conditions. At this case, the hull is simulated over a distance equivalent to approximately 10 ship lengths, applying the default condition of SHIPFLOW. Thus, based on the constant operational speed and the fixed distance, the total time of the simulation results in

$276sec$ (nearly $4.6min$), in which the solver manages to complete 3200 iterations, so as to converge properly.

When simulation finished, time series data for all relevant parameters (positions, velocities, accelerations, forces, moment and resistance) is created. This data were utilized in the below visualizations and calculations.

In the present thesis, the simulations were performed on a PowerEdge R7515 Rack server (AMD EPYC 7543P 2.8GHz, 32C/64T, 256M Cache (225W) DDR4-3200, RAM 256Gb), utilizing only 6 threads (due to the educational license), the simulation for one regular state used to take 4-5 hours, while for one irregular condition the duration reached up to 48 hours of continuous running.

5.3 Calm water

Initially, calm water simulations were conducted for a wave height value almost zero ($0.001\ m$), in order to collect data for added resistance in waves through the calm water resistance of the DTC hull. Although is not strictly required, simulations were performed for all the aforementioned frequencies of regular waves, which exhibited slight differences among them, so as to verify the value of the resistance in calm water. Consequently, it was calculated that the average value of the resistance in calm water of the DTC hull is presented below.

Table 5.1: Average calm water resistance of DTC hull.

Resistance in calm water R_c	3490 (kN)

Table 5.2: Calm water resistance of DTC hull (head seas).

Wave frequency ω (rad/sec)	Resistance in calm water R_c (kN)
0.20	3493.4
0.30	3485.5
0.40	3493.4
0.45	3485.4
0.50	3492.5

0.60	3485.4
0.70	3493.5
0.80	3493.0
1.00	3485.1
1.20	3485.8

5.4 Time-series results

Below are presented the time series of the positions, velocities and accelerations of the ship's center of gravity (CG) in each of the 6 degrees of freedom (DOF), for every one of the four headings.

Table 5.3: Description of time series values.

Title	Description
eta_at_CG	Surface elevation of the undisturbed incident wave field at the center of gravity (m)
P1	Position of the center of gravity in the x-direction (m)
P2	Position of the center of gravity in the y-direction (m)
P3	Position of the center of gravity in the z-direction (m)
P4	Roll angle (Euler angle) (◦)
P5	Pitch angle (Euler angle) (◦)
P6	Yaw angle (Euler angle) (◦)
V1	Velocity of the center of gravity in the x-direction (m/s)
V2	Velocity of the center of gravity in the y-direction (m/s)
V3	Velocity of the center of gravity in the z-direction (m/s)
V4	Roll angular velocity (Euler angle) (◦ /s)
V5	Pitch angular velocity (Euler angle) (◦ /s)

V6	Yaw angular velocity (Euler angle) (◦ /s)
A1	Acceleration of the center of gravity in the x-direction (m/s^2)
A2	Acceleration of the center of gravity in the y-direction (m/s^2)
A3	Acceleration of the center of gravity in the z-direction (m/s^2)
A4	Roll angular acceleration (Euler angle) (◦ /s^2)
A5	Pitch angular acceleration (Euler angle) (◦ /s^2)
A6	Pitch angular acceleration (Euler angle) (◦ /s^2)

The diagrams presented below have been generated and analyzed through programming, specifically using Python (Hetland, 2017; Pajankar, 2022).

5.4.1 Regular waves – Following seas

Below are presented the time series of the free surface elevation, positions, velocities and accelerations of the CG for regular following waves, with heading 0°.

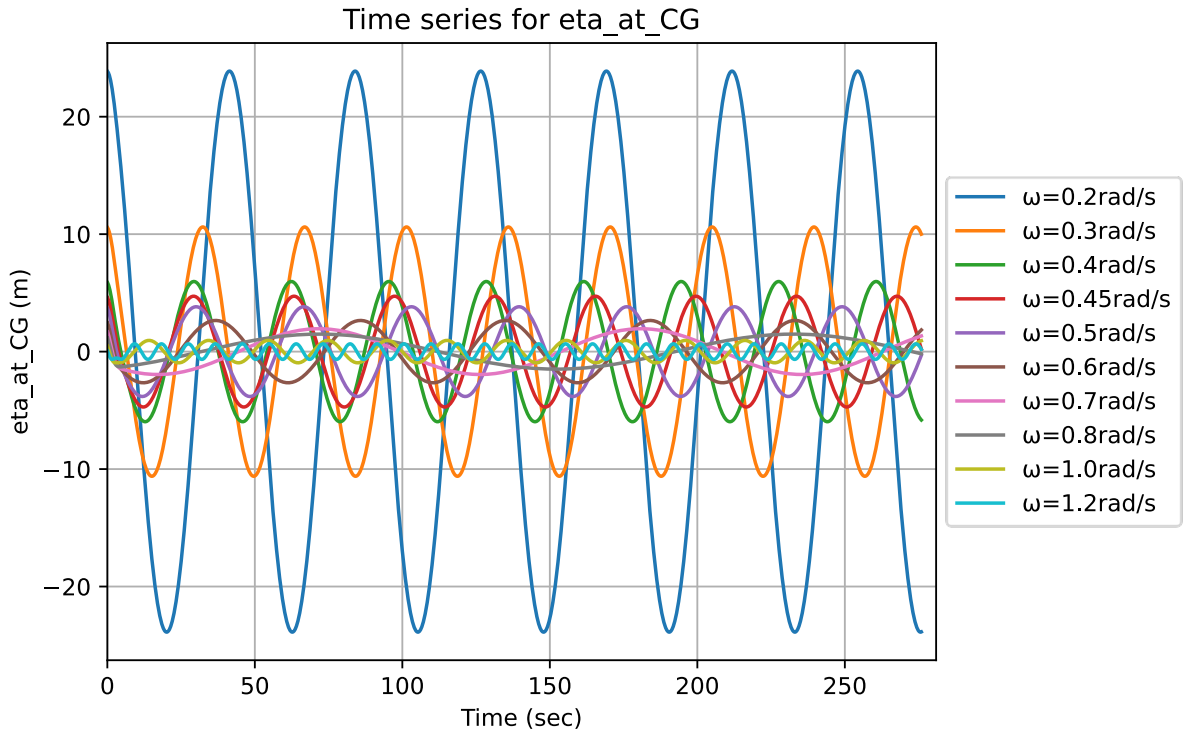

Figure 5.1: Time series of CG free surface elevation in regular following waves.

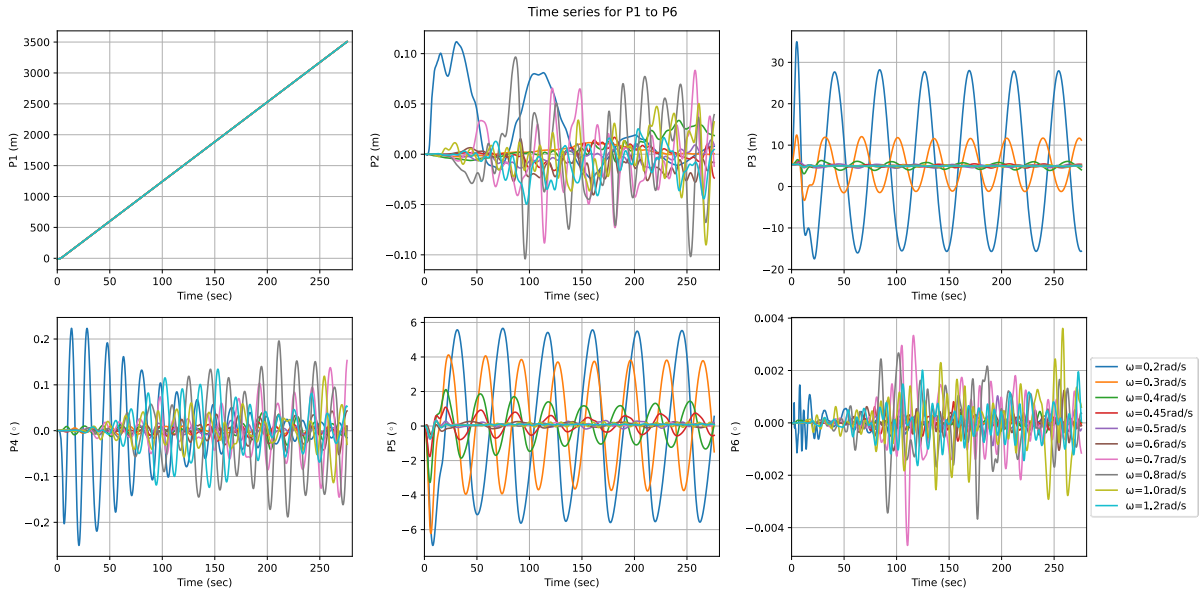

Figure 5.2: Time series of CG positions in regular following waves.

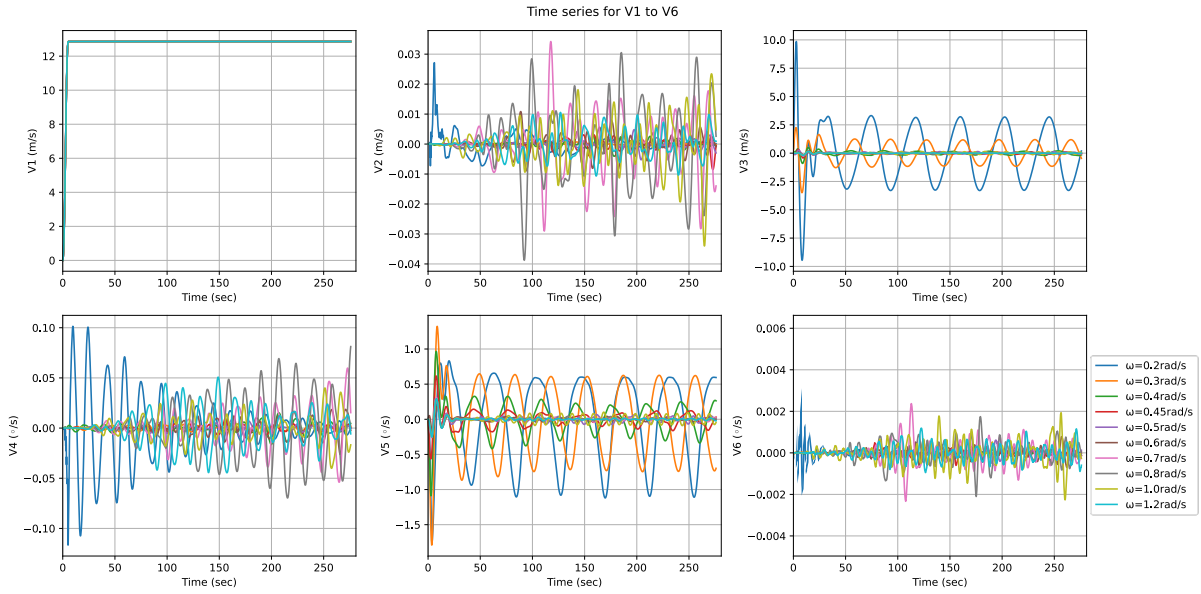

Figure 5.3: Time series of CG velocities in regular following waves.

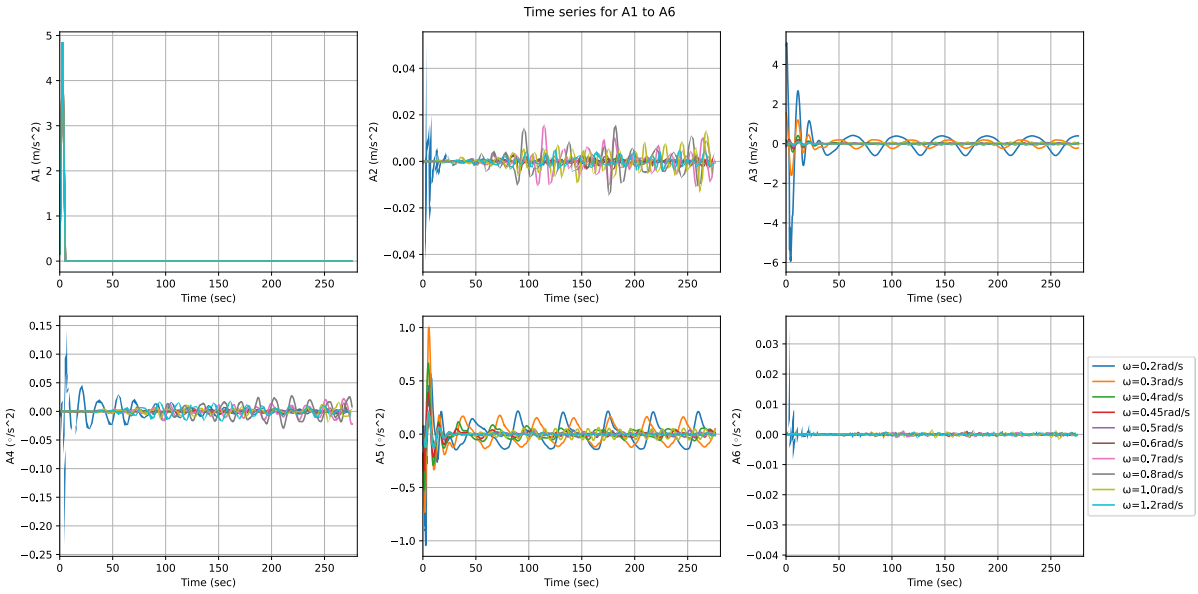

Figure 5.4: Time series of CG accelerations in regular following waves.

It is observed that the positions on the y-axis (P2) and roll angle (P4) develop small oscillations, while the yaw angles (P6) are negligible, since the waves are following and thus significant lateral responses are not generated. On the other hand, significant values are observed for positions on the z-axis (P3) and pitch angles (P5), which graphically resemble the shape of the free surface elevation, while yaw angles are practically zero. Additionally, the time series of velocities and accelerations at the CG match those of the positions and angles, confirming the validity of the results, while being periodical during time, as indicated when solver converges.

5.4.2 Regular waves – Quartering seas

Below are presented the time series of the free surface elevation, positions, velocities and accelerations of the CG for regular quartering waves, with heading 30°.

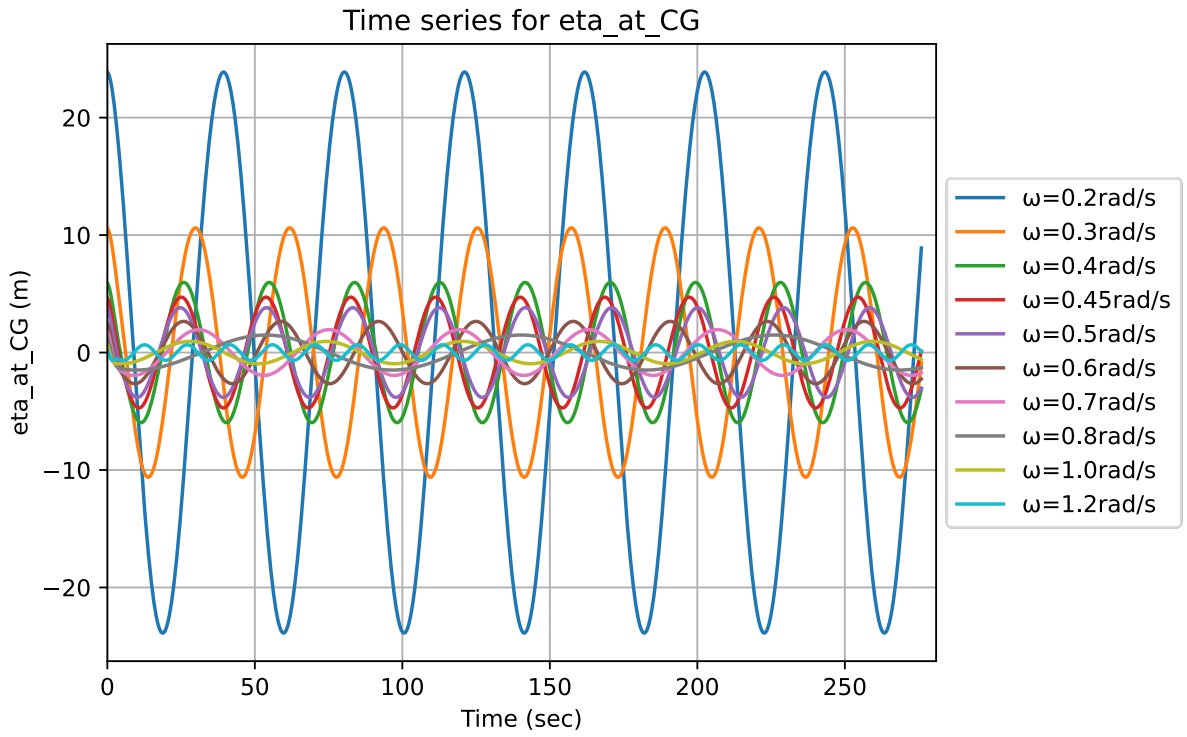

Figure 5.5: Time series of CG free surface elevation in regular quartering waves.

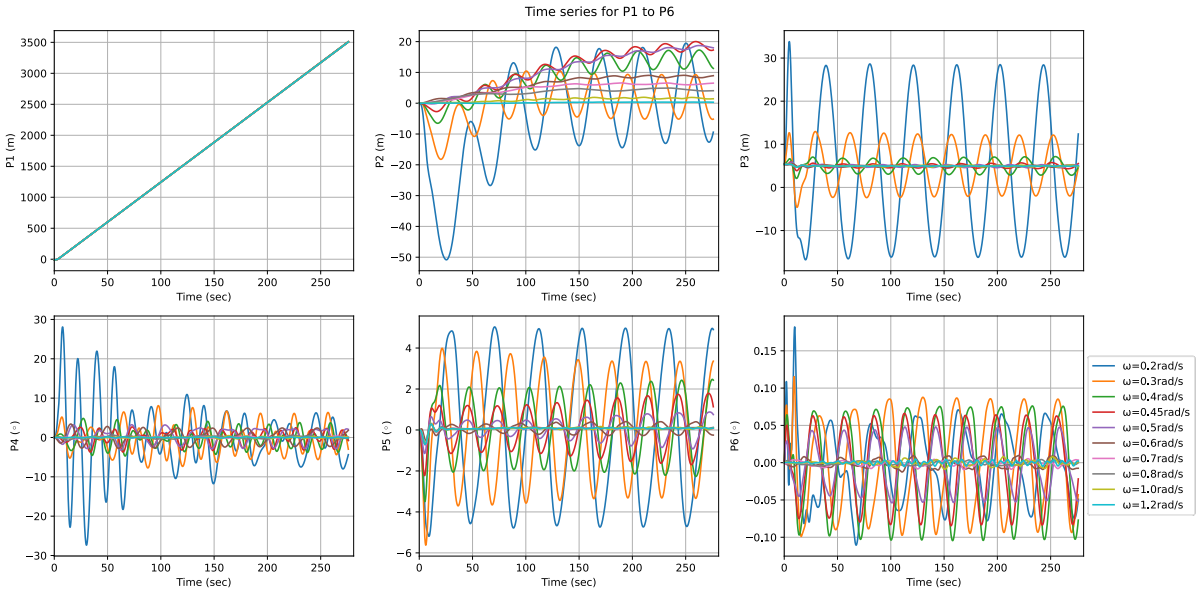

Figure 5.6: Time series of CG positions in regular quartering waves.

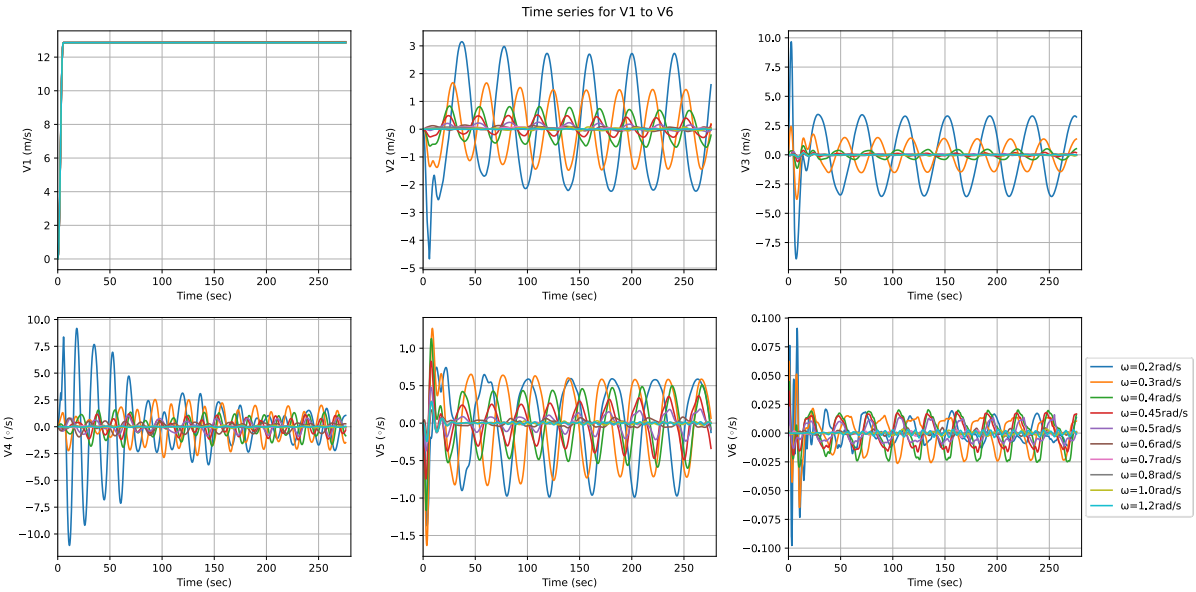

Figure 5.7: Time series of CG velocities in regular quartering waves.

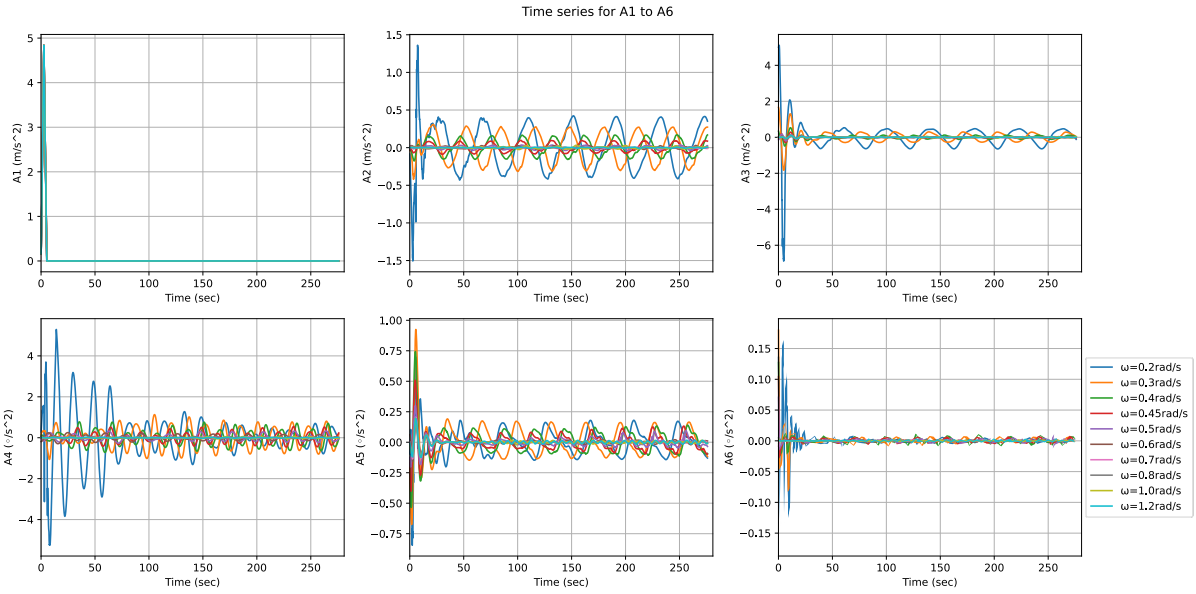

Figure 5.8: Time series of CG accelerations in regular quartering waves.

It is observed that the time series of positions in the z-axis (P3) and the pitch angles (P5) continue to exhibit significant oscillations, but this time for waves heading 30°, significant effects are displayed on the positions on the y-axis (P2) and the roll angles (P4), while yaw angles (P6) are also increased, compared to the respective results of following waves. These phenomena occur because the quartering waves, additionally, affect the sway and roll responses. Also, velocities and accelerations at these positions and angles demonstrate interesting patterns.

5.4.3 Regular waves – Beam seas

Below are presented the time series of the free surface elevation, positions, velocities and accelerations of the CG for regular beam waves, with heading 90°.

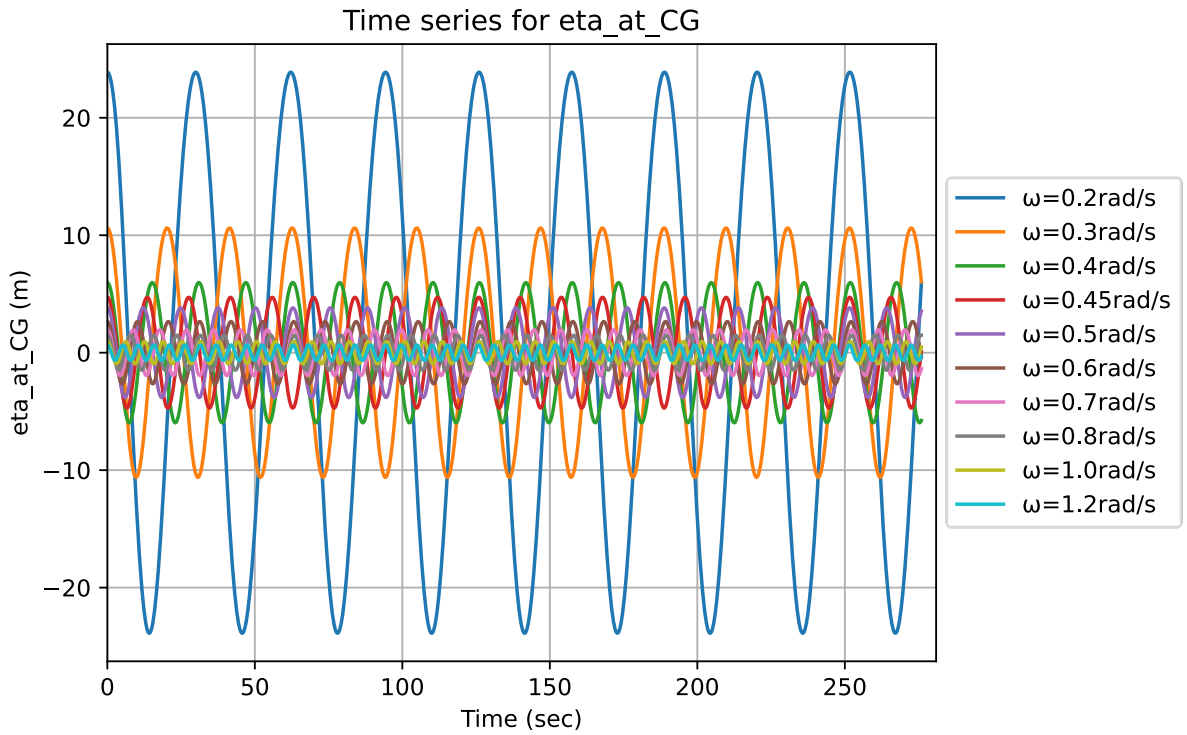

Figure 5.9: Time series of CG free surface elevation in regular beam waves.

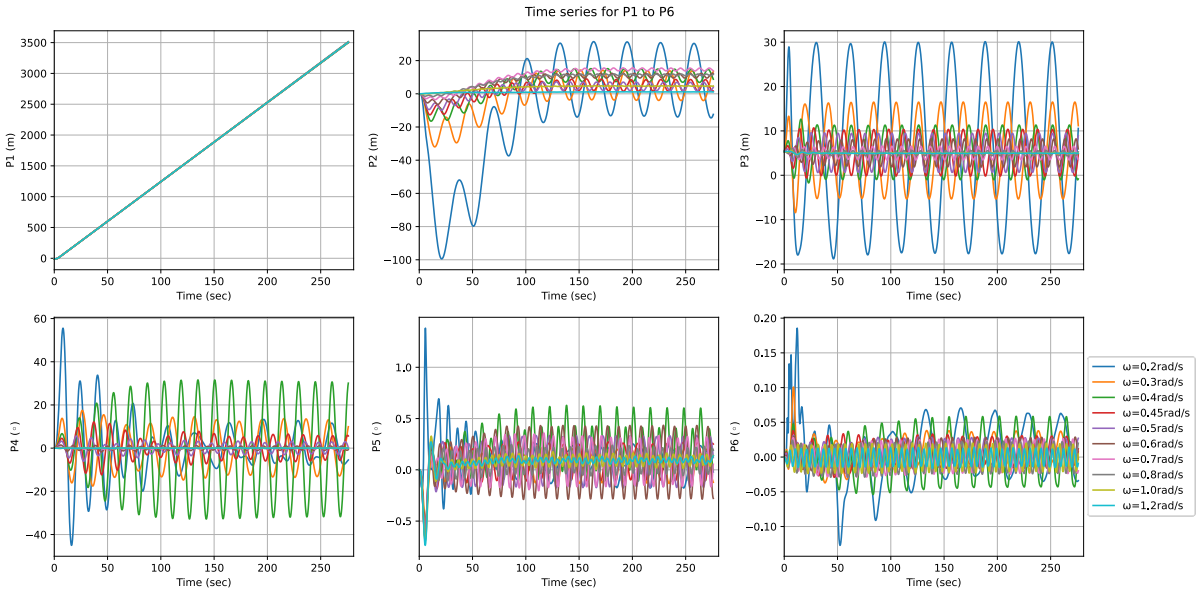

Figure 5.10: Time series of CG positions in regular beam waves.

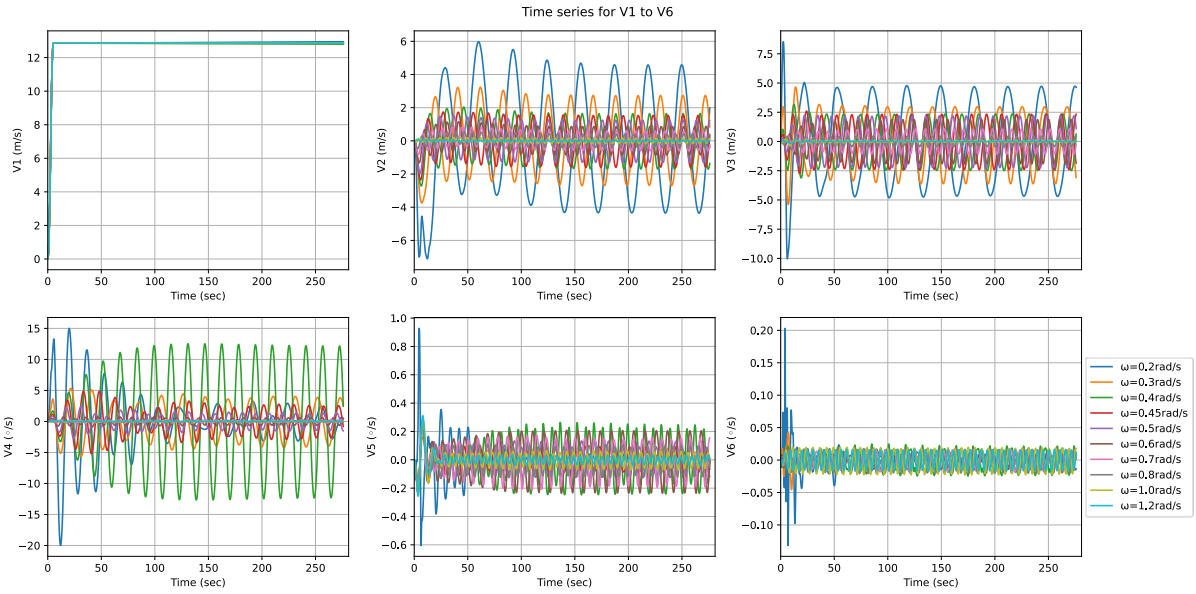

Figure 5.11: Time series of CG velocities in regular beam waves.

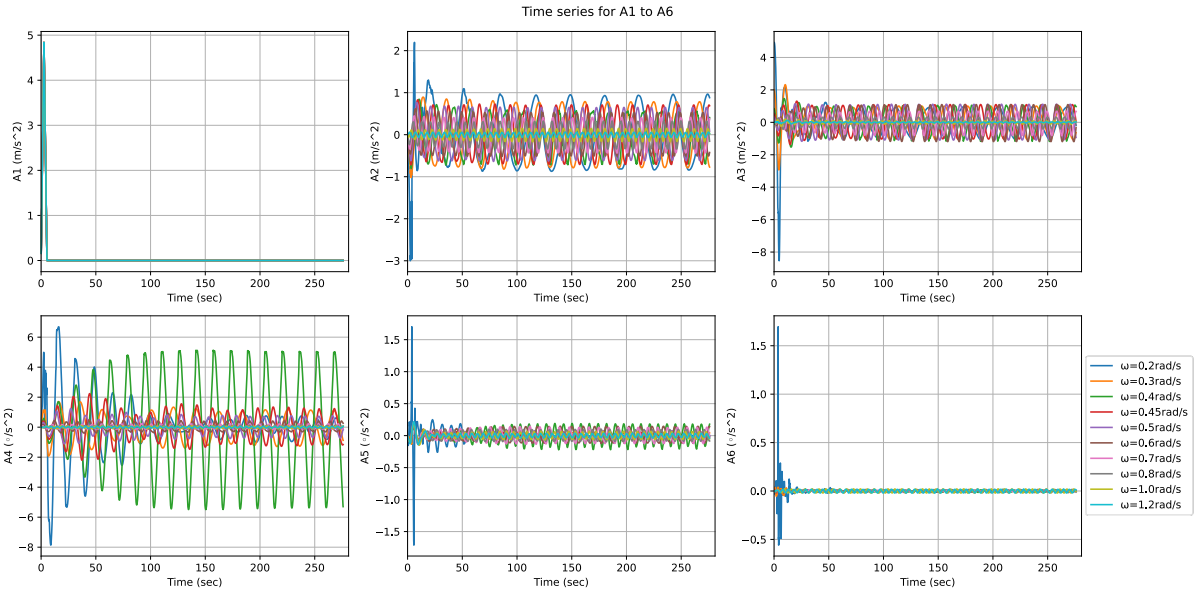

Figure 5.12: Time series of CG accelerations in regular beam waves.

It is observed that beam waves strongly influence all positions and angles, particularly the positions in the y-axis (P2) and z-axis (P3) and the roll angles (P4). More specifically, positions in y-axis (P2) present notable oscillations until convergence, especially for small wave frequencies, where ship "moves" along with waves, and beam seas are highly affecting responses in y-axis. Correspondingly, the velocities and accelerations of these positions and angles are important, exhibiting considerable harmony sequence as they evolve over time. Also, it may be worth pointing out that the highest values of roll angles occur at the wave frequency of 0.4 rad/sec.

5.4.4 Regular waves – Heading seas

Below are presented the time series of the free surface elevation, positions, velocities and accelerations of the CG for regular heading waves, with heading 180°.

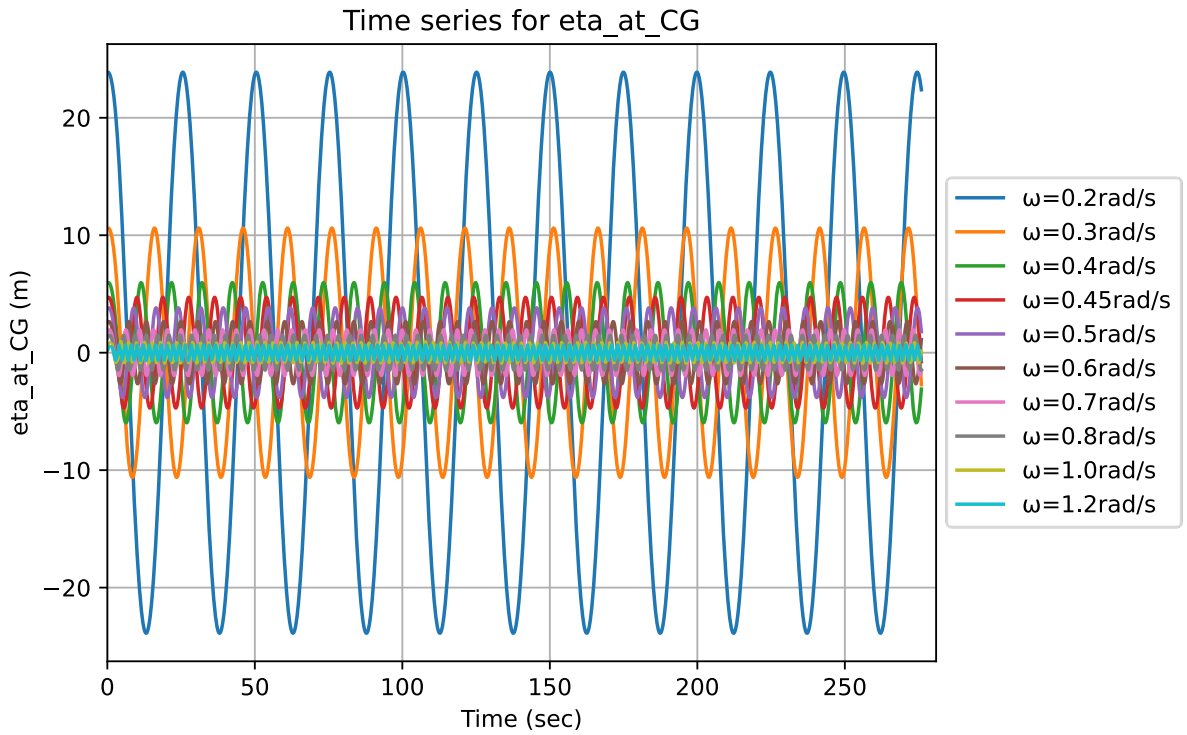

Figure 5.13: Time series of CG free surface elevation in regular heading waves.

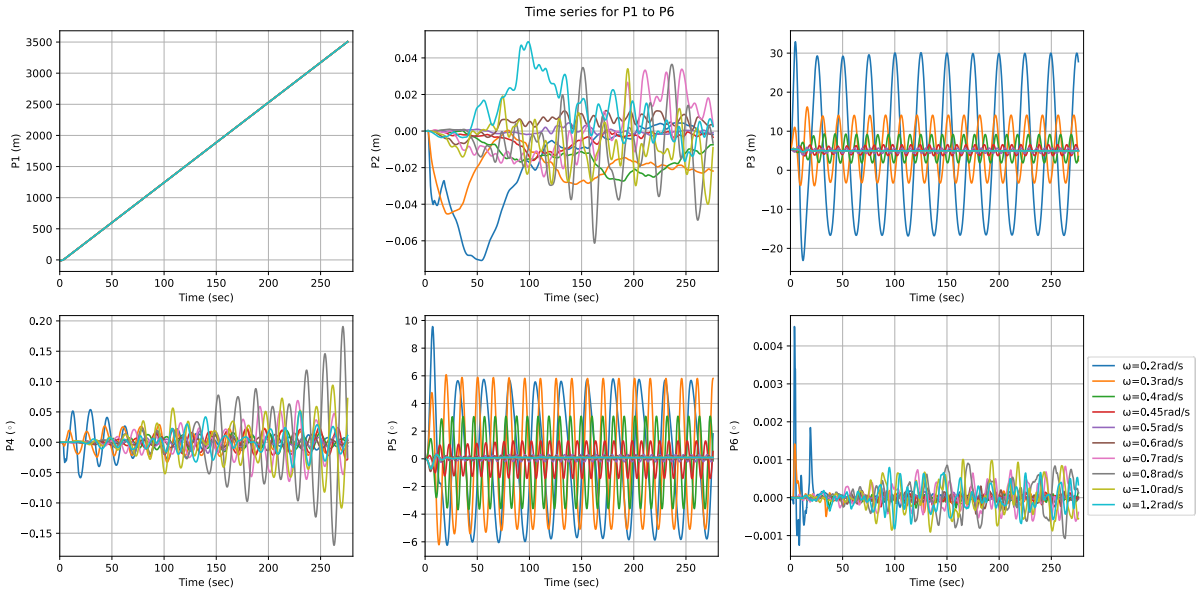

Figure 5.14: Time series of CG positions in regular heading waves.

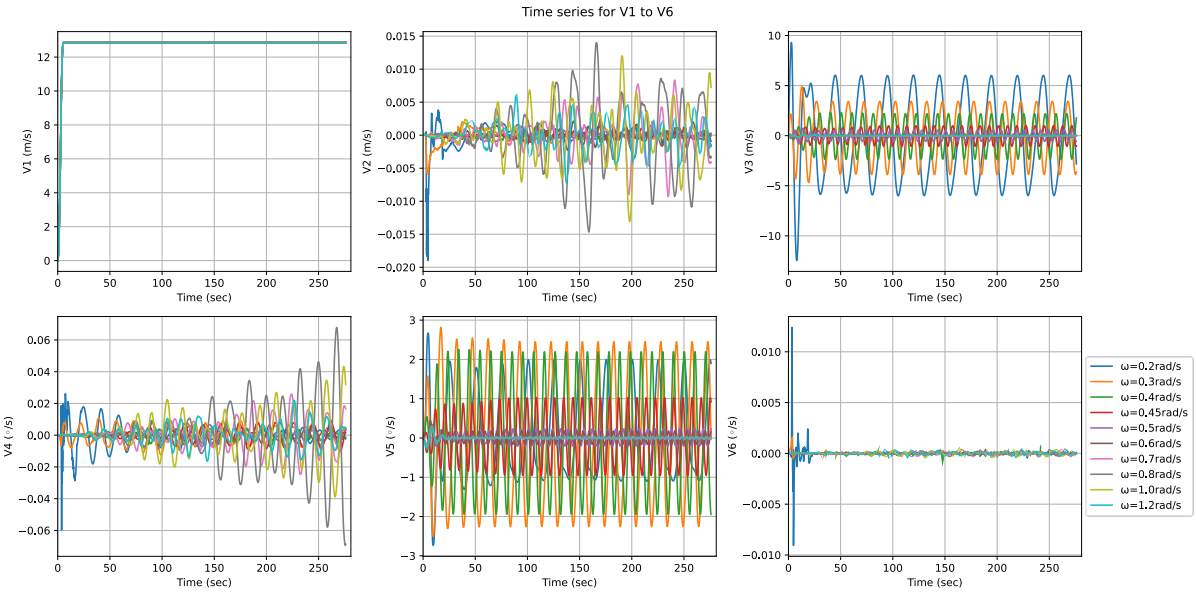

Figure 5.15: Time series of CG velocities in regular heading waves.

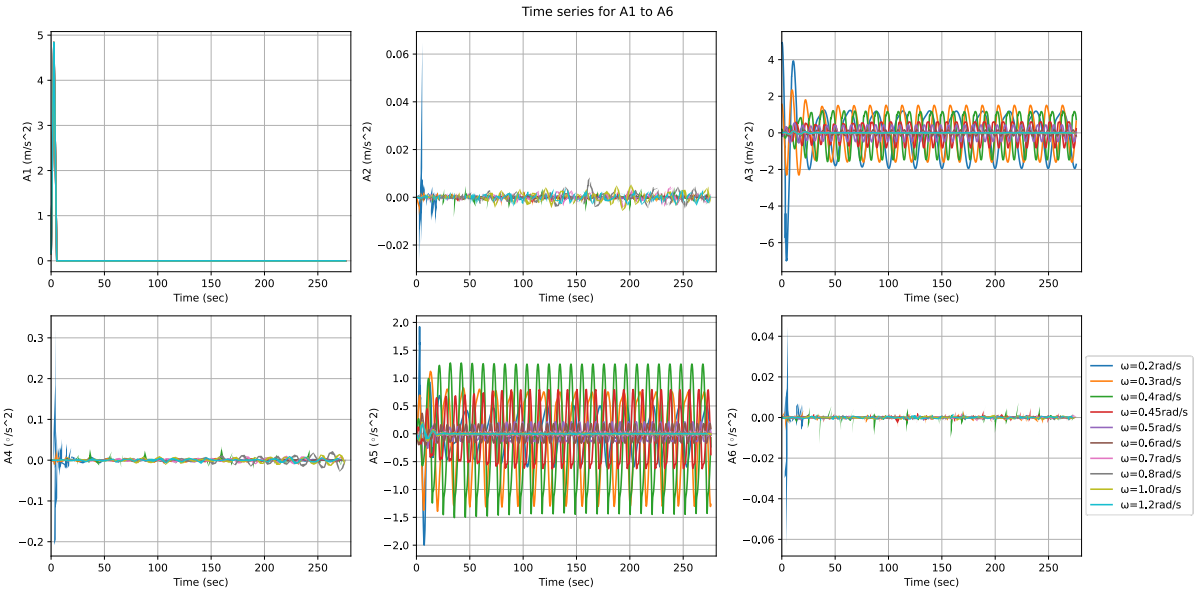

Figure 5.16: Time series of CG accelerations in regular heading waves.

It is observed that the results of the time series for heading waves resemble those of following waves, with only the positions in the z-axis (P3) and the pitch angles (P5) being significantly affected. Furthermore, the amplitudes of these positions and angles follow the amplitudes of the free surface, for the respective wave frequencies. Similarly, the same applies to the time series of velocities and responses.

Some significant general observations and comments for the time series plots are:

1. The above diagrams clearly indicate that for regular waves (harmonic), both the time series and responses will be harmonic, verifying the linear theory. A low-frequency wave implies a wave of large amplitude and period, while conversely, a high-frequency wave has a small amplitude and period. This is evident in all the presented time series, based on the imported small steepness condition of this case study.
2. The entire oscillations of both the free surface and the positions, velocities and accelerations (P2, V2, A2, P4, V4, A4) are significant in quartering seas and even more bold in beam seas compared to following and heading seas because the waves impact on the hull at an angle, resulting in more frequent responses within the same time frame.
3. The time series of positions, velocities and accelerations on the x-axis (P1, V1, A1) suggest that the vessel starts from zero velocity and as waves approach, it quickly reaches service speed, which is maintained steady for the rest of the simulation, as it converges. This verifies the conditions defined in the software and justifies the initial noise presented in these time series plots.
4. At the beginning of each diagram, an irregular/jumpy distribution is observed for all results of positions, velocities and accelerations. This is because the vessel has not yet reached its steady operational speed and the simulation is evolving. This is graphically depicted as noise. Subsequently, when analyzing the results, this noise at the beginning of the time series will be neglected.
5. In summary, it is worth pointing out that, as reflected the time series graphs, heave and pitch motions are primarily influenced by following and head waves, whereas sway and roll motions are more affected by quartering and beam waves.

5.5 RAOs and Phases

The following graphics depict the RAOs (Response Amplitude Operators) of the six motions in ship's CG, for all wave headings examined.

Table 5.4: RAOs descriptions.

Title	Description
RAO1	Surge amplitude / wave amplitude (-)

RAO2	Sway amplitude / wave amplitude (-)
RAO3	Heave amplitude / wave amplitude (-)
RAO4	Roll amplitude / (wave number * wave amplitude) (-)
RAO5	Pitch amplitude / (wave number * wave amplitude) (-)
RAO6	Yaw amplitude / (wave number * wave amplitude) (-)
PHASE 1	Surge phase angle relative incident wave at CG (°)
PHASE 2	Sway phase angle relative incident wave at CG (°)
PHASE 3	Heave phase angle relative incident wave at CG (°)
PHASE 4	Roll phase angle relative incident wave at CG (°)
PHASE 5	Pitch phase angle relative incident wave at CG (°)
PHASE 6	Yaw phase angle relative incident wave at CG (°)

Below the diagrams of the RAOs and phases are presented, with respect to the wave frequency, for each of the headings.

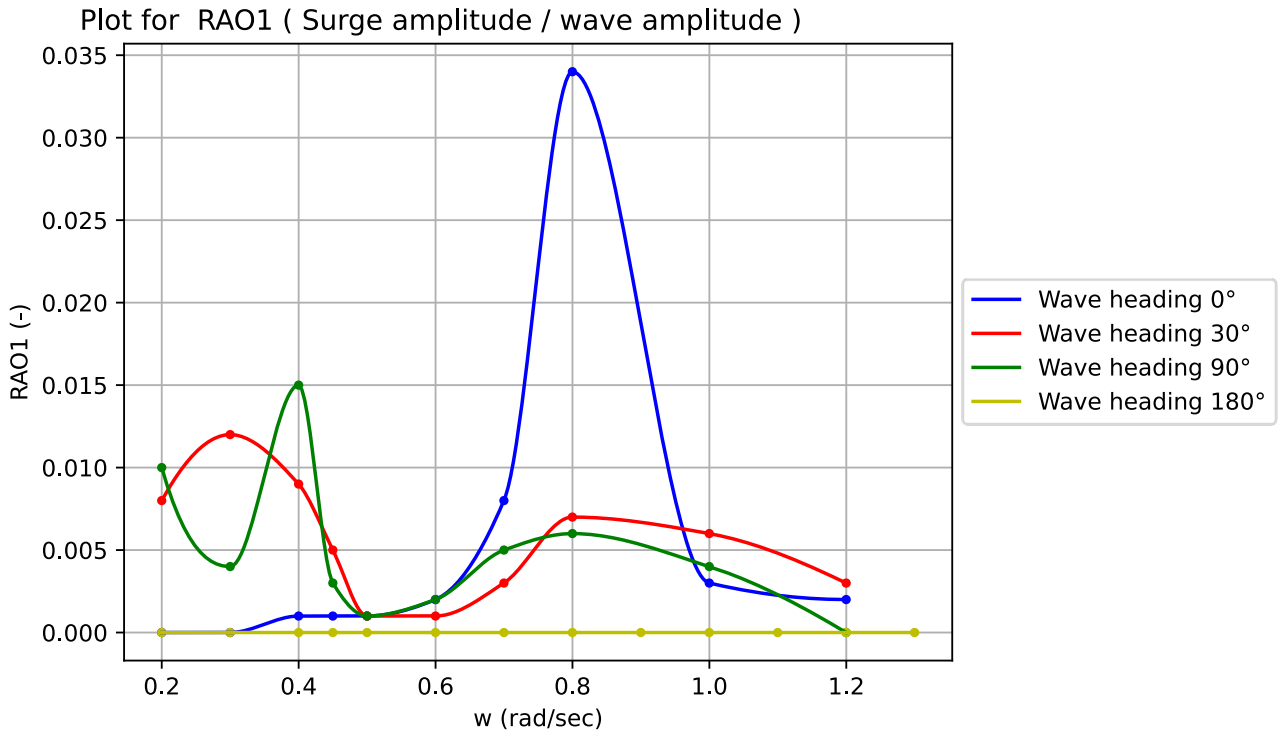

Figure 5.17: Surge RAOs with respect to wave frequency.

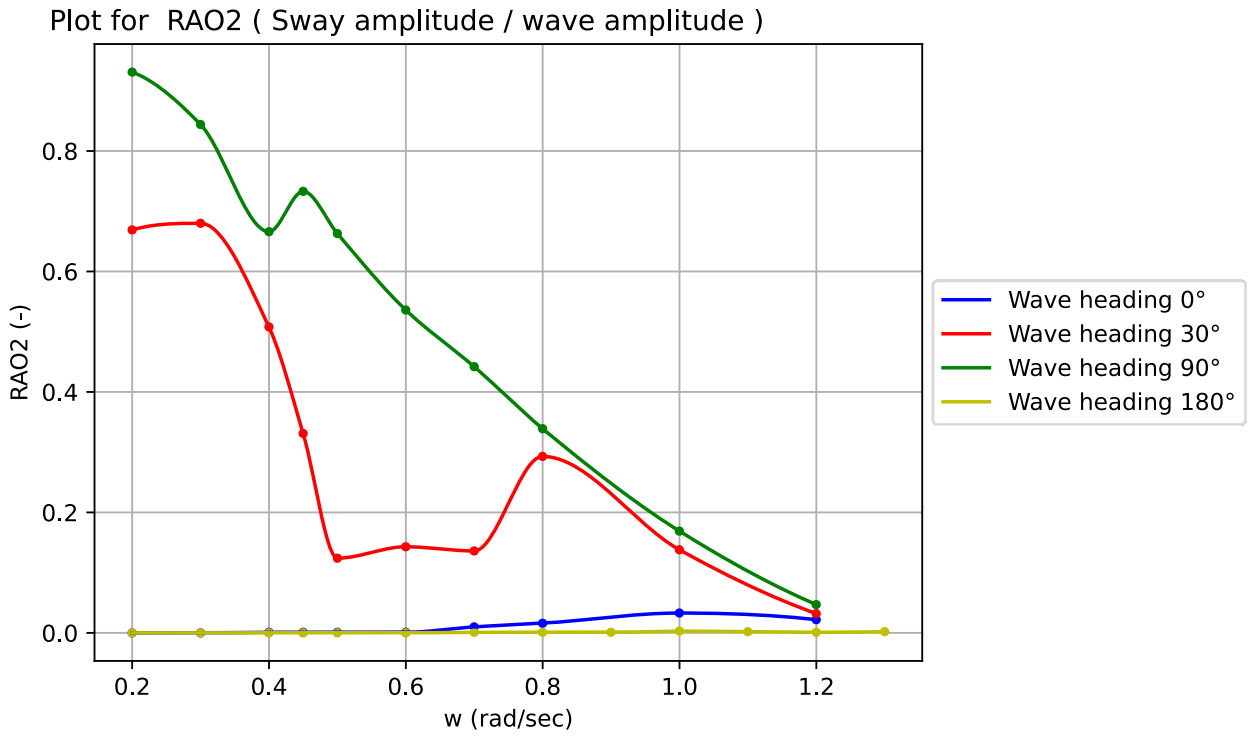

Figure 5.18: Sway RAOs with respect to wave frequency.

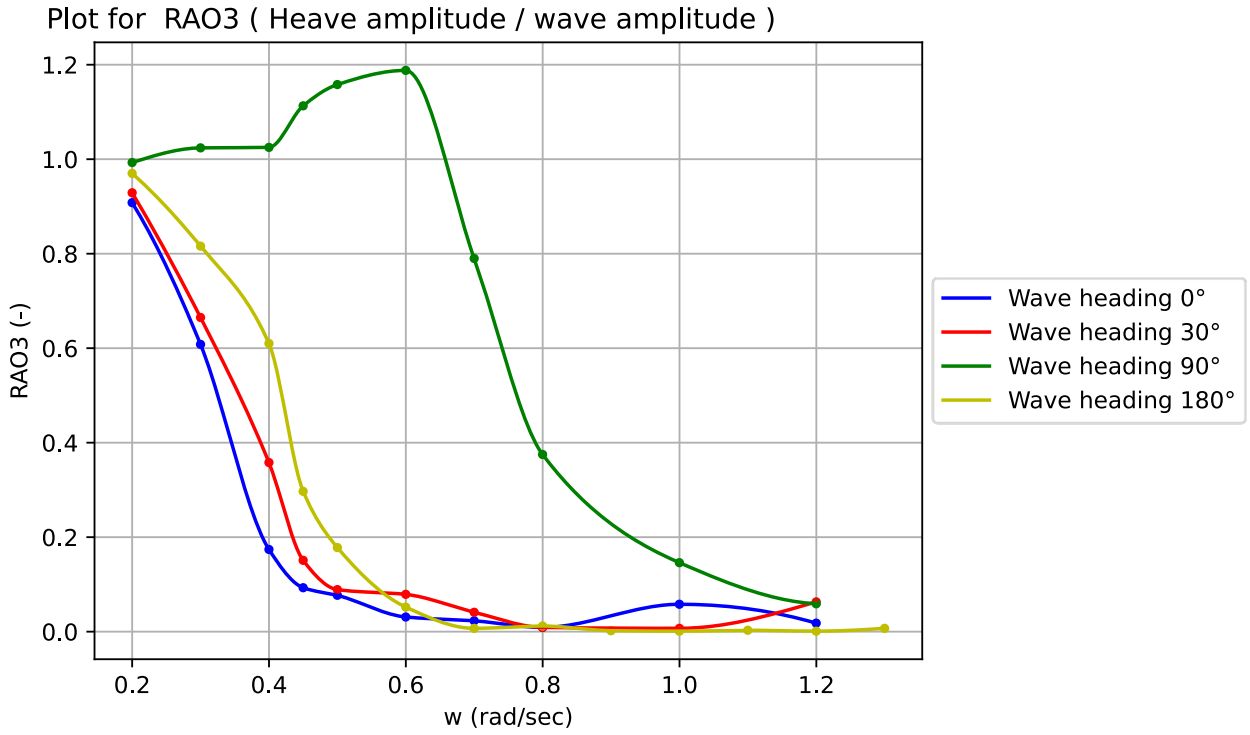

Figure 5.19: Heave RAOs with respect to wave frequency.

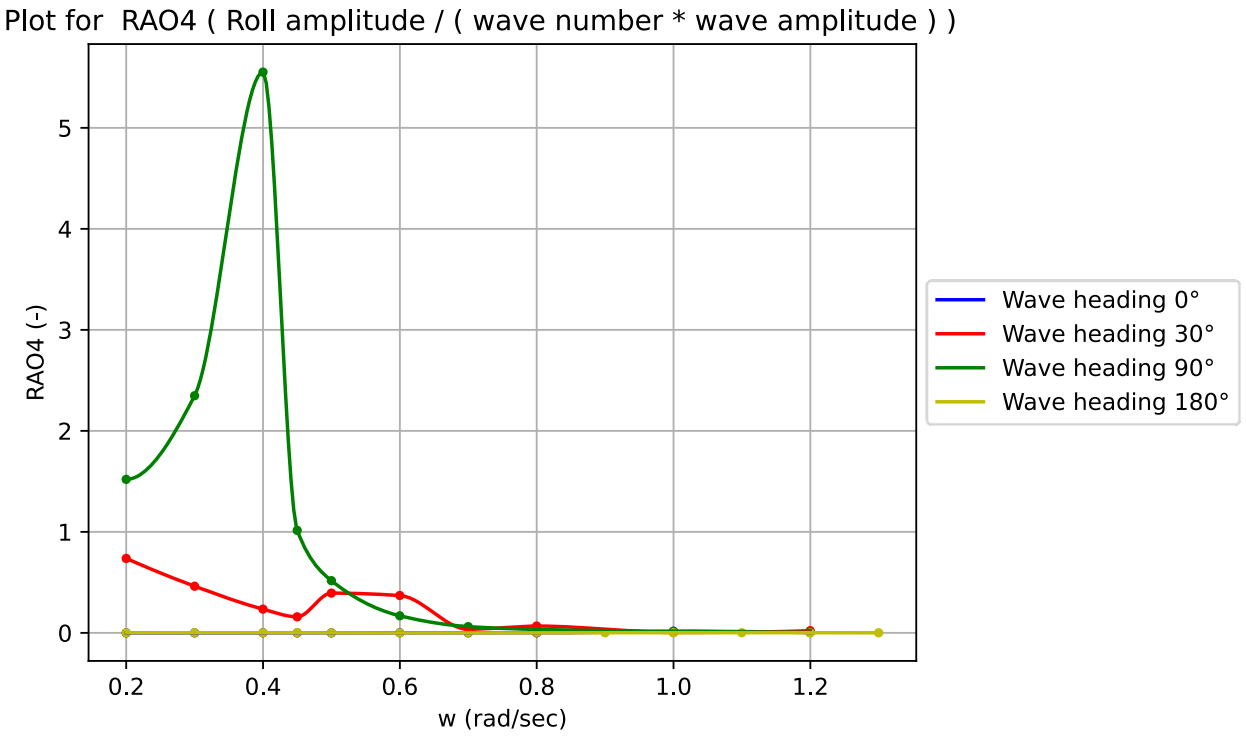

Figure 5.20: Roll RAOs with respect to wave frequency.

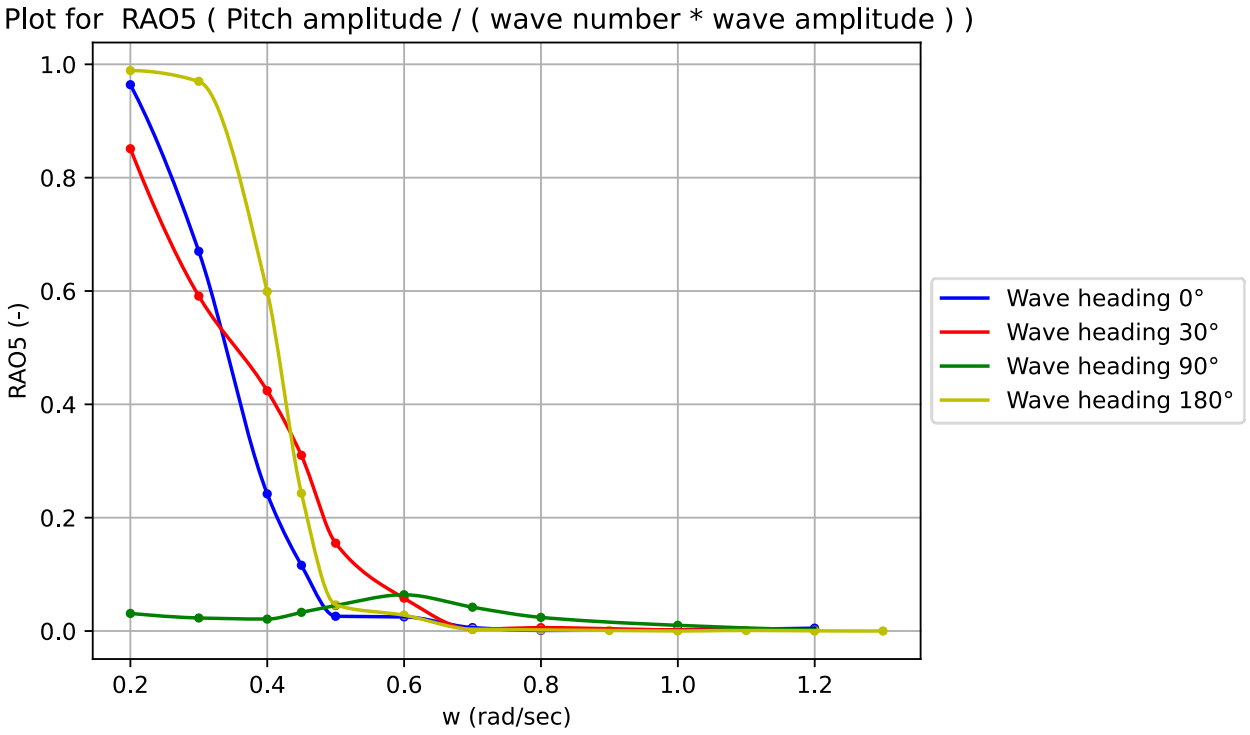

Figure 5.21: Pitch RAOs with respect to wave frequency.

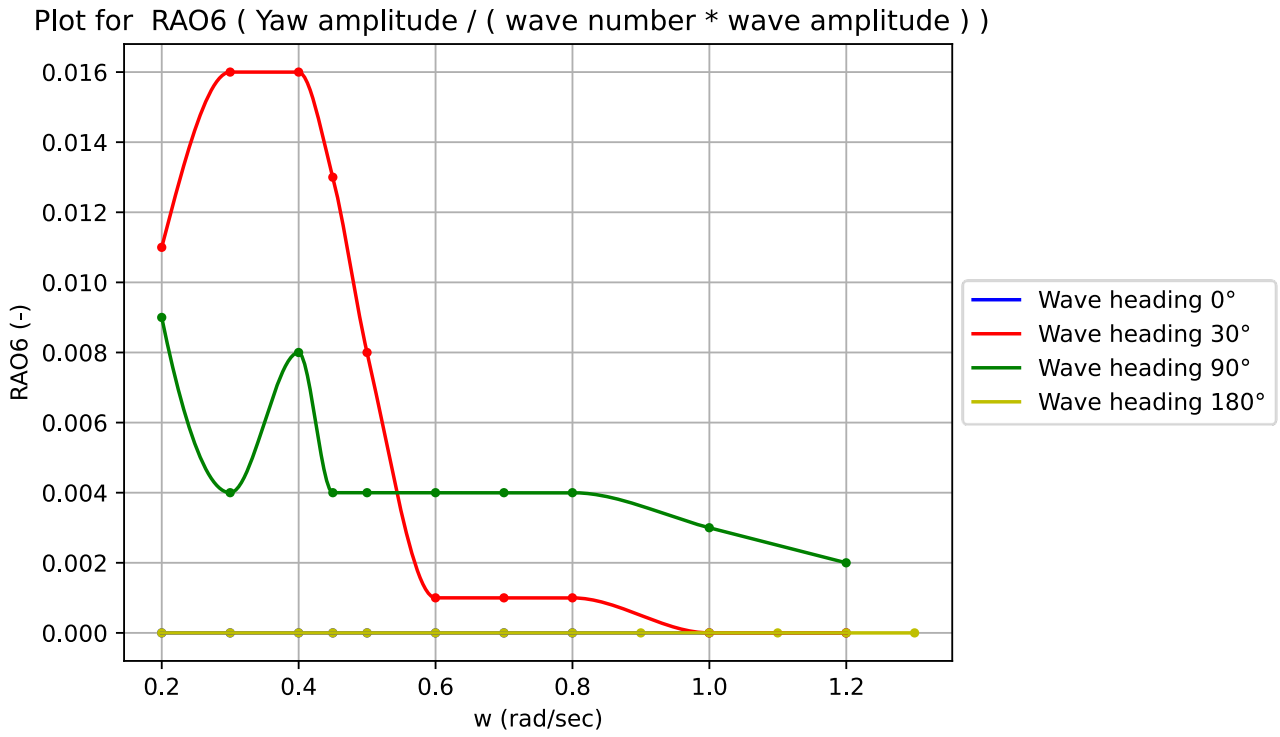

Figure 5.22: Yaw RAOs with respect to wave frequency.

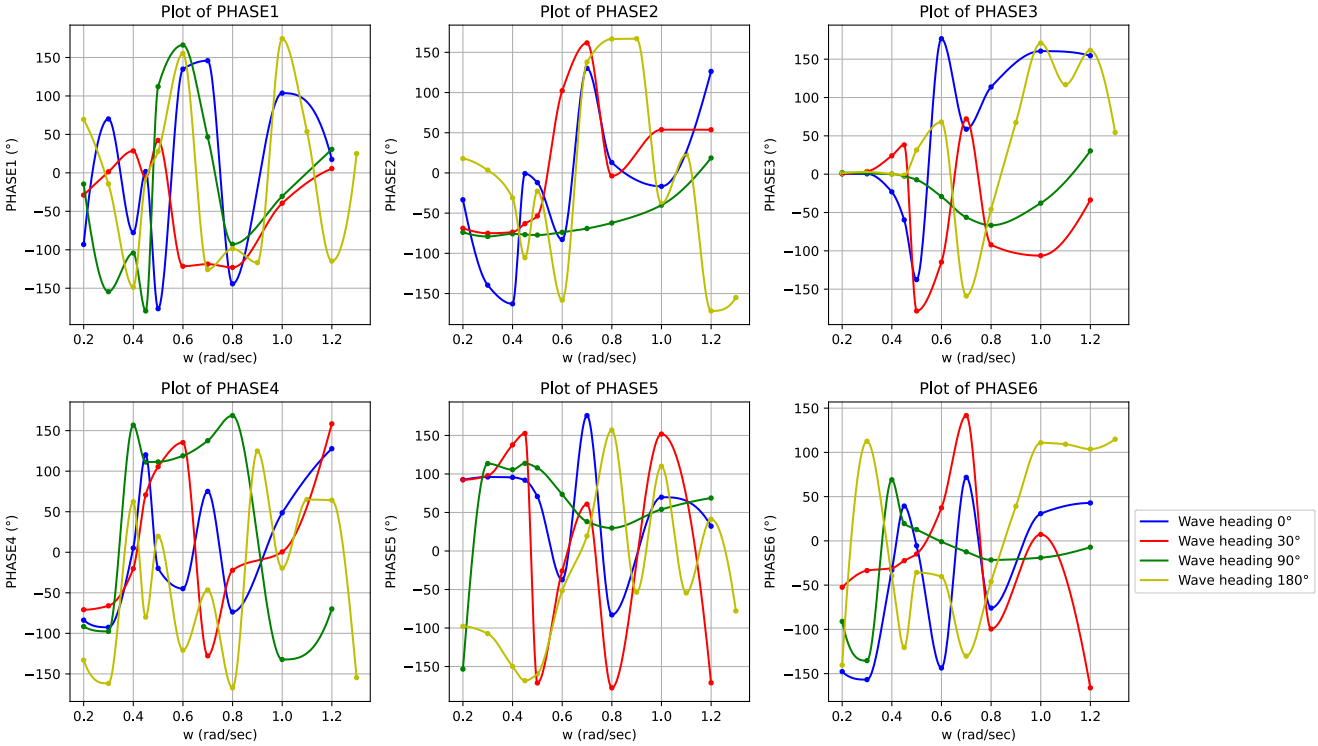

Figure 5.23: Motions phases with respect to wave frequency.

Below the diagrams of the RAOs and phases are presented, with respect to the dimensionless wavelength ratio (λ/Lpp) of wavelength to ship's length between perpendiculars, for each of the headings.

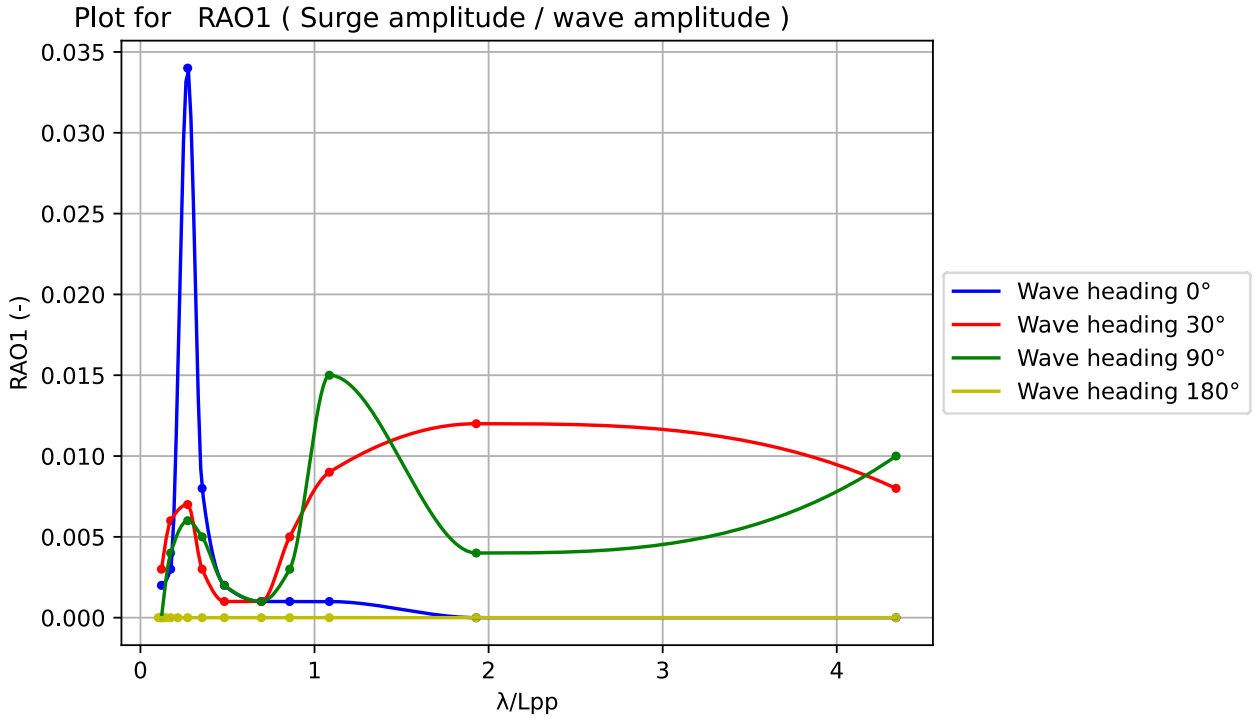

Figure 5.24: Surge RAOs with respect to dimensionless wavelength.

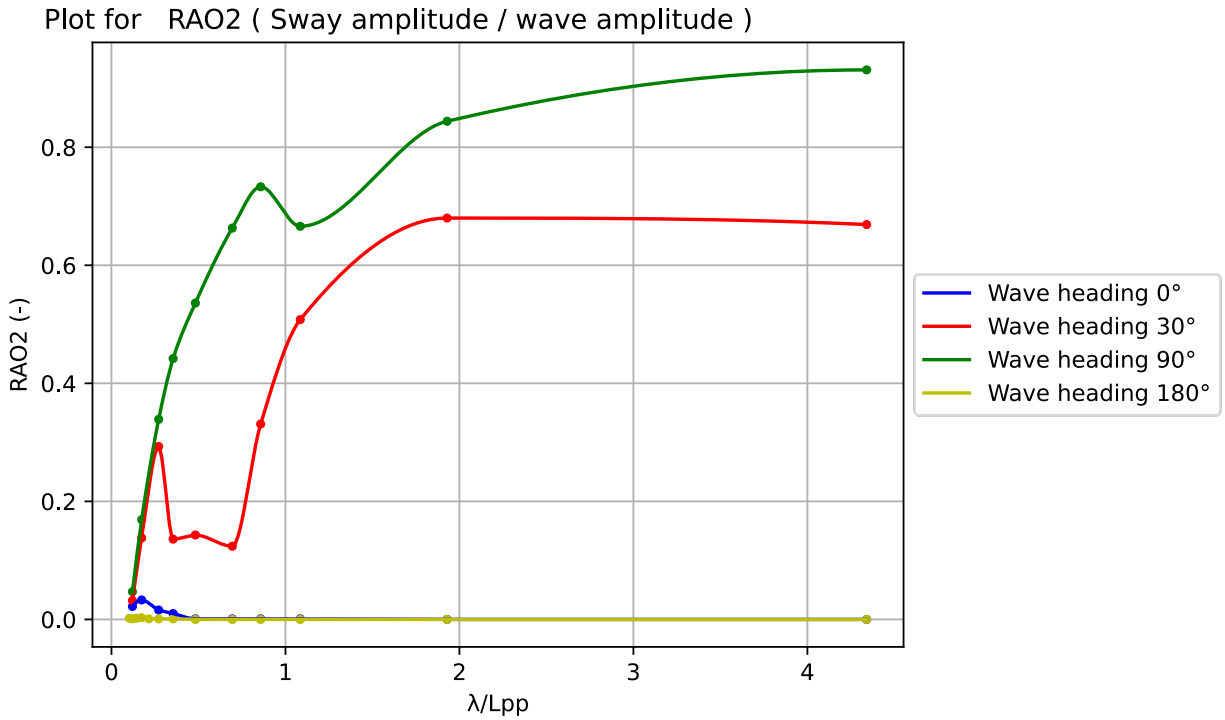

Figure 5.25: Sway RAOs with respect to dimensionless wavelength.

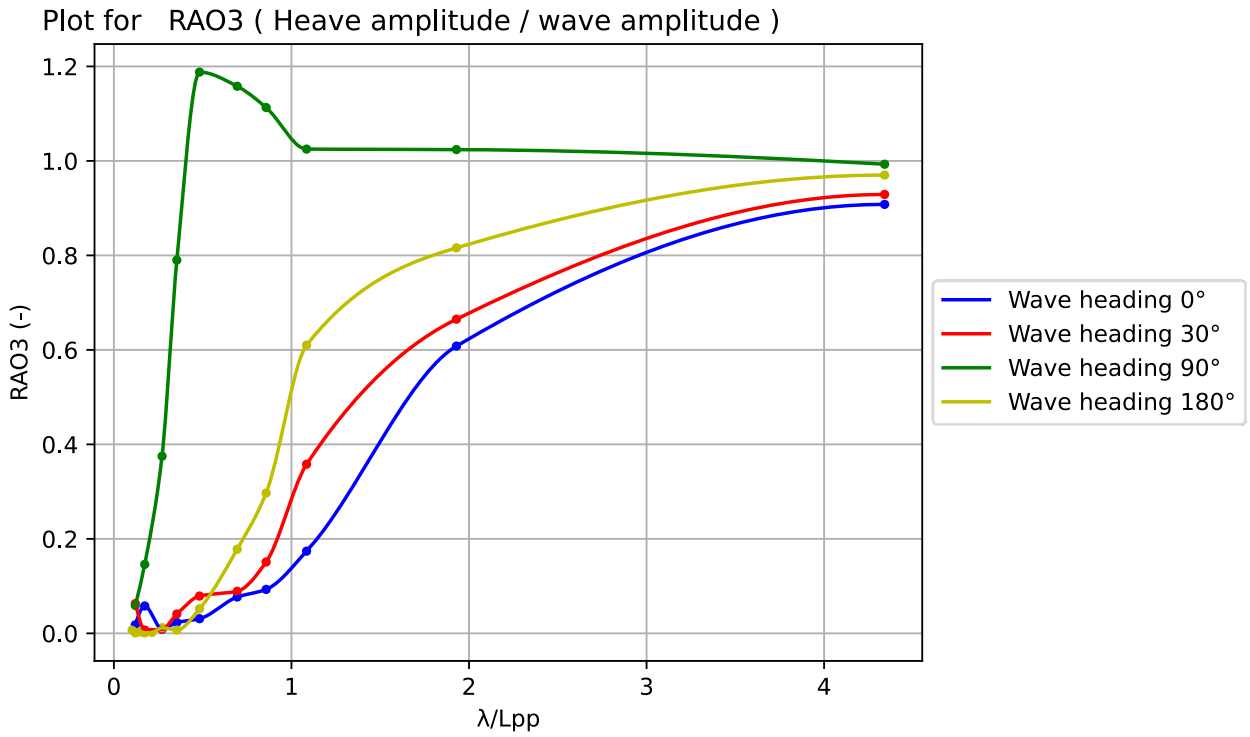

Figure 5.26: Heave RAOs with respect to dimensionless wavelength.

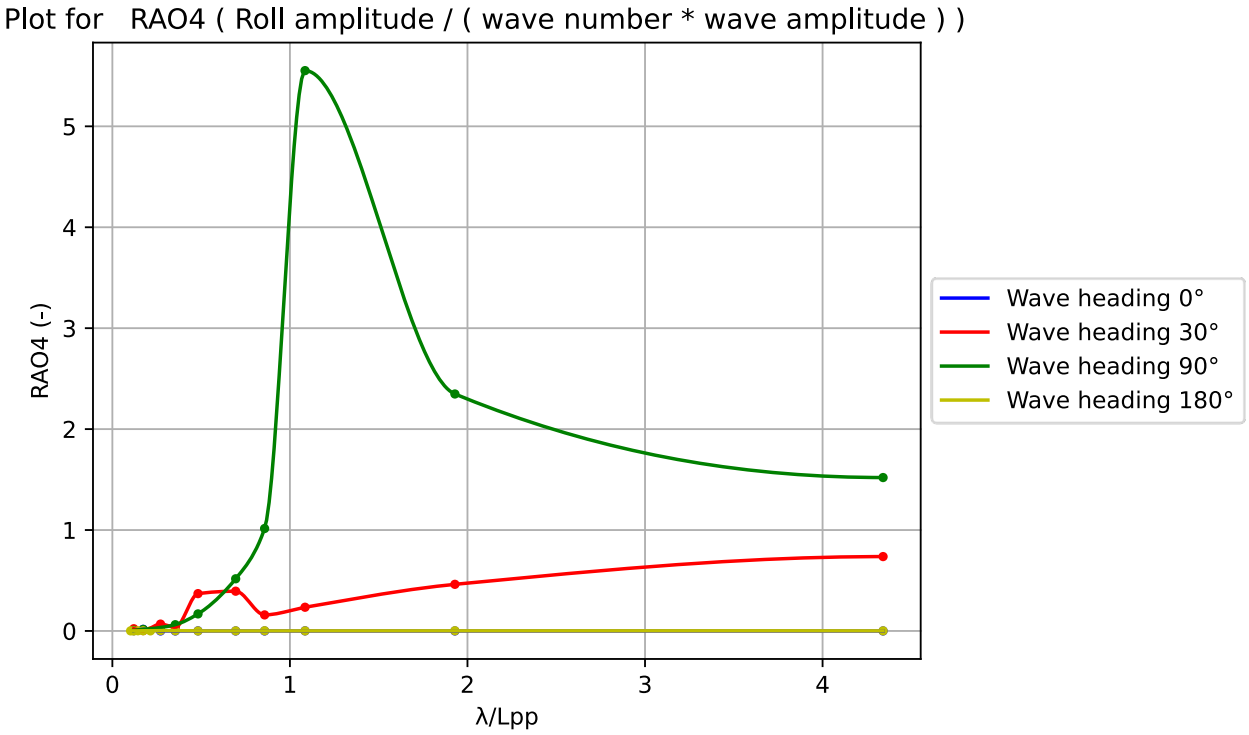

Figure 5.27: Roll RAOs with respect to dimensionless wavelength.

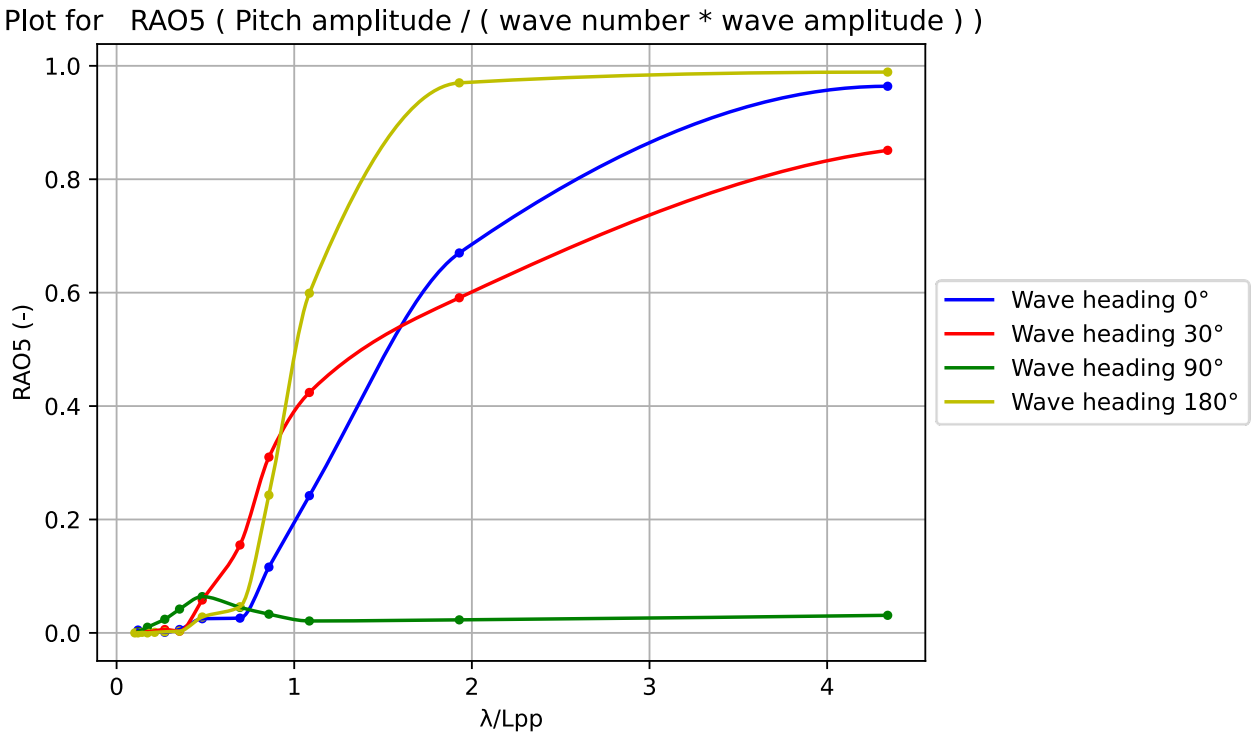

Figure 5.28: Pitch RAOs with respect to dimensionless wav length.

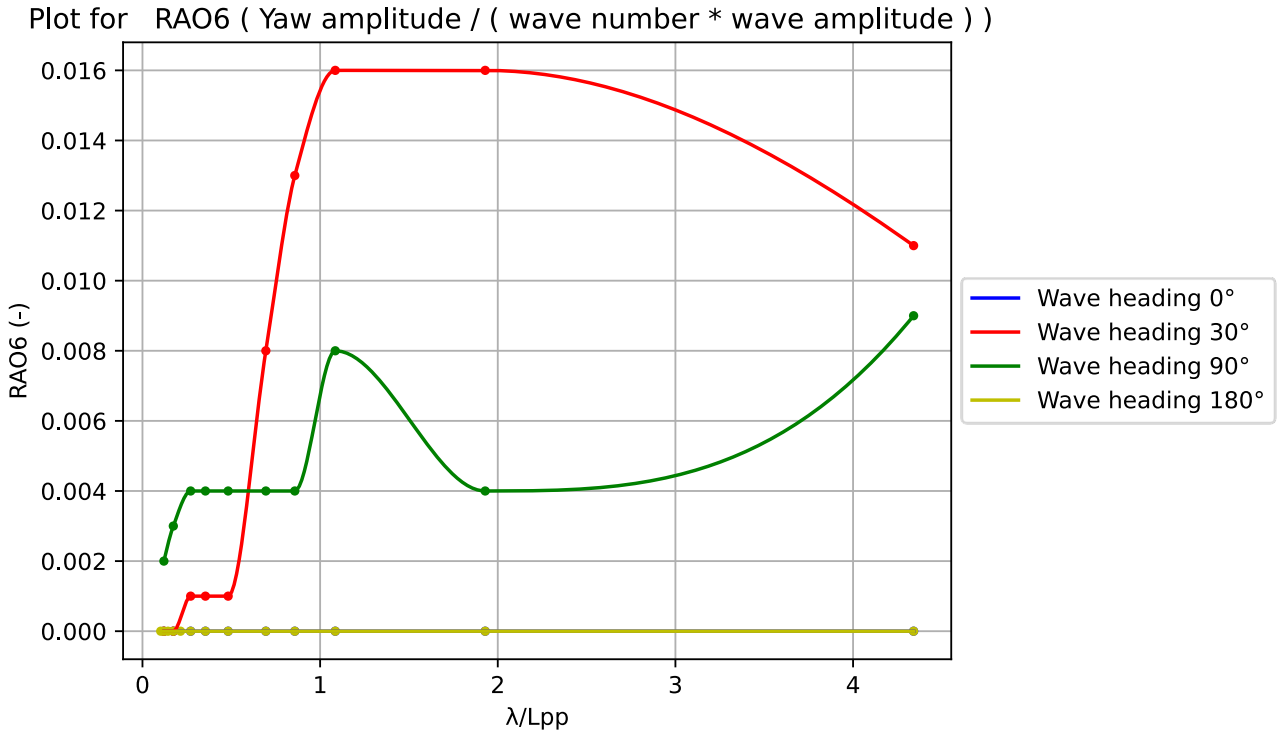

Figure 5.29: Yaw RAOs with respect to dimensionless wavelength.

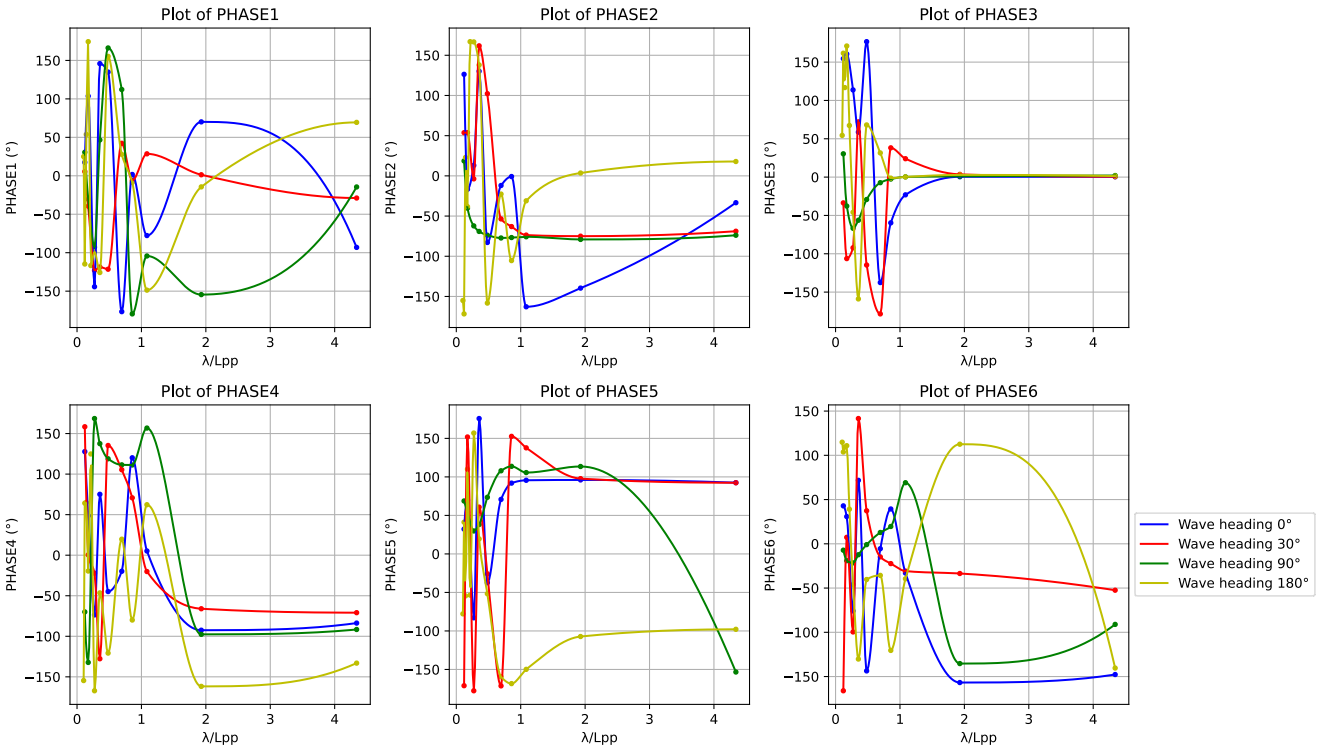

Figure 5.30: Motions phases with respect to dimensionless wavelength.

Some significant general observations and comments for the time series plots are:

1. Initially, it should be reminded that the dimensioned RAOs represent the ratio of response amplitude to wave amplitude. The RAOs presented here concern the responses at the ship's center of gravity (CG), in regular waves.

2. For regular waves with constant steepness, as in this case study, it indicates that large value of ratio of dimensionless wavelength corresponds to small wave frequency, where the wavelengths are much greater than that of the ship's length L_{PP}. This is why there are differences in the graphical representations with respect to wave frequency and dimensionless wavelength, in which the RAO results remain common for both cases.

3. The RAO in surge (RAO1) (Figure 5.17, Figure 5.24) could be considered negligible, as it does not show significant results. The surge RAO diagram, as a function of wave frequency, was generated and presented solely for plenitude in the RAOs representation in all motions. As previously mentioned, in the simulation conditions, surge was considered constant, so as to maintain the vessel's steady speed. Therefore, it is verified by the diagram that the surge RAO is negligible.

4. From the sway RAO diagram (RAO2) (Figure 5.18, Figure 5.25) the corresponding results from the time series are validated, showing significant values for regular waves in quartering and beam seas, while being negligible for following and heading seas. For low frequency values ($0.2 - 0.5\ rad/sec$), sway RAO values appear to be the highest, which is reasonable, since at these wave frequencies have significant height and length, which practically means that the ship moves along with the wave and thus is significantly affected by its amplitude.

5. From the heave RAO diagram (RAO3) (Figure 5.19, Figure 5.26), it is observed that for beam seas, the RAOs differ from those of the other wave headings. It is thus certified that lateral wave headings strongly influence heave motion. The maximum value of the RAO heave for beam seas is approximately 1.2 and occurs at a frequency of approximately $0.6\ rad/sec$, where the wave has a characteristic wavelength of $171m$ and wave height $5m$. This is tenable, as this specific regular wave has half the length of the ship, making the situation risky. An important comment is that the heave RAOs are expected to start from a value greater than 1. In this case study, they start almost from unity, which is due to the minimum wave frequency of $0.2\ rad/sec$ limit. Overall, it is verified that the heave response for all wave directions starts from a maximum value and decreases as the wave frequency increases, following the principle that for low wave frequencies (large wave height and length), the ship moves along with the wave, while for high wave frequencies (small wave height and length), the ship remains essentially unaffected, almost like sailing in calm water conditions.

6. From the RAO roll diagram (RAO4) (Figure 5.20, Figure 5.27), it is evident that the roll motion is influenced only by beam seas, to a lesser extent by quartering seas and not at all by following and heading seas. Specifically, the maximum value of the RAO roll is recorded for a wave frequency of almost $0.4\ rad/sec$, with characteristics of wavelength $385m$ and wave height $12m$. This is entirely expected, as in this case, the wavelength approaches the length of the ship, representing the most unfavorable condition where resonance and extreme ship responses can occur.

7. The RAO pitch diagram (RAO5) (Figure 5.21, Figure 5.28) indicates agreement for following, quartering and heading seas, while for beam seas, the pitch is negligible. Similar to heave, the RAO pitch exhibits a maximum value close to unity and is significant at low wave frequencies.

8. The RAO yaw diagram (RAO6) (Figure 5.22, Figure 5.29) is equally unimportant to the RAO surge one, as the values and responses are minimal and nearly zero. When compared to the wave directions, there seems to be a small yaw response for quartering seas, then less for beam seas and finally negligible for following and heading seas.
9. The data points on the graphs are derived from the results of SHIPFLOW simulations, while the curves are smoothed using monotonic cubic spline interpolation. This interpolation method ensures that the values of new points are calculated utilizing monotonic cubic splines, preserving the order of the data. Also, it considers the intermediate values and the derivatives at the endpoints, ensuring smooth and accurate representation of the data.
10. Regarding the phases of the RAOs, they are characterized by intense randomness when the phenomena are actively evolving.

5.6 Resistance

Additionally, resistance was calculated for these conditions to determine the added resistance due to waves and the coefficient of added resistance. The added resistance due to waves was determined by the difference between the total resistance in waves and the total resistance in calm water. Subsequently, the coefficient of added resistance was calculated using the formula (Equation 2.66), which is validated both by research work (Chirosca et al., 2023) and by the manual of the SHIPFLOW software.

The calculated resistances and their descriptions are presented in the Table below.

Table 5.5: Description of resistance parameters.

Title	Description
R_W	Wave resistance from pressure integration (Wave making) (kN)
R_F	Friction resistance (kN)
R_T	Total resistance (kN)
R_C	Resistance in calm water (kN)
R_{AW}	Added resistance due to waves (kN)
C_{AW}	Coefficient of added resistance due to waves (-)

Below the diagrams of the aforementioned resistances and coefficient are presented, with respect to the wave frequency, for each of the headings.

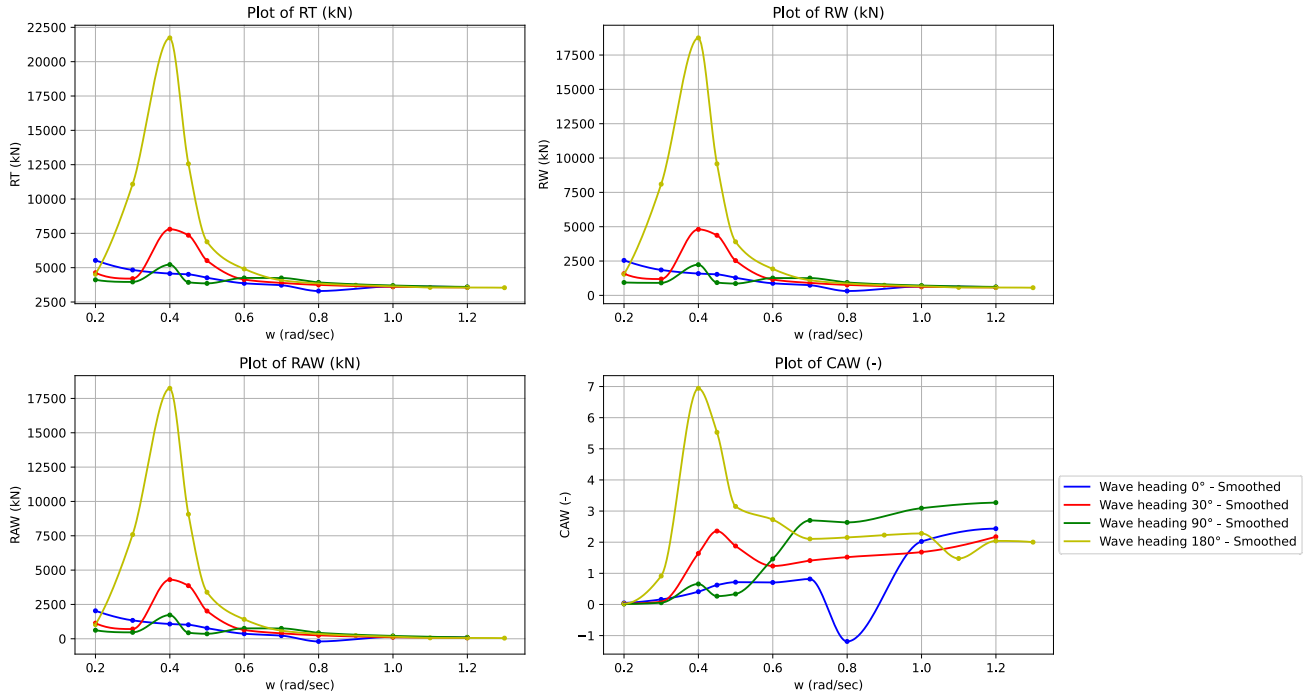

Figure 5.31: Resistance with respect to wave frequency.

Additionally, the same diagrams are presented, with respect to the dimensionless wavelength ratio (λ/Lpp) of wavelength to ship's length between perpendiculars, for each of the headings.

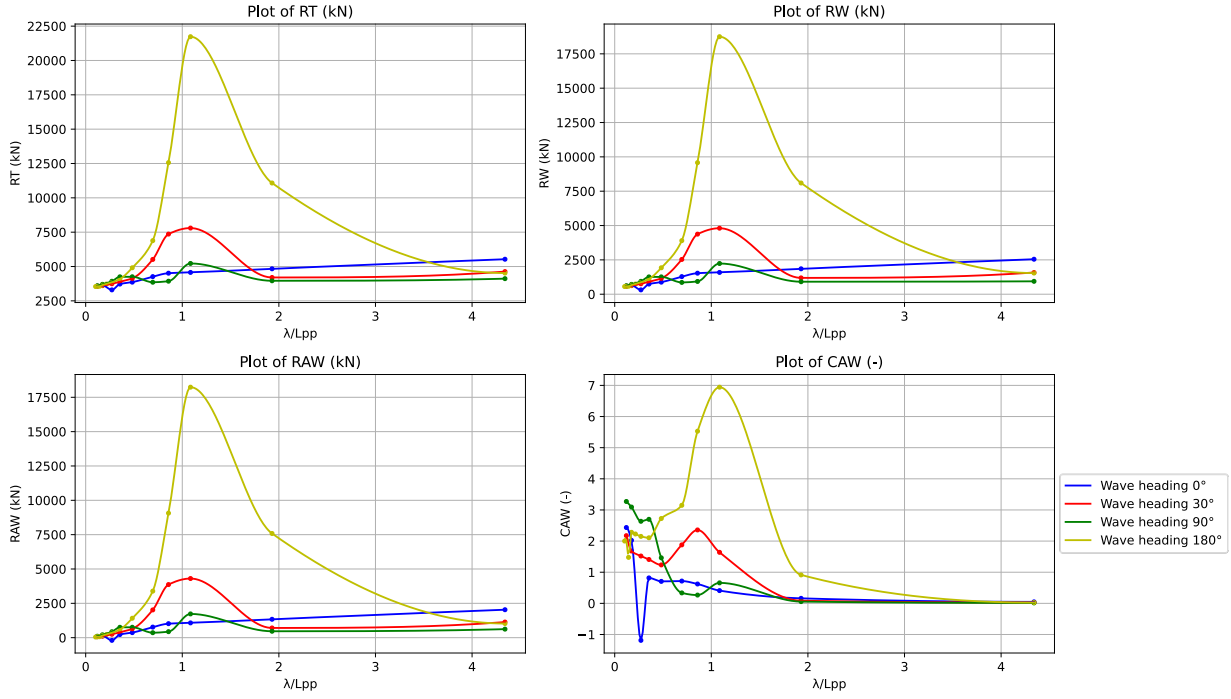

Figure 5.32: Resistance with respect to dimensionless wave length.

Some significant general observations and comments for the time series plots are:

1. The total resistance of the vessel in waves appears to reach its maximum value for heading seas at a frequency of $0.4\,rad/sec$, where the wavelength of the waves is nearly equal to the vessel's length. At this specific frequency, the total resistances peak in all wave directions, except for following seas, where the total resistance is very low. Given that the maximum total resistance occurs for heading waves, where the heave and pitch responses were significant and greater than those of the other motions, it is inferred that these contributed to the maximum total resistance. Similarly, for quartering seas, the sway, heave, and pitch motions contribute to the resistance, while for beam seas, the sway, heave, and more importantly, roll motions do.
2. Likewise, the same applies to wave making resistance, as both wave making and friction resistance contribute to the total resistance. The friction resistance remains constant because it depends on the vessel's Reynolds number and wetted surface. Therefore, it is reasonable for wave resistance to follow the pattern of the total resistance.
3. The value of friction resistance calculated by SHIPFLOW is based on the ITTC 57, and depends on the variation of the ship's wetted surface (ITTC, 2011). For validation purposes of the results, calculations using the ITTC 57 formulas for the reference value of the wetted surfaced presented in Table 4.2. Specifically, the Reynolds number for the ship's operational speed in sea water and the coefficient of friction resistance C_F were numerically calculated, while based on these the friction resistance was computed. The difference between the value of friction resistance calculated by SHIPFLOW and that of the ITTC 1957 theory is 2%. This minimal difference arises from the unimportant variance in the wetted surface area computed by the software compared to the reference one of the DTC hull, as the coefficient C_F is same in both methods.
4. The added resistance presents the same pattern and peak values at the same frequencies as those of the total resistance, as explained by the calculation method. Additionally, the similar distribution of added resistance to that of wave resistance indicates that added resistance is the primary contributing resistance for the respective phenomena, particularly when approaching the wave frequency of $0.4\,rad/sec$.

5. Finally, the coefficient of added resistance is of interest. Its maximum value is encountered for a wave frequency of $0.4\ rad/sec$ in following seas, as the coefficient value depends on the added resistance. The diagram confirms the aforementioned points regarding the resistances. Specifically, the coefficient shows small values for following seas and larger values for quartering and beam seas. Of particular interest is the abrupt increase in the coefficient for beam seas at a wave frequency of nearly $0.6\ rad/sec$, which aligns with the steep increase in RAO heave for the same conditions, indicating that the heave motion contributed to this increase of the coefficient.

Chapter 6 Responses in irregular waves

In this chapter, the results of the ship responses to irregular waves are presented, based on the weather data obtained from the statistical analysis of a specific reference route.

6.1 Reference route

Definitive and crucial parameters for seakeeping analysis include meteorological data, such as wind, wave (wind and swell waves) and current. In this particular study, since we are examining the hydrodynamic behavior of our vessel, we are interested in the factors of wind and swell waves, as well as when they will be extreme entailing maximum ship responses. This aims to assess the satisfaction of the seakeeping criteria under the most extreme sea conditions that are likely to occur.

It is widely known that one of the sea areas, where the most extreme weather phenomena occur, is the North Pacific Ocean area. Therefore, the reference route is in the North Pacific Ocean and on this route, the three northernmost points were selected, as shown in the Figure 6.1. For these three indicative points, meteorological data were extracted from the NOAA database (hindcast data for the last 4 years, with a 3-hour frequency), which pertained to significant wave height Hs, peak period Tp and mean direction of seas and swell. Subsequently, the time series data were used to implement probability analysis in order to capture a depiction of the Hs and Tp pairs that are of interest for the simulation of the DTC hull in irregular waves.

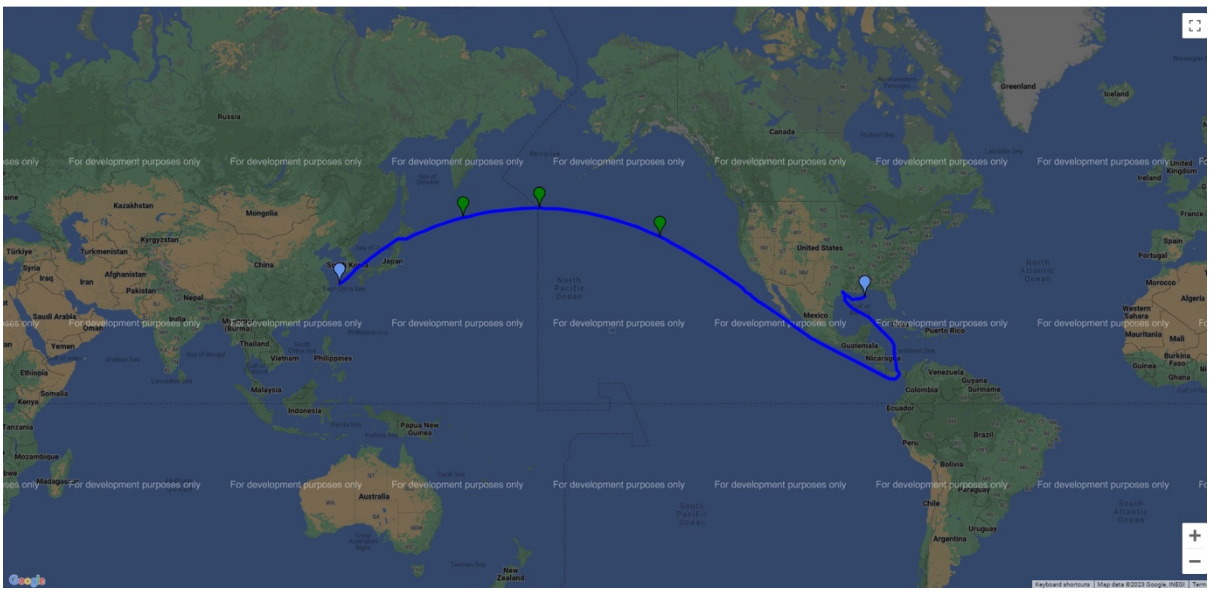

Figure 6.1: Reference route.

The three points of interest (green points) are presented in Table 6.1.

Table 6.1: Points of reference route.

Points	Points Coordinates in decimal degrees (°)
Point 1	(42, -146)
Point 2	(47.7, -179.5)
Point 3	(46, 159.3)

6.2 Sea state data

Irregular waves

Regarding the irregular waves, two sources were used to obtain sea state data, as mentioned previously: hindcast weather data for the reference route and weather data provided from studies and analyses.

6.2.1 Statistical analysis

In order to obtain useful data from irregular wave conditions, a statistical analysis of wave data recording was conducted. The recording of the free surface elevation is statistically analyzed by taking a sample of multiple values at equal time intervals, i.e., equal time steps.

Weather data retrieved from NOAA for the three pairs of coordinates were collected and subjected to statistical analysis, implementing the theory of probability density function, so as to determine the likelihood of sea state occurrences based on significant wave height and peak period.

By extracting the time series weather data, spectral data with a 3-hour frequency have been collected. To visualize the probability of their occurrence, the following univariate and bivariate parameter histograms (significant wave height, peak period, and their combination) were created. These histograms are based on long-term statistics and the distribution of possible values. Essentially, the number of occurrences in each interval is determined, and by dividing by the total number of occurrences initially, and then by the width of the interval (when univariate) or the corresponding interval area (when bivariate), the probability is calculated.

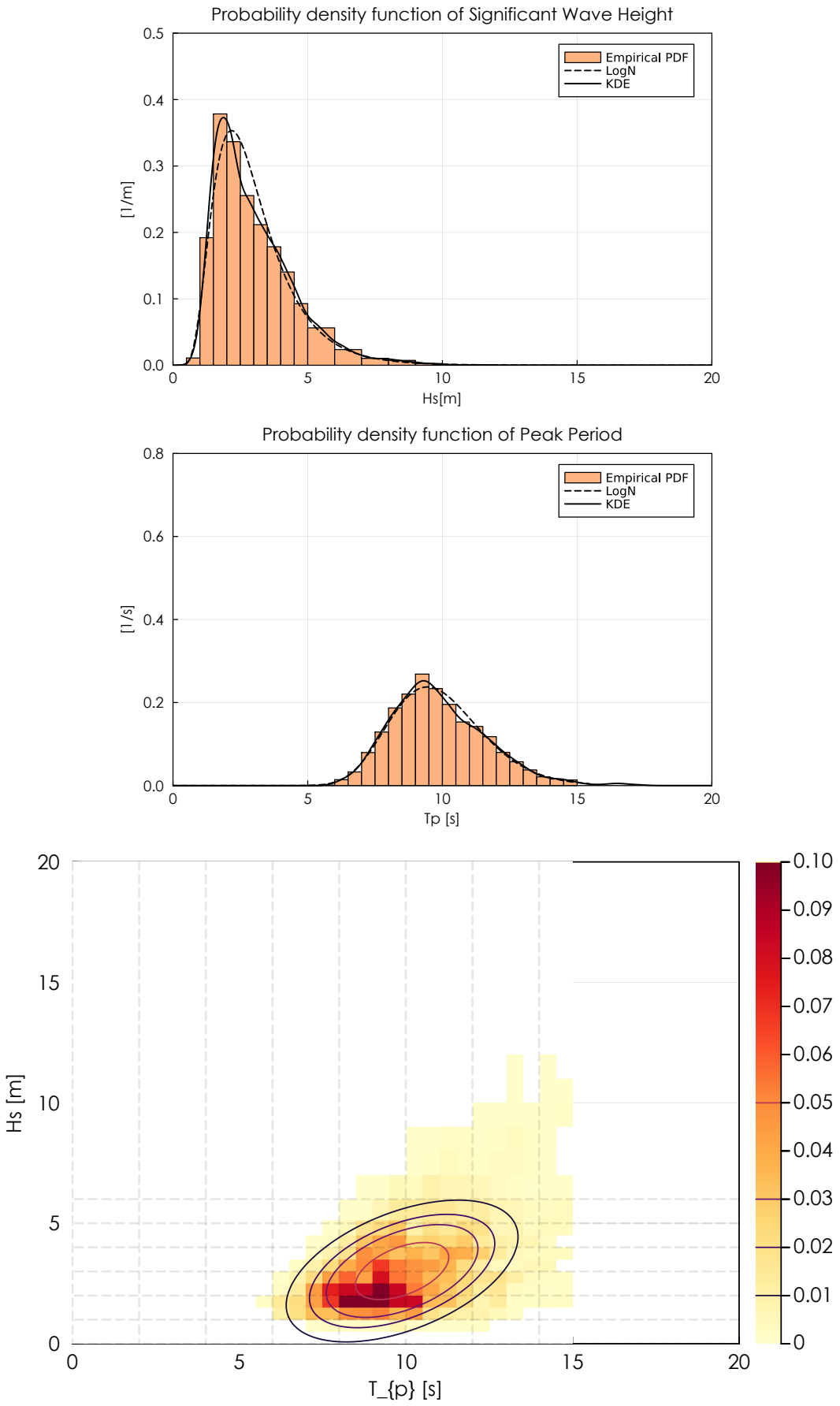

Figure 6.2: Univariate and bivariate probability analysis of Point 1.

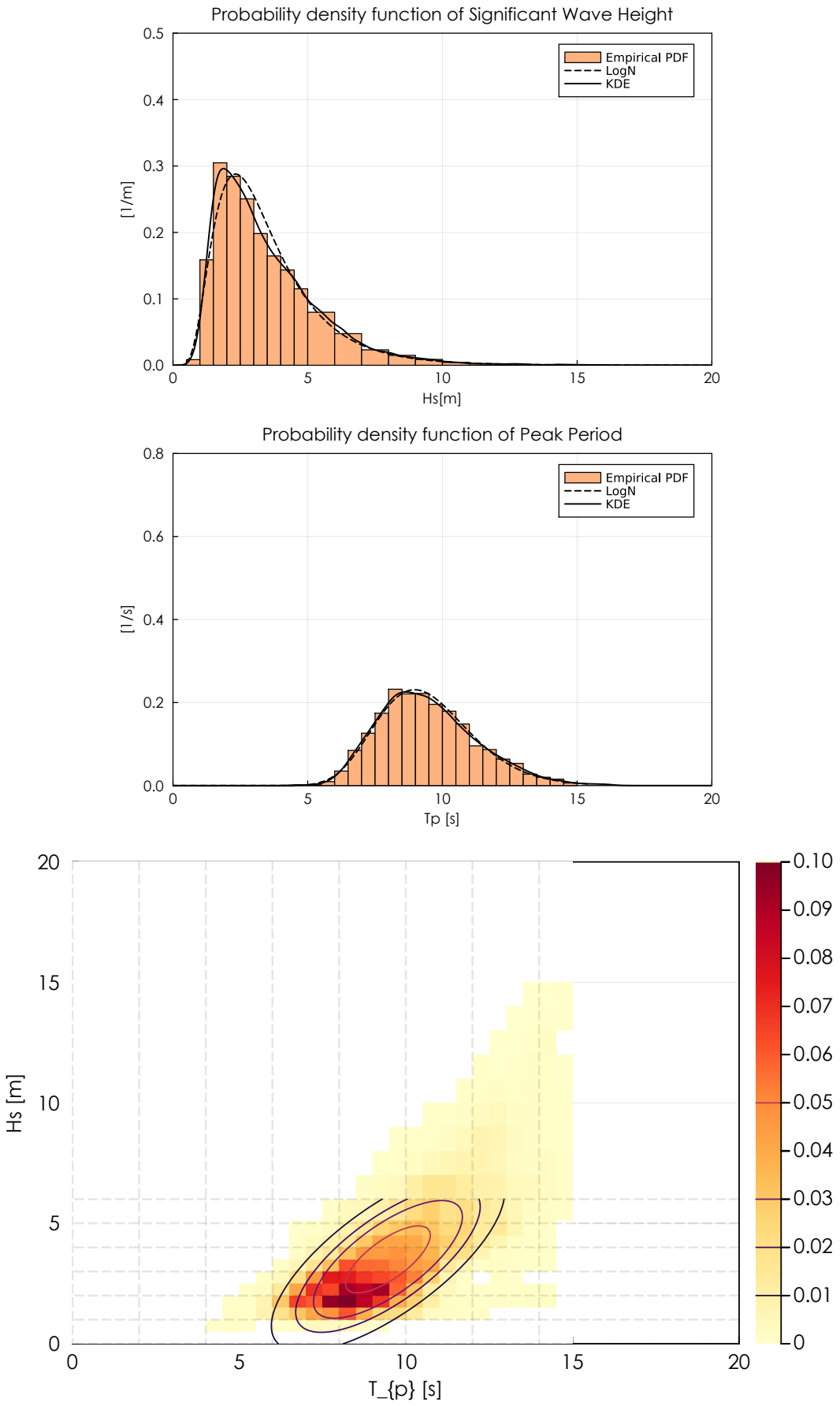

Figure 6.3: Univariate and bivariate probability analysis of Point 2.

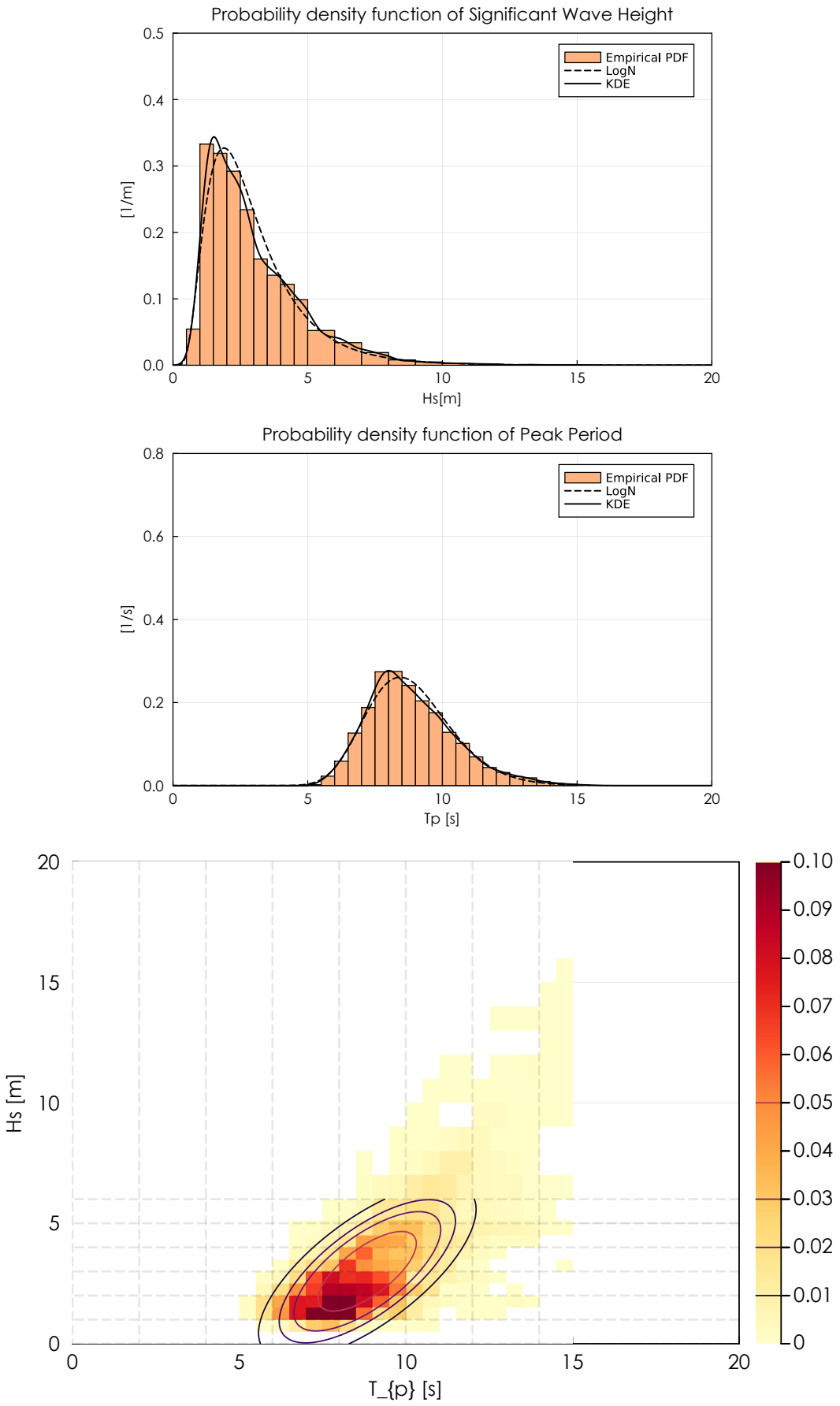

Figure 6.4: Univariate and bivariate probability analysis of Point 3.

Additionally, data for sea states were gathered from class reports (ABS, 2021; DNV-GL, 2018; IACS, 2001) and from the MARIN report (MARIN, 2022), in which the responses of a wide range of containerships were investigated, in order to determine the conditions under where the most intense and significant seakeeping phenomena occur. More specifically, the main basis for selecting pairs of significant wave height and peak period was the report by MARIN on limiting sea state conditions for containerships. This report refers to limiting sea state conditions in a specific geographical area with shallow water, where extreme phenomena of accelerations, bottom contact and green water were observed, calculated and recorded for various types of containerships. In the case study of this thesis, the vessel operates and be simulated in deep water and therefore, the results of these phenomena from this report could not be confirmed or compared, thus are considered as an extra weather data source. However, data for extreme sea conditions were extracted from it. Additionally, information regarding the probability occurrence of various sea states was derived from guidelines provided by ABS and DNV, utilizing scatter diagrams for worldwide operations. Therefore, from the aforementioned sources, specific extreme and possible to occur sea state data were extracted, which were confirmed to be existing through probability analysis conducted using real historical weather data that occurred on the reference route.

Thus, the combination of these two ways defining extreme weather data, contributed to identifying some indicative irregular conditions that were used in this study.

The entire test matrix used in the simulation for irregular waves is displayed in Table 6.2.

Table 6.2: Sea state conditions in irregular waves.

Sea state conditions	Wave significant height $H_s(m)$	Wave peak period $T_P(\text{sec})$	Waves direction (°)	WMO sea state code
Sea state 1	5.2	11.9	180°	Very rough (SS6)
Sea state 2	6.5	12.4	180°	High (SS7)
Sea state 3	6.5	14.5	180°	High (SS7)
Sea state 4	7.5	14.5	180°	High (SS7)
Sea state 5	5	15.5	180°	Very rough (SS6)

Significant observations include:

- The fundamental requirement for determining the final weather conditions was the testing, simulation and analysis of multiple conditions to conclude in comprehensive results of interest.
- Through this testing process, the encounter frequency was found in which the peaks of the wave spectrum and the ship's CG responses spectrums coincide to compare and verify the RAOs. Specifically, from the results of the regular wave simulations, the frequency of the wave causing the highest total resistance was identified and based on this, the peak period was calculated, and the respectively significant wave height was determined with the assistance of the two aforementioned sources.

6.3 Time-series results

Below are presented the time series of the positions, velocities and accelerations of the ship's center of gravity (CG) in each of the 6 degrees of freedom (DOF), for every one of the five irregular seas stated.

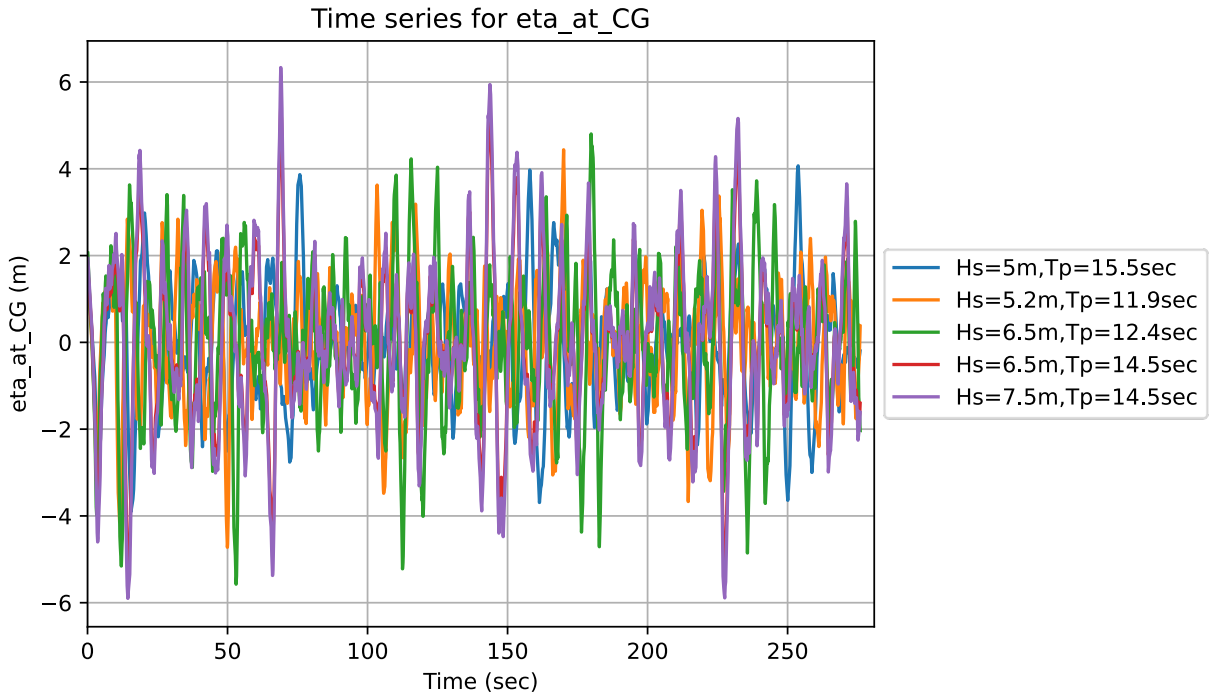

Figure 6.5: Time series of CG free surface elevation in irregular waves.

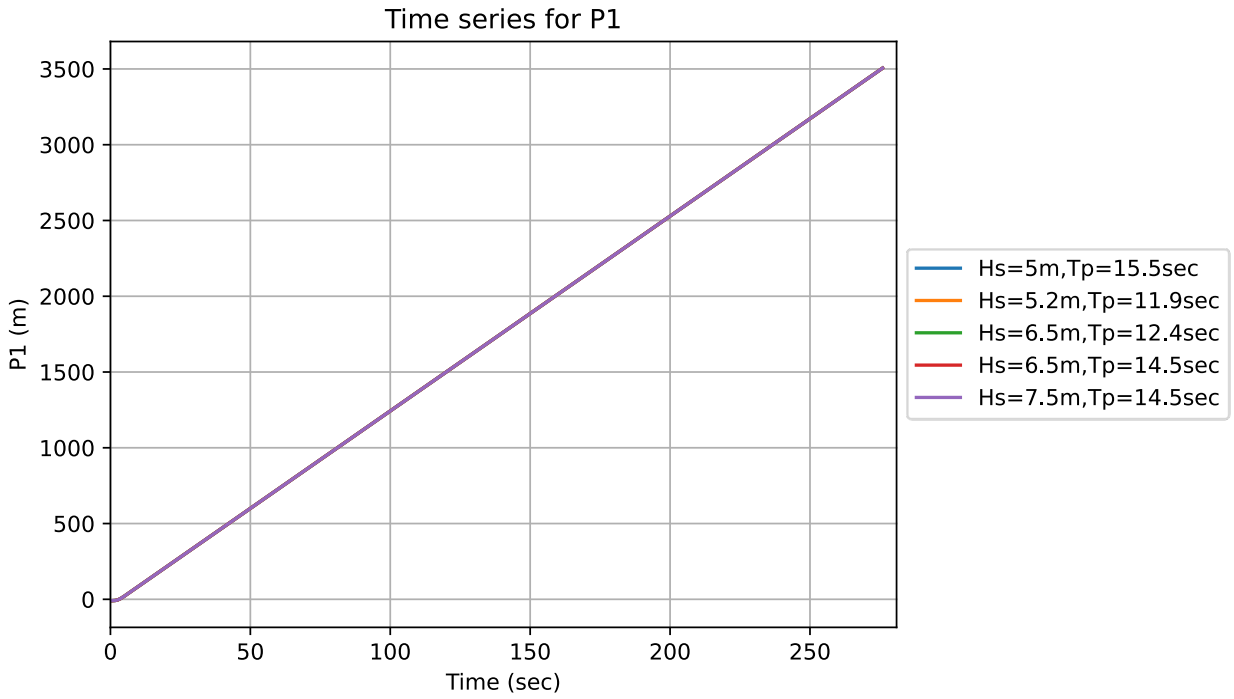

Figure 6.6: Time series of P1 in irregular waves.

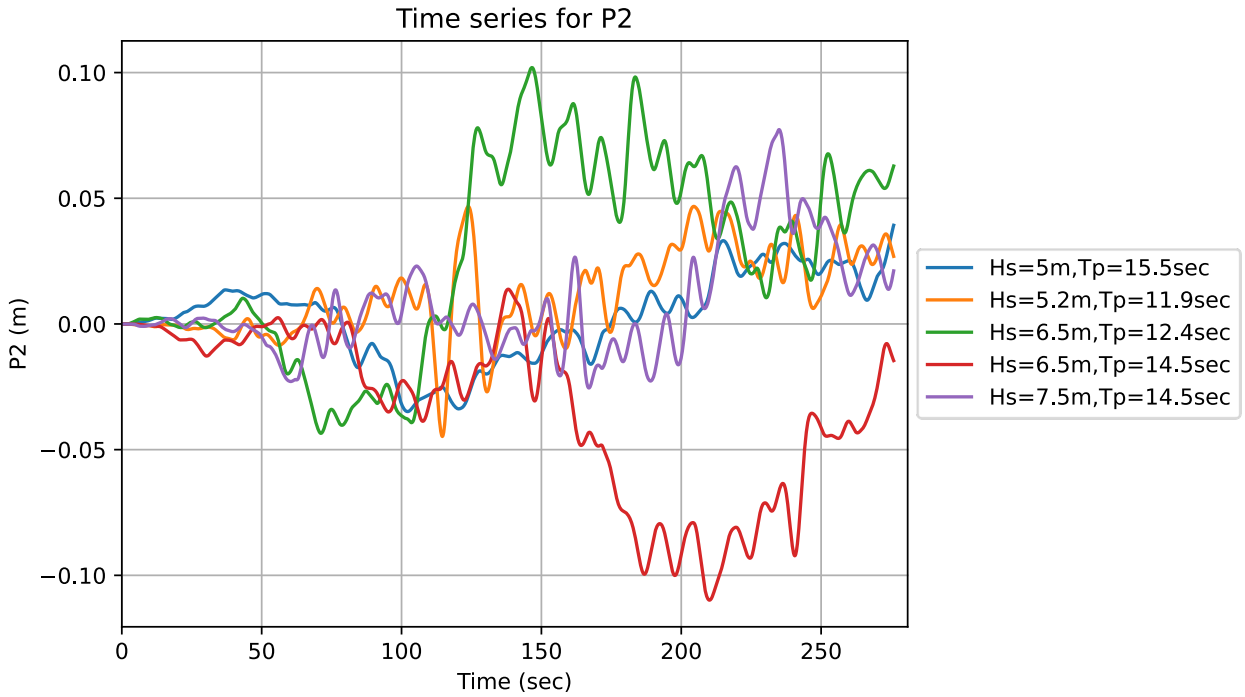

Figure 6.7: Time series of P2 in irregular waves.

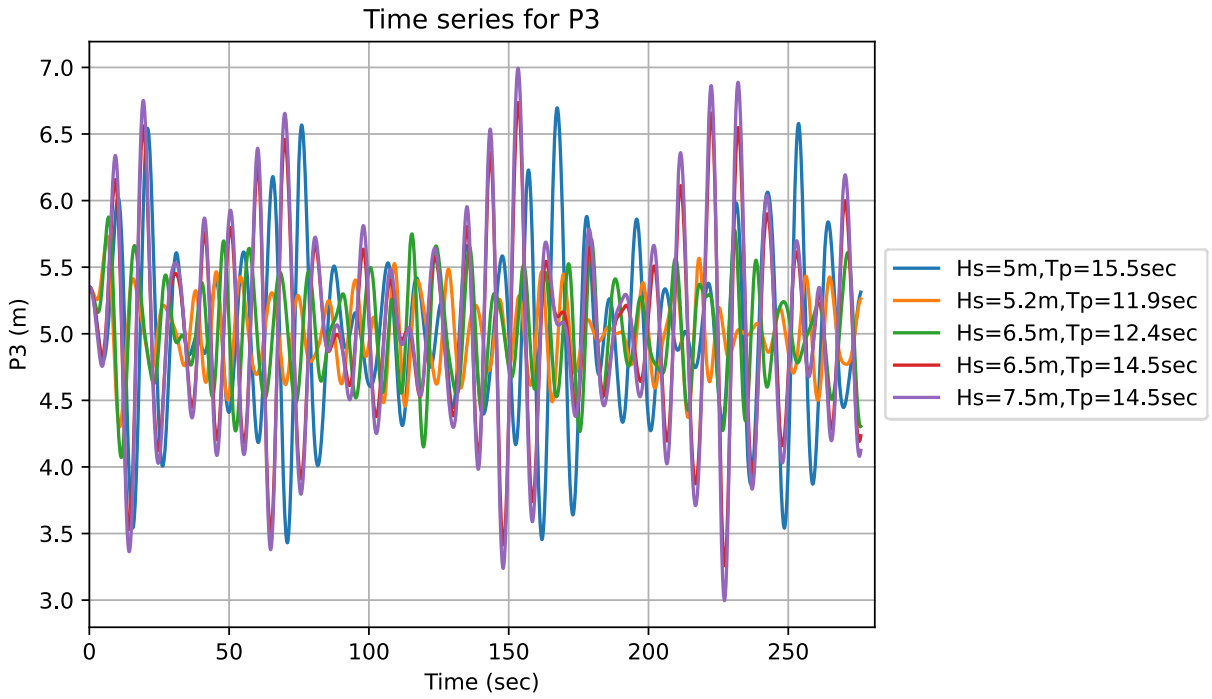

Figure 6.8: Time series of P3 in irregular waves.

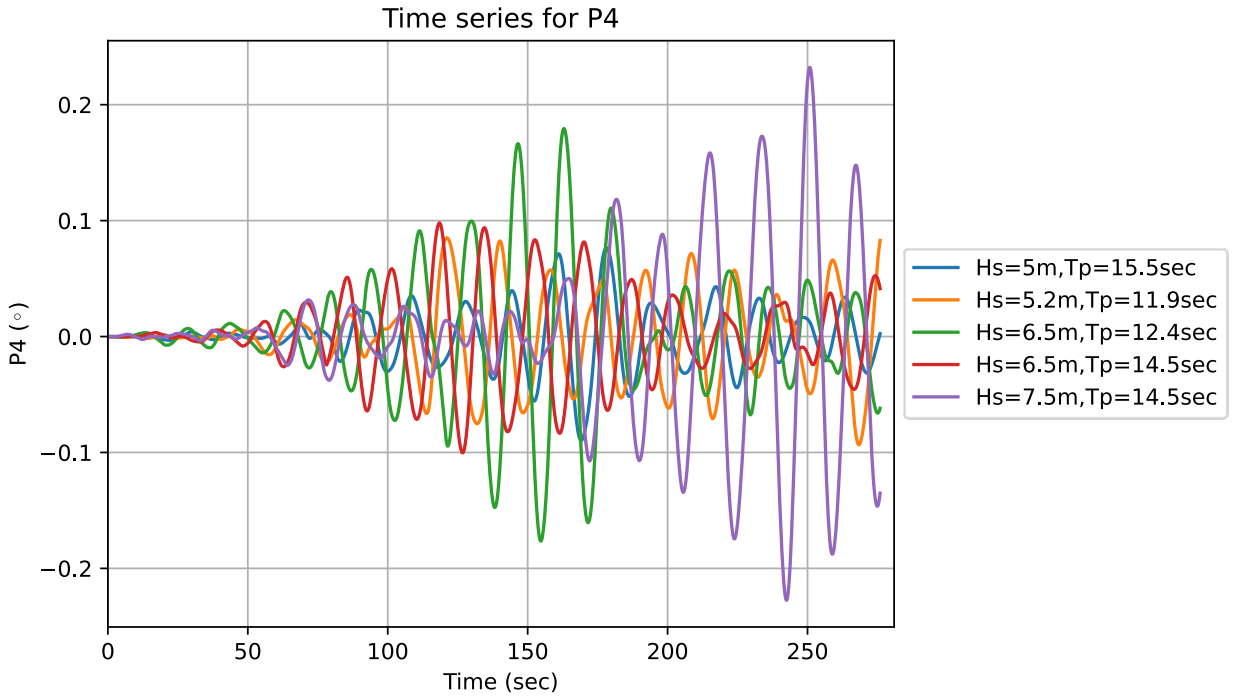

Figure 6.9: Time series of P4 in irregular waves.

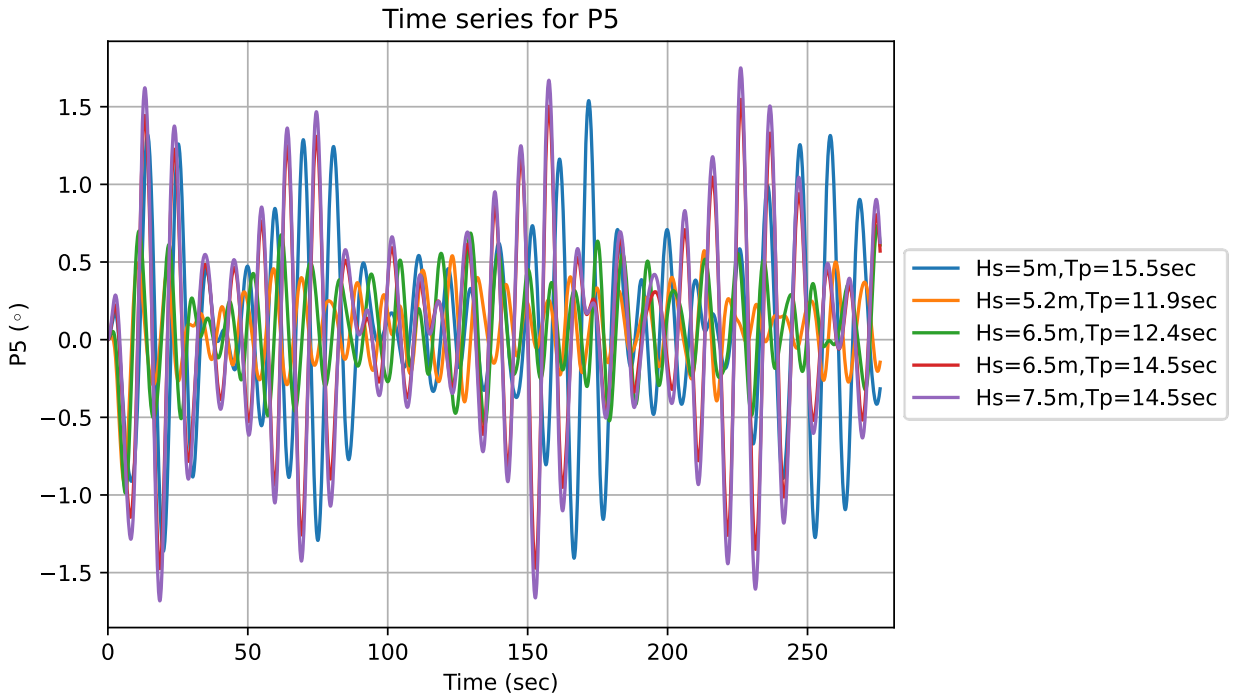

Figure 6.10: Time series of P5 in irregular waves.

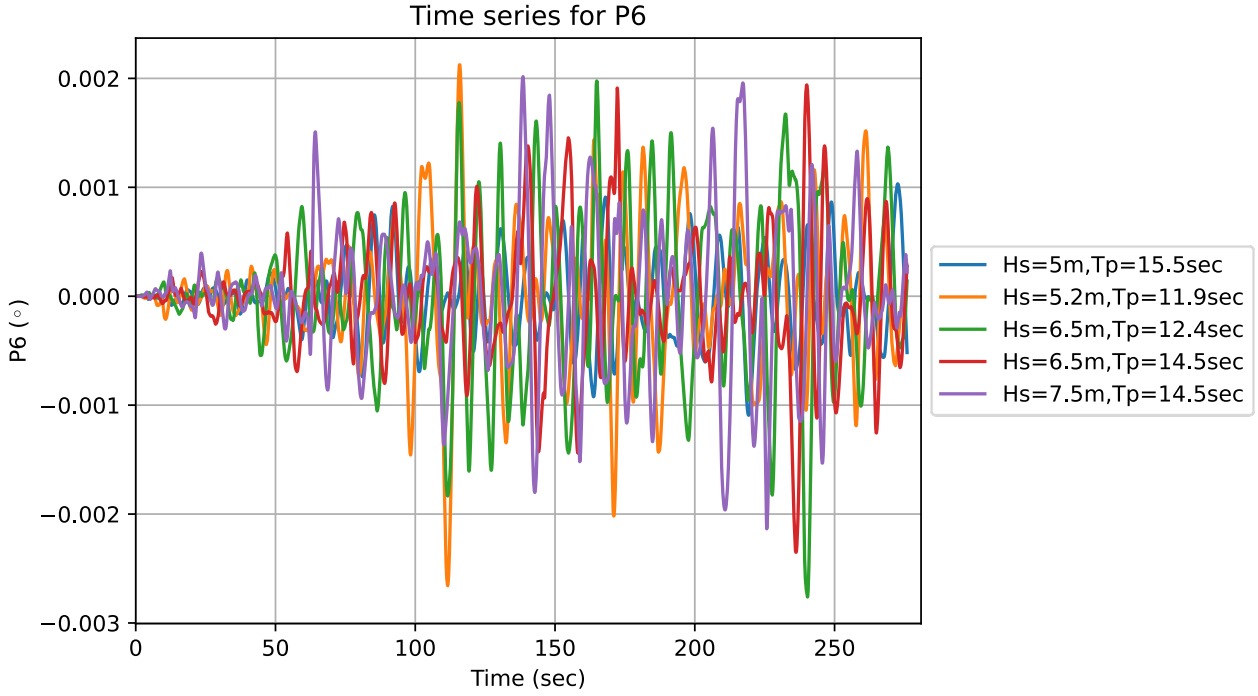

Figure 6.11: Time series of P6 in irregular waves.

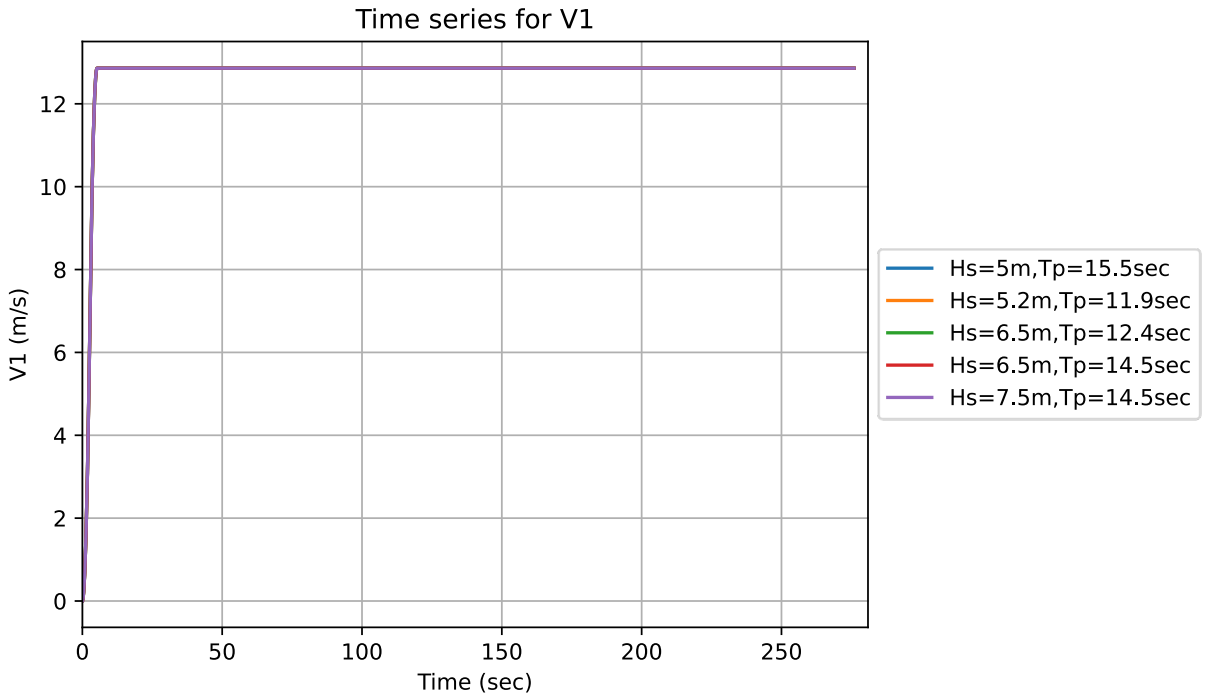

Figure 6.12: Time series of V1 in irregular waves.

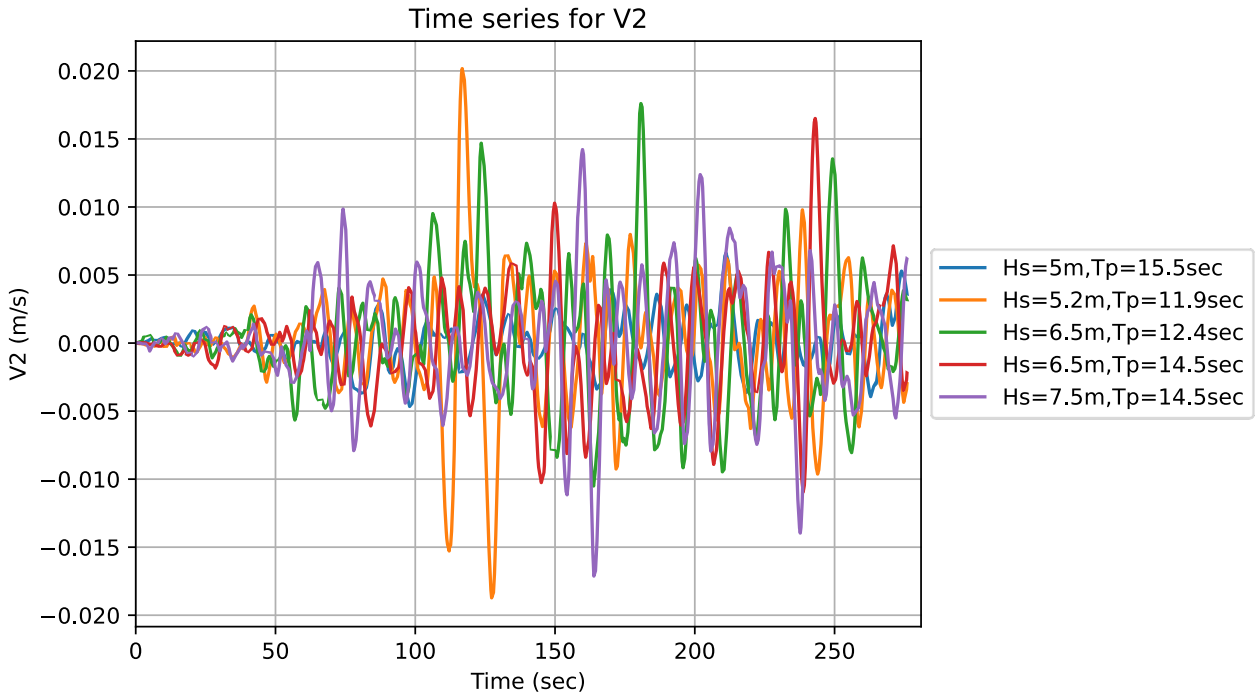

Figure 6.13: Time series of V2 in irregular waves.

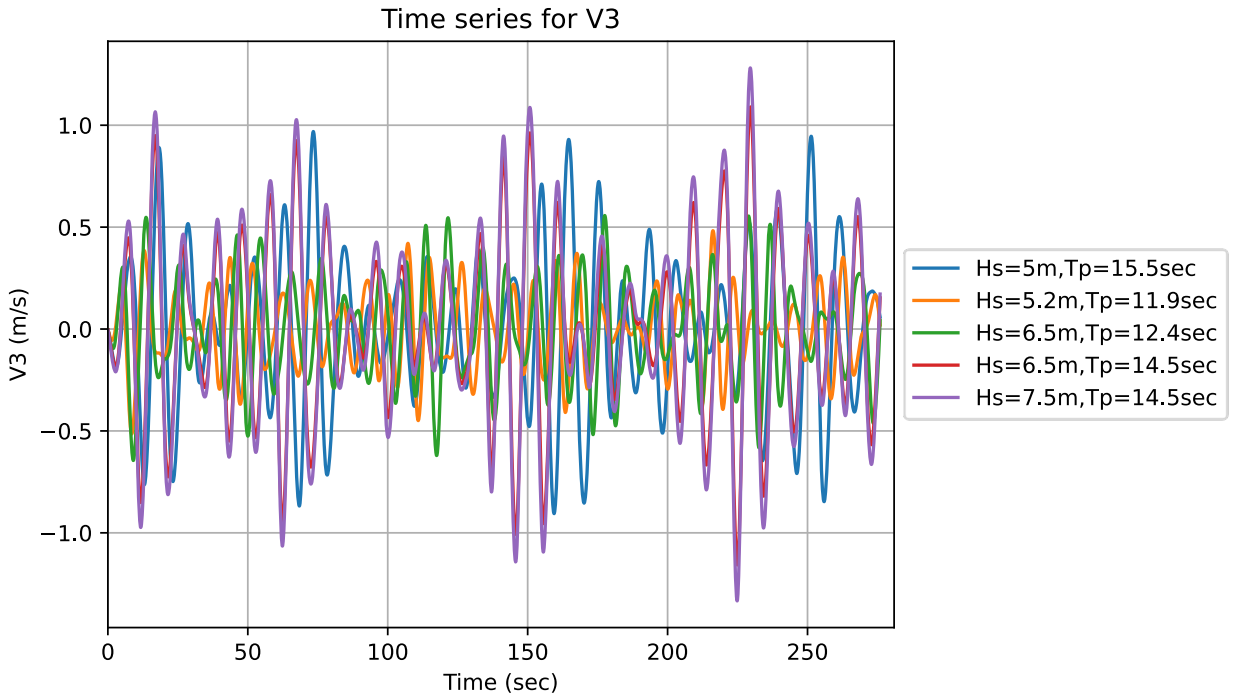

Figure 6.14: Time series of V3 in irregular waves.

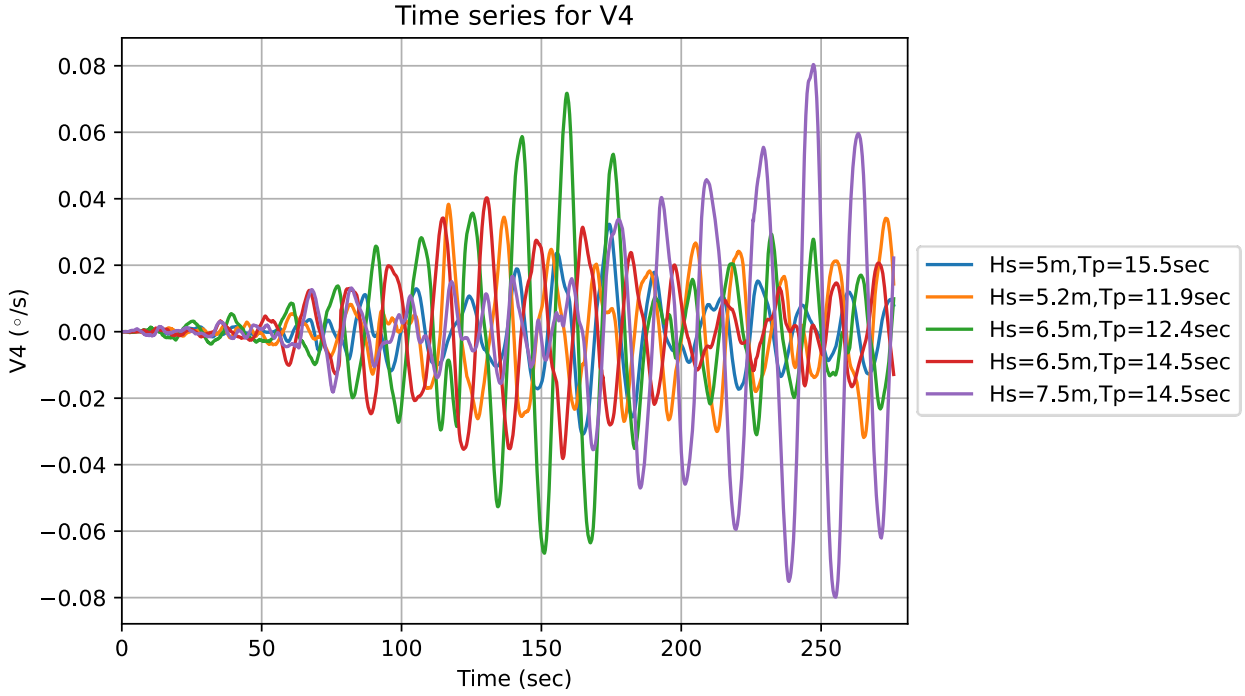

Figure 6.15: Time series of V4 in irregular waves.

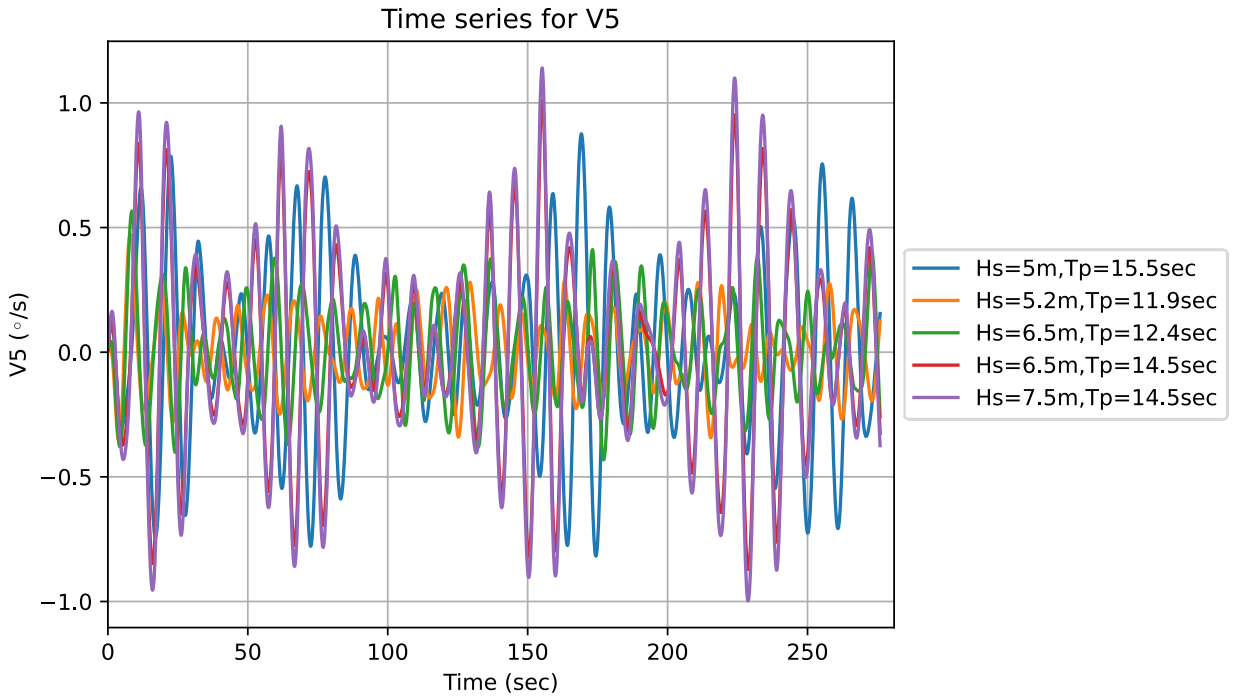

Figure 6.16: Time series of V5 in irregular waves.

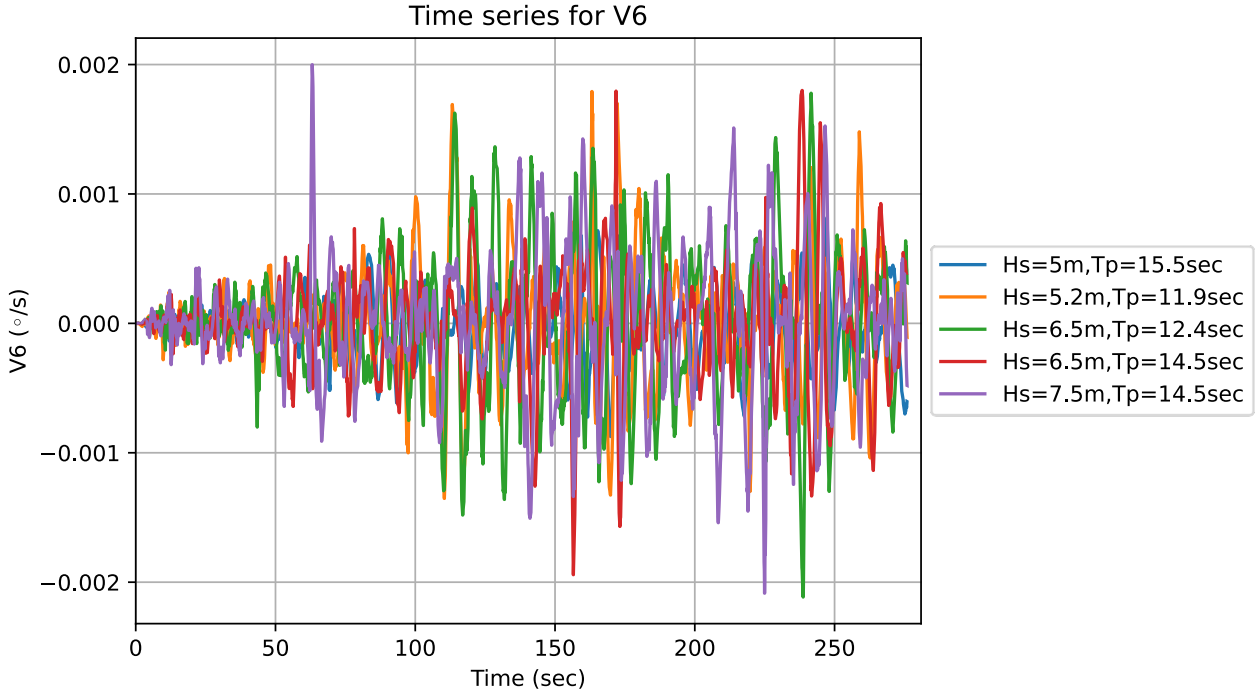

Figure 6.17: Time series of V6 in irregular waves.

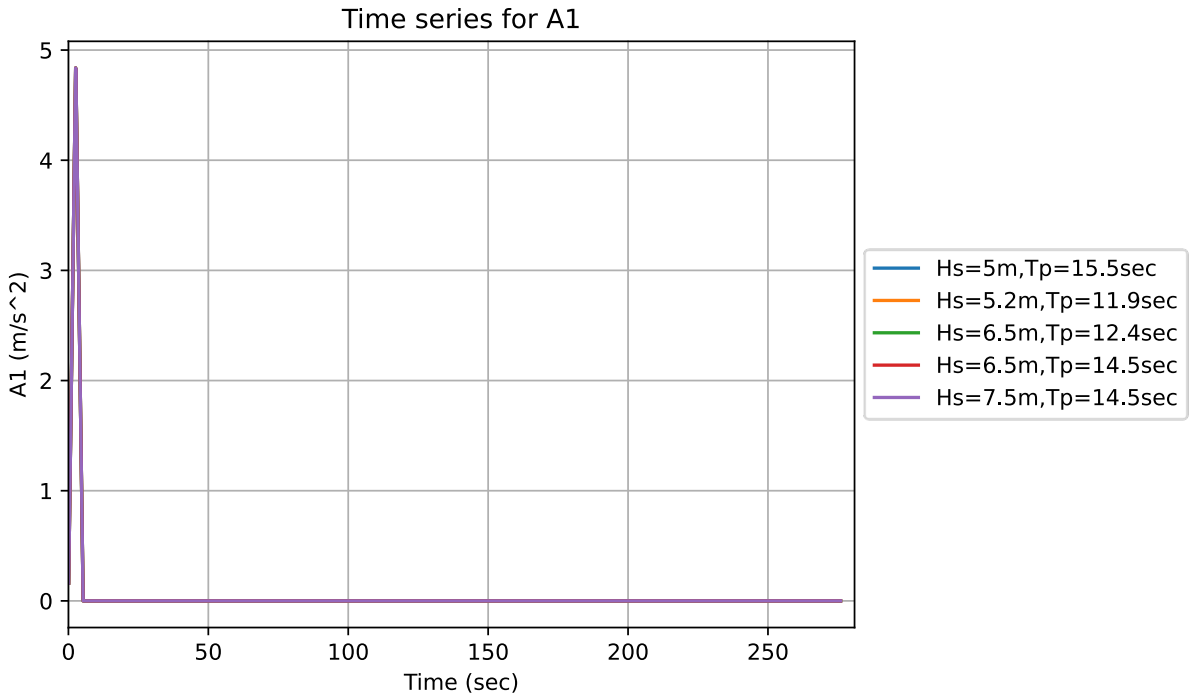

Figure 6.18: Time series of A1 in irregular waves.

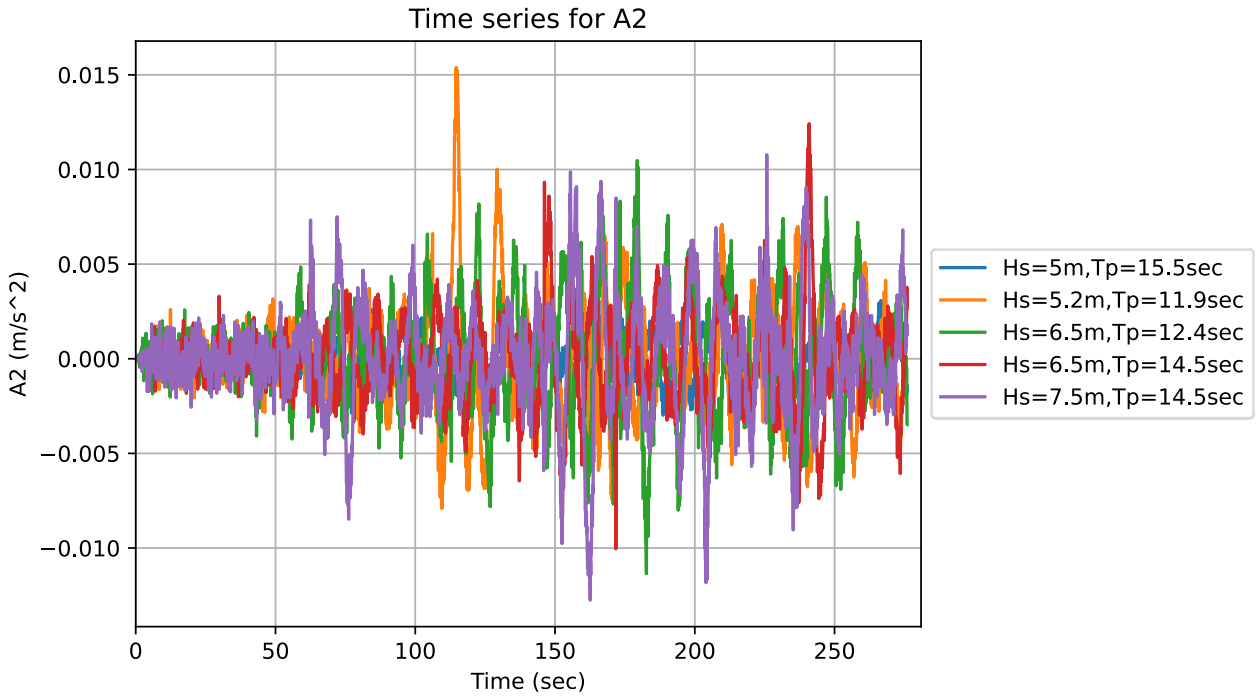

Figure 6.19: Time series of A2 in irregular waves.

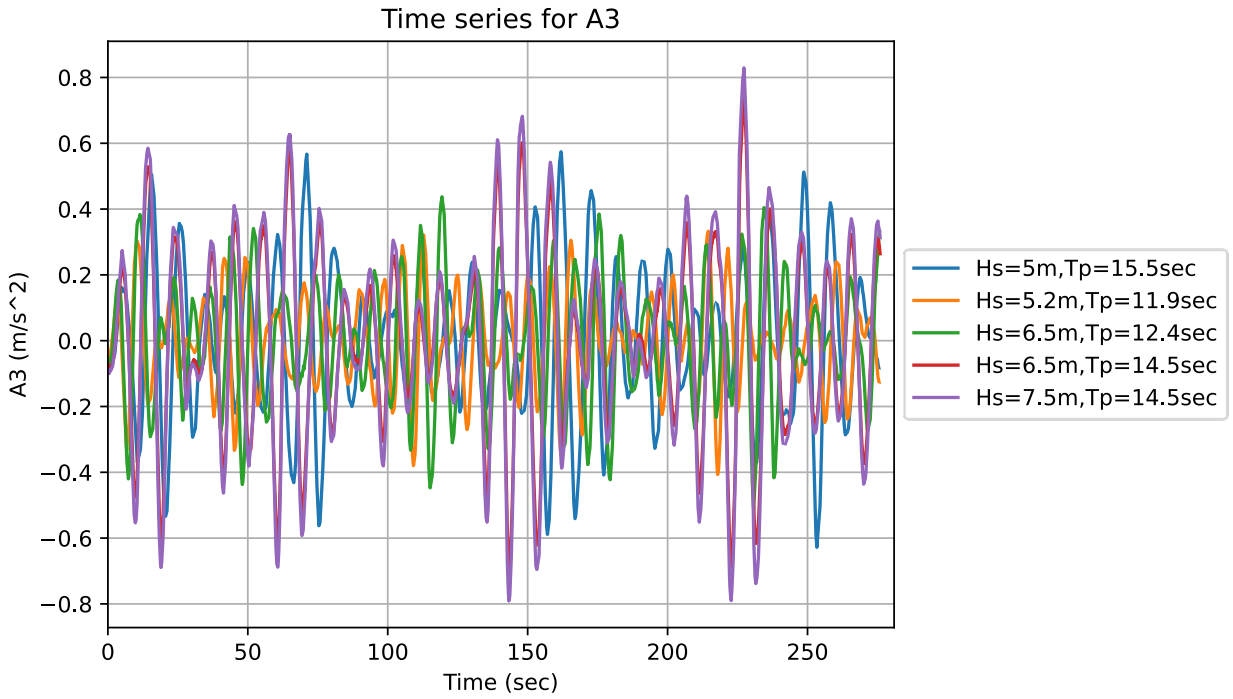

Figure 6.20: Time series of A3 in irregular waves.

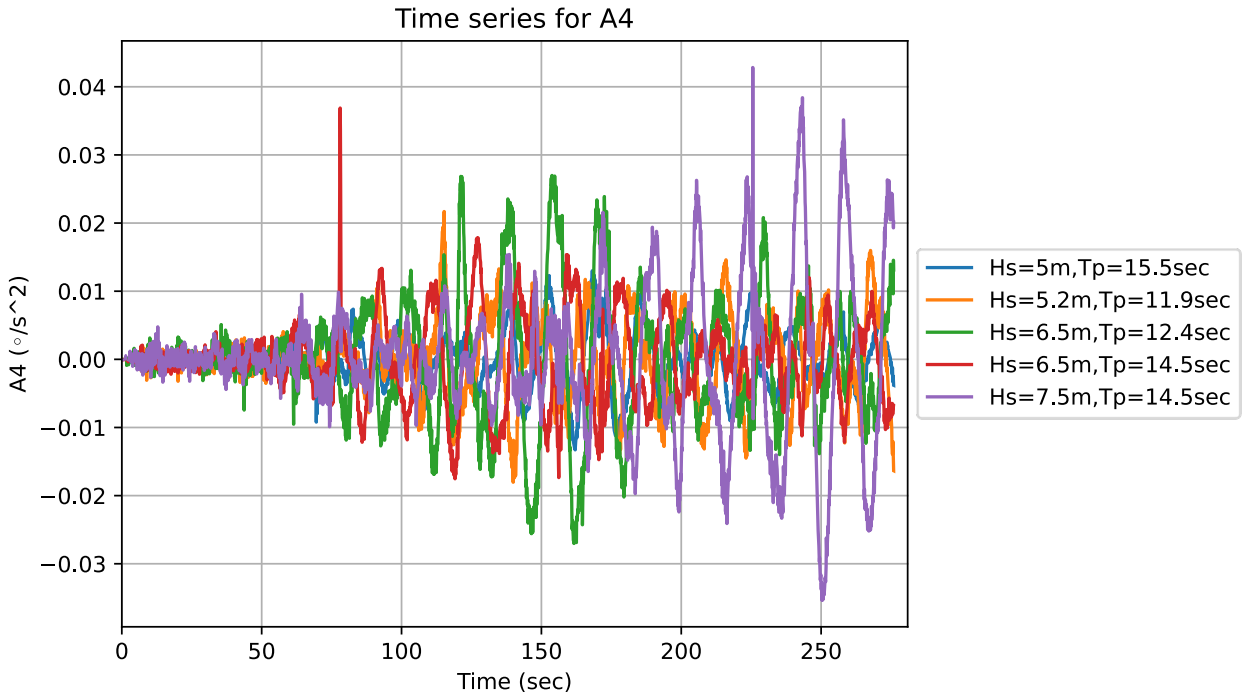

Figure 6.21: Time series of A4 in irregular waves.

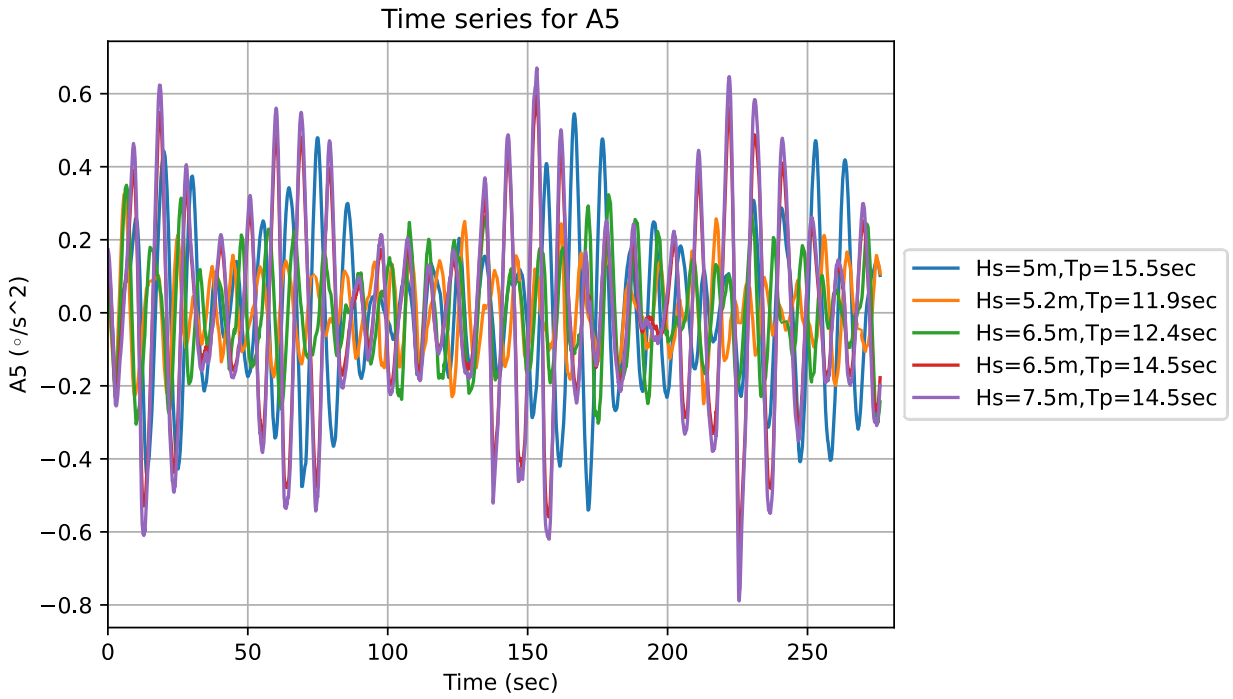

Figure 6.22: Time series of A5 in irregular waves.

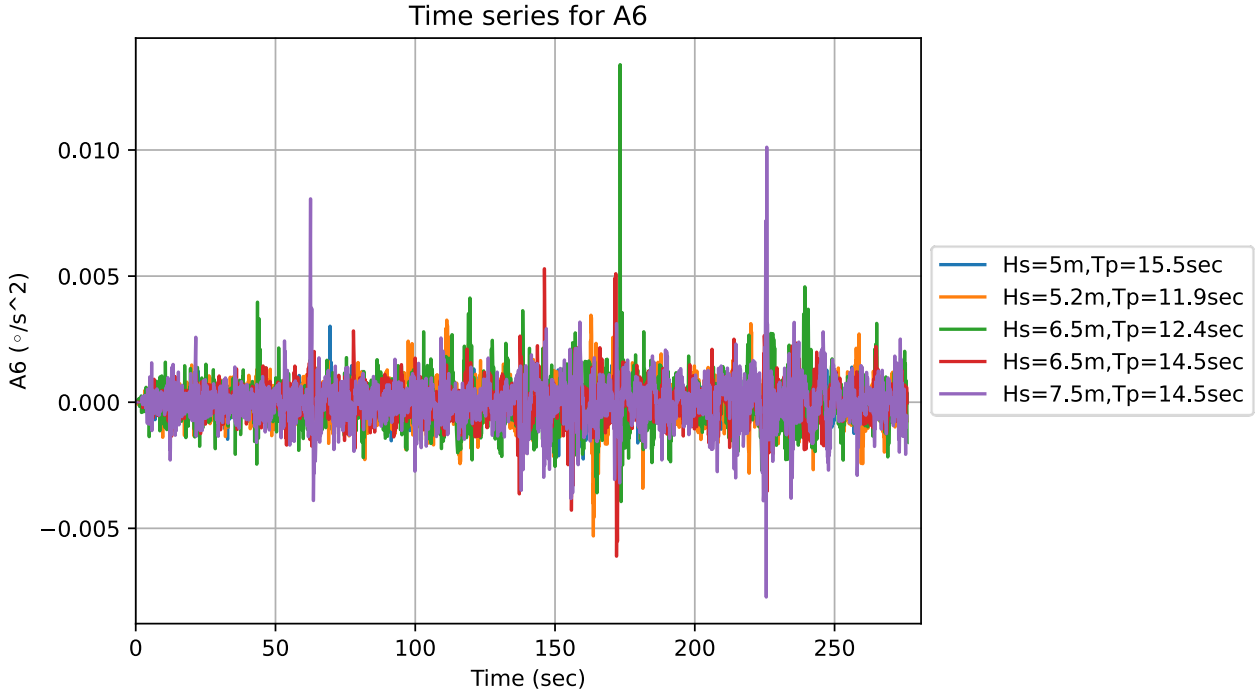

Figure 6.23: Time series of A6 in irregular waves.

Some significant general observations and comments for the time series plots are:

1. Observing the time series of free surface elevations in irregular waves, the difference compared to regular waves is evident, as randomness prevails. As known from theory, irregular waves are represented as the superposition of multiple regular waves of different frequencies and random phases. The free surface elevation represents a realization of a sea state with a specified significant wave height and peak period. The time series of the free surface elevation is derived from the calculations of the SHIPFLOW software using the inverse Fourier transformation method (IFFT). Specifically, before starting the simulation, the type of spectral sea model (JONSWAP for this thesis) and its parameters are defined. Consequently, the software first generates the sea spectrum (frequency domain) and then the corresponding time series (time domain).
2. Similar to regular waves, in irregular waves, the ship's speed remains constant, meaning surge remains constant, as shown in the time series of surge position (P1), velocity (V1), and acceleration (A1).
3. As shown in the plots, no significant phenomena are observed in the sway position (P2), velocity (V2) and acceleration (A2) due to heading seas. Additionally, differences in the evolution of phenomena are apparent for irregular waves with the same Hs and different Tp.
4. According to the positions on the z-axis (P3), dominant phenomena are observed in heave, with extreme values appearing in irregular conditions with larger Hs, as expected, especially for heading seas. Peak period also seems to play a significant role, as larger peak periods contribute to larger position amplitudes on the z-axis. These observations are also reflected in the time series of velocity (V3) and acceleration (A3).
5. Concerning the angles on the x-axis (P4), for roll motion, no significant phenomena are observed due to heading seas. In this case as well, larger position amplitudes of the response are observed in irregular conditions with larger Hs, with the ones on sea states 3 and 5 being predominant. An interesting observation is that for the significant wave height of $6.5m$, more intense phenomena are observed in the smaller peak period of $12.4sec$ compared to $14.5sec$, indicating that responses depend on both height and period, i.e., the frequency of wave occurrences. The above also apply to the time series of velocities (V4) and accelerations (A4).

6. According to the time series of angles on the y-axis (P5), the phenomena are predictable. Similar to the corresponding P3 time series, extreme values are located in sea states with the largest Hs, but mainly with the largest peak period (sea states 1, 4, 5), indicating that the value of the peak period significantly affects the angles on the y-axis. Additionally, the time periods of maximum values of P5 coincide with those of P3, in which the maximum values of free surface elevation occur, as shown in Figure 6.5. The above also apply to the time series of velocities (V5) and accelerations (A5).
7. Regarding the angles on the z-axis (P6), the values of the time series are almost negligible, as expected for heading seas, while no significant differentiation of results for the given sea states is observed. The above also apply to the time series of velocities (V6) and accelerations (A6), where results stand out at specific time periods but are not significant.
8. Finally, observing all the time series, some dominant frequencies stand out, in which abrupt fluctuations and variations of the responses were distinguished at specific time stamps. Therefore, there appear to be certain wave frequencies that excite more intense response phenomena.

Chapter 7 Seakeeping Criteria satisfaction

In this chapter, the calculation of seakeeping criteria and the corresponding operability analysis, according to linear and non-linear theory, are presented.

7.1.1 Points of interest except the ship's CG

To inspect the seakeeping criteria satisfaction, it is necessary to include in the calculations and simulations some points of interest on the vessel besides the center of gravity (CG), in order to calculate and analyze the amplitudes, velocities and accelerations of the responses at these points. To estimate the exact coordinates of these points, the software Rhinoceros and the General Arrangement of a containership, with the same dimensions and characteristics as the DTC vessel from Danaos Shipping CO. LTD, were utilized.

The table below lists the extra points of interest and their coordinates with respect to the offset coordinate system.

Table 7.1: Points of interest).

Points	Point Coordinates (m)
Point 1 at the center of propeller's hub	(x, y, z) = (10, 0, 5)
Point 2 at the deck in Forward Perpendicular (FP)	(x, y, z) = (355, 0, 31.5)
Point 3 at the bow in Forward Perpendicular (FP)	(x, y, z) = (355, 0, 1.8)
Point 4 at the bridge	(x, y, z) = (221, 0, 61.7)

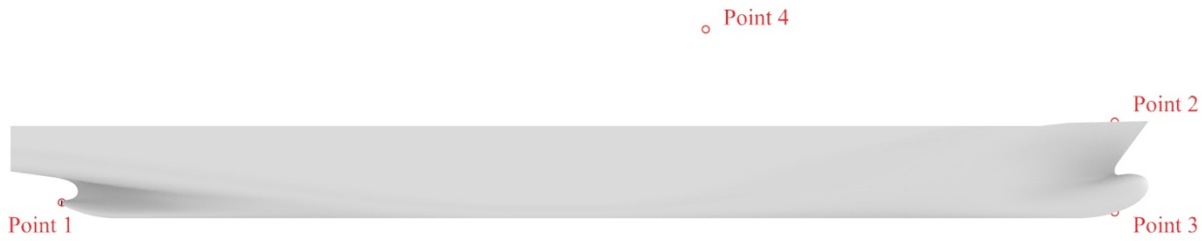

Figure 7.1: Visualization of points in the 3D DTC hull.

7.1.2 Probes in areas of interest

In irregular wave conditions, for the verification of seakeeping criteria, two probe areas were defined in the SHIPFLOW software, as it is known from theory (Chapter 2) that in order to

calculate moments and rms values at points of interest except the CG, it is necessary to have the time series record for the free surface at these points. According to the criteria for verification, the areas of interest were confined to be at the forward perpendicular (FP) and the end of the propeller shaft, so as to coincide with the positions of the points of interest that have been defined. The positions of the probes are presented in the table below.

Table 7.2: Probes.

Probes	Probe Coordinates (m)
Probe 1 at the center of propeller's hub	(x, y) = (10, 0)
Probe 2 at Forward Perpendicular (FP)	(x, y) = (355, 0)

Figure 7.2: Visualization of probes in the 3D DTC hull.

7.2 Operability analysis

In order to conduct a completed seakeeping analysis, it is useful to perform an operability analysis. Specifically, the operability analysis investigates and delineates the threshold values of a ship's seakeeping criteria across a wide range of sea state conditions that may occur during a voyage. In this thesis, an operability analysis of the DTC hull is conducted on the reference route presented in 6.1. The purpose of this analysis is to investigate and compute the threshold values of the fundamental seakeeping criteria along the reference route, using the actual sea state values obtained from the statistical analysis in 6.2.1 (pairs of significant wave height and peak period). Thus, it is possible to assess the vessel's performance not only in specific extreme weather conditions but also across a multitude of them.

For the operability analysis, two methodologies were utilized (frequency domain and time domain), so as to compare the results obtained from the application of these two methods.

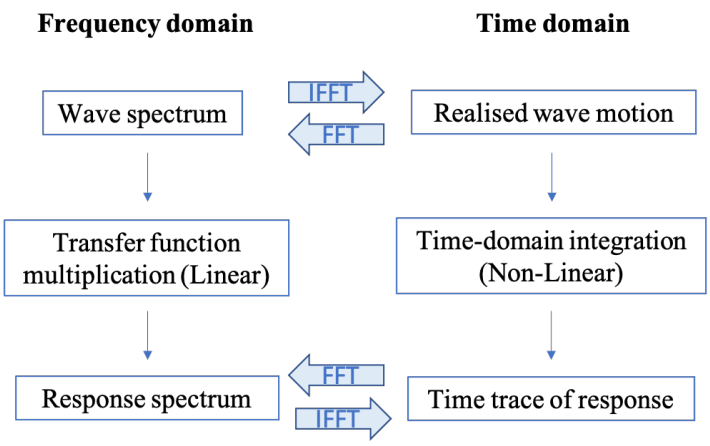

Figure 7.3: The two methodologies used for operability analysis.

In the frequency domain, using the wave spectrum and the RAOs in regular waves, as calculated by the software (as a function of frequency), the response spectrum is computed. This spectrum is then used to calculate the seakeeping criteria for the operability analysis. On the other hand, in the time domain, the time responses derived from simulations in irregular waves are utilized, and with appropriate analysis and transformation, the response spectrum is generated, which will form the basis for the criteria calculation.

7.2.1 Method 1: Frequency domain

Conducting operability analysis for ship's seakeeping, requires having calculated the ship's responses in various sea state conditions, and given that the computational run time of SHIPFLOW software is slow because of its non-linear algorithms, it was more feasible to perform the operability analysis using the linear theory.

The methodology followed for the operability analysis using linear theory was as follows:

- Initially, the RAOs have to be defined for three types of cases:
  - The Response Amplitude Operators (RAOs), as calculated and extracted from SHIPFLOW software methods, for regular heading waves were utilized for the seakeeping criteria referring to the ship's center of gravity (CG).
  - As the SHIPFLOW software cannot calculate and visualize the RAOs in specific points other than CG (e.g., bridge), that are necessary for seakeeping criteria, both the Fourier transform method and a method for identifying the crests and troughs of the time signal of the responses (to regular waves) were used. Specifically, as simulating regular waves, regular responses will be formulated, thus the response amplitude can be segmented into many parts, and the mean value of amplitude calculated. With the help

of PyWafo (WAFO, 2017), the waves are segmented, identifying the crests and troughs and from the successive values the corresponding heights are calculated. Based on this, the mean value of all heights is evaluated, and from this the mean value of the amplitude. The FFT method is a more complex one, and transforms time series data into frequency data, while identifies the dominant frequency component. The sinusoidal signal is reconstructed based on this dominant frequency and the corresponding amplitude. Both methods resulted in accurate amplitude calculations, however the identification of crest and troughs was preferred for the final results (as indicated in Figure 7.4, due to less complexity). Then, given the known wave amplitude on each wave frequency, the RAOs are calculated at this specific point. Additionally, by simulating regular wave conditions and inputting coordinate information about the points of interest, SHIPFLOW returns time series for their motions, velocities and accelerations. Consequently, the RAOs of velocities and accelerations can be calculated accordingly.

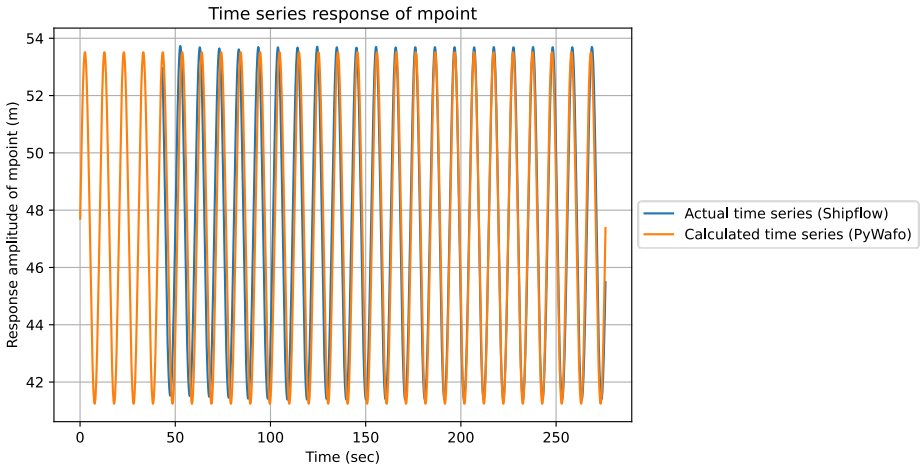

Figure 7.4:Calculated time series for point of interest response amplitude (PyWafo).

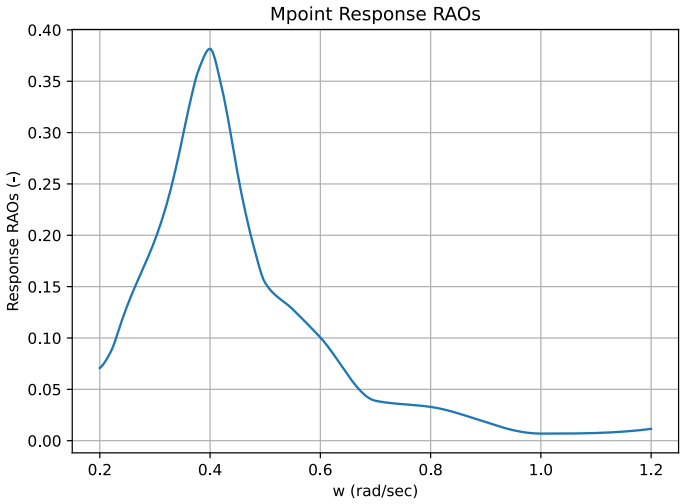

Figure 7.5: RAOs of vertical acceleration at bridge.

- For seakeeping criteria related to free surface elevation (e.g., slamming, green water deck) SHIPFLOW software cannot provide direct results, of either calculations or RAOs. Thus, it was necessary to use the mathematical expression for calculating the elevation amplitude of the free surface using complex numbers. Having the RAOs of regular waves, their phases, as well as the longitudinal distance of the point to the FP from the CG, allowed to compute the RAOs based on the response amplitude formula of the relative response of a specific point regarding to waves.

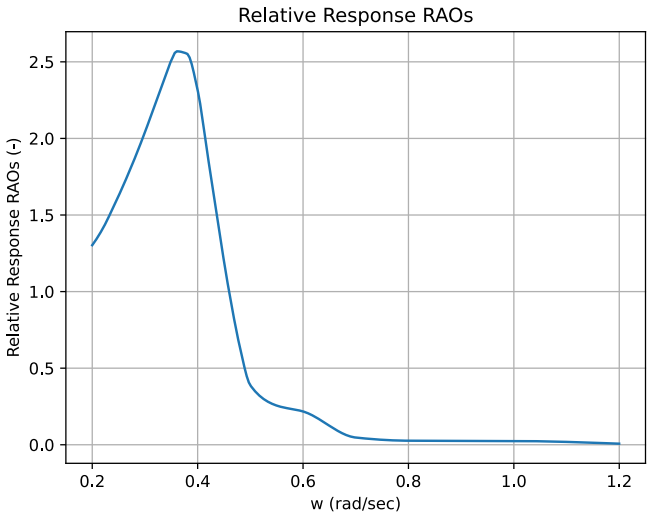

Figure 7.6: RAOs of vertical amplitude at FP.

- Subsequently, with the assistance of the PyWafo library, wave spectra were created in Python according to the JONSWAP spectrum, for a large number of possible combinations of significant wave height (Hs) and peak period (Tp) derived from the statistical analysis of the reference route. The aforementioned wave spectra are modeled with respect to the wave frequencies, so they were properly transformed to the same ones with respect to the encounter frequencies.
- According to linear theory, the response spectra were calculated using the respective RAOs and wave spectra, with respect to the encounter frequency.
- Having calculated the response spectra of the amplitudes, velocities and accelerations, the required moments and root mean square (RMS) values were computed, which are essential for the calculation of the criteria.
- Finally, the seakeeping criteria were calculated for various combinations of sea state conditions, so as to find the limit values, above of which the criteria are not satisfied. This method allows to conduct an operability analysis, indicating ship's performance and seakeeping.

7.2.2 Seakeeping criteria results

The sea states examined for the operability analysis are based on the results of the statistical analysis of the reference route. Thus, pairs of significant wave height and peak period values were created for $Hs = 1 - 15m$ and $Tp = 4 - 15sec$ and heading seas (180°).

Below are the results of the criteria for this multitude of sea states, forming a comprehensive picture of the impact of weather data on the respective seakeeping criteria.

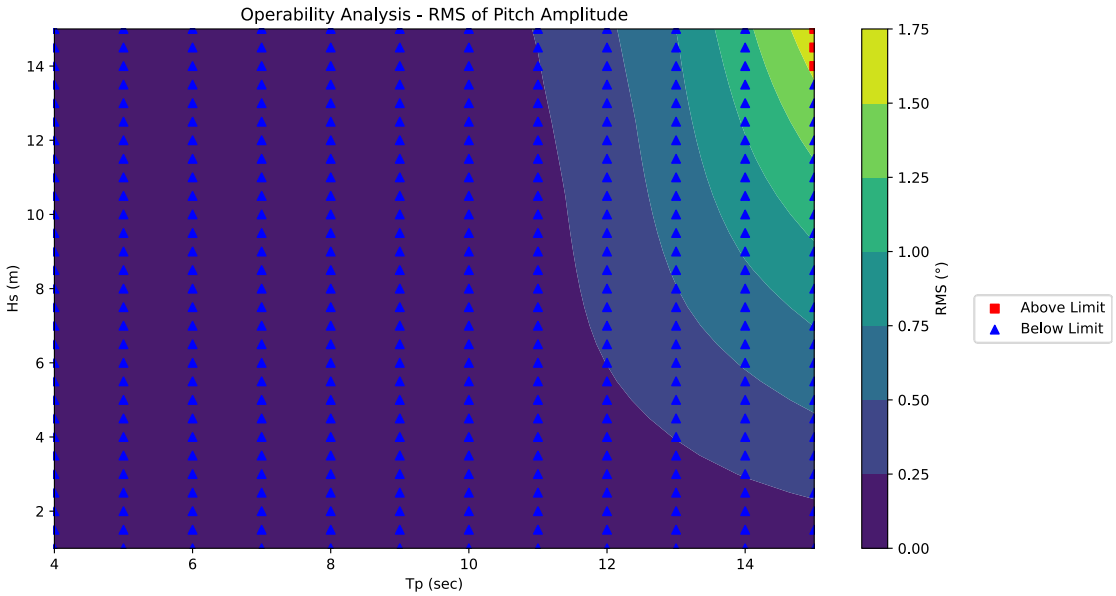

Figure 7.7: Pitch amplitude criterion.

In the Figure 7.7, the operability analysis of the criterion for pitch amplitude is depicted, with a threshold value of $RMS = 1.5°$ (NATO STANAG 4154, Table 1.1, Equation 2.51). This threshold value appears to be exceeded, indicating that the criterion is not satisfied, only for 3 sea states. Specifically, these sea states concern significant wave heights greater than $12m$, which, as indicated by the statistical analysis of the weather data from the reference route, are extremely unlikely to occur. In the broader context, the criterion is satisfied for a wide range of sea states, while the rms value of the pitch amplitude seems to increase for pairs of large significant wave height and peak period values.

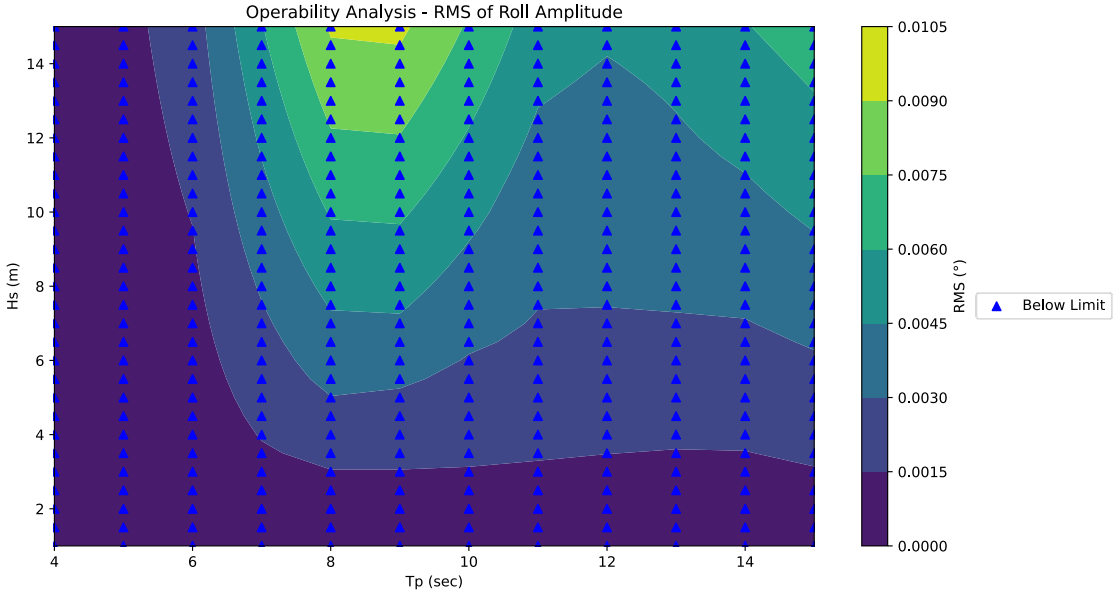

Figure 7.8: Roll amplitude criterion.

In the Figure 7.8, the operability analysis of the criterion for roll amplitude is presented, with a threshold value of $RMS = 4.0°$ (NATO STANAG 4154, Table 1.1, Equation 2.52). This threshold value is not exceeded in any of the sea states, and basically, it does not even exceed $0.01°$. This occurs due to the heading waves, so it is reasonable for the responses to roll to be extremely small, as demonstrated by the recorded RAOs of the roll motion in heading seas. However, based on the distribution, there is a slight increase in the rms roll amplitude for pairs of wave conditions with high Hs and moderate Tp values. Nevertheless, due to the very small responses of the vessel in roll motion, it is quite likely that errors are involved.

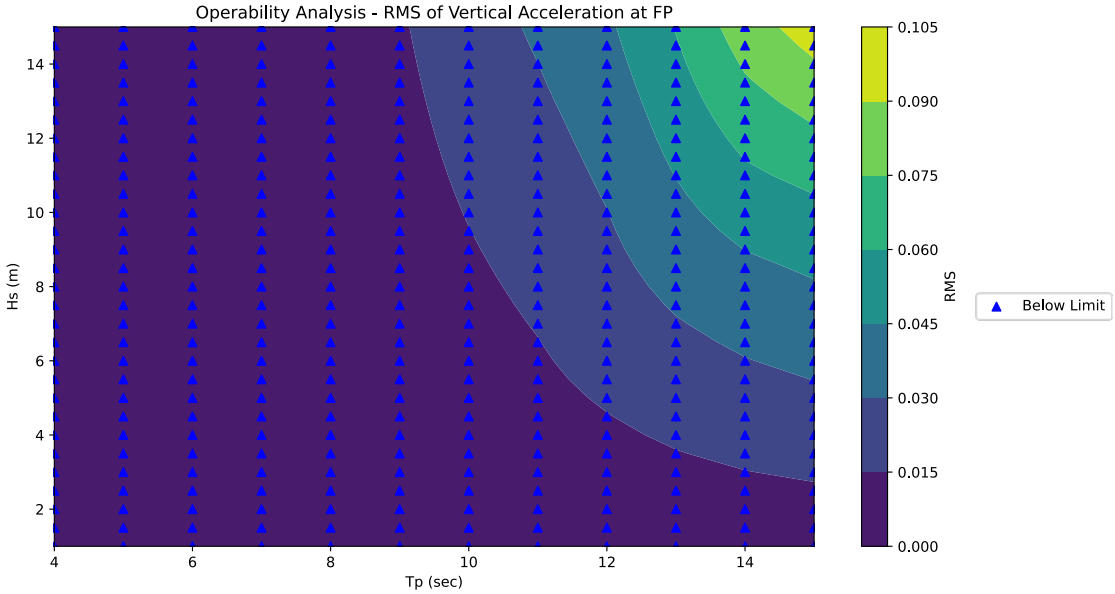

Figure 7.9: Vertical acceleration at FP criterion.

In the Figure 7.9, the operability analysis of the criterion for vertical acceleration at the ship's FP is presented, with a threshold value of $RMS = 0.05g$ (NORDFORSK 1987, Table 1.1, Equation 2.53) which appears to be satisfied in almost all pairs of sea states. Specifically, these sea states concern significant wave heights greater than $12m$, which, as indicated by the statistical analysis of the weather data from the reference route, are extremely unlikely to occur. In the broader context, the criterion is satisfied for a wide range of sea states, while the rms value of the pitch amplitude seems to increase for pairs of large significant wave height and peak period values.

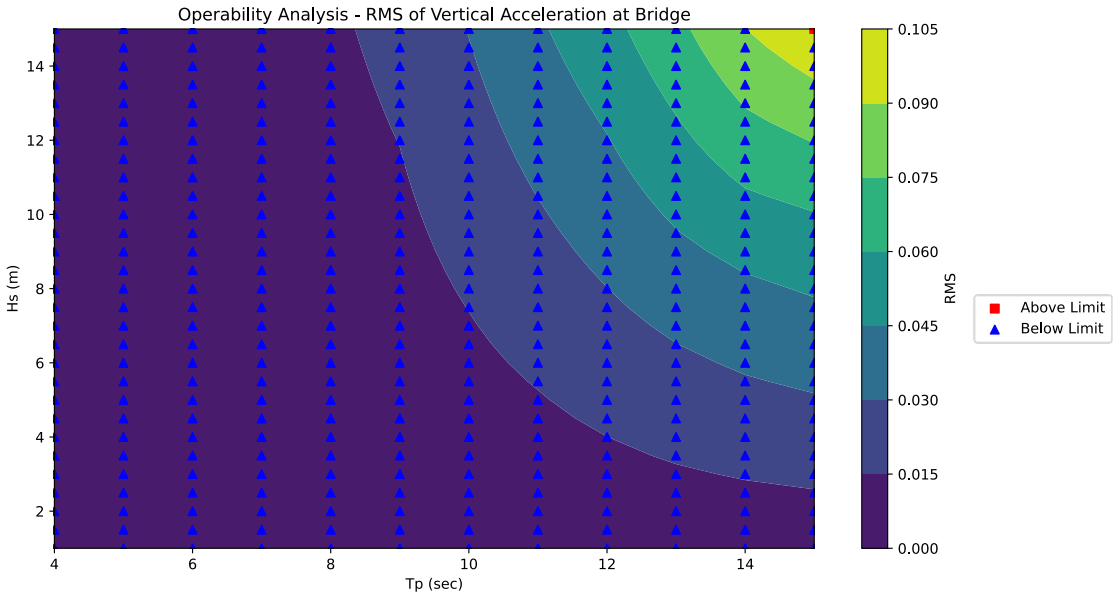

Figure 7.10: Vertical acceleration at bridge criterion.

In the Figure 7.10, the operability analysis for vertical acceleration at the bridge is presented, with a threshold value of $RMS = 0.10g$ (NATO STANAG 4154, Table 1.1, Equation 2.55). Overall, the criterion is satisfied for all sea states, showing only one instance where the criterion is not met for $Hs = 15m$ and $Tp = 15sec$, which is a highly extreme wave condition and quite unlikely to occur. Generally, due to the distribution, it is evident that the criterion value increases as the values of significant wave height and peak period increase, which is logical as the wave conditions become extreme and can affect more the vertical acceleration at bridge.

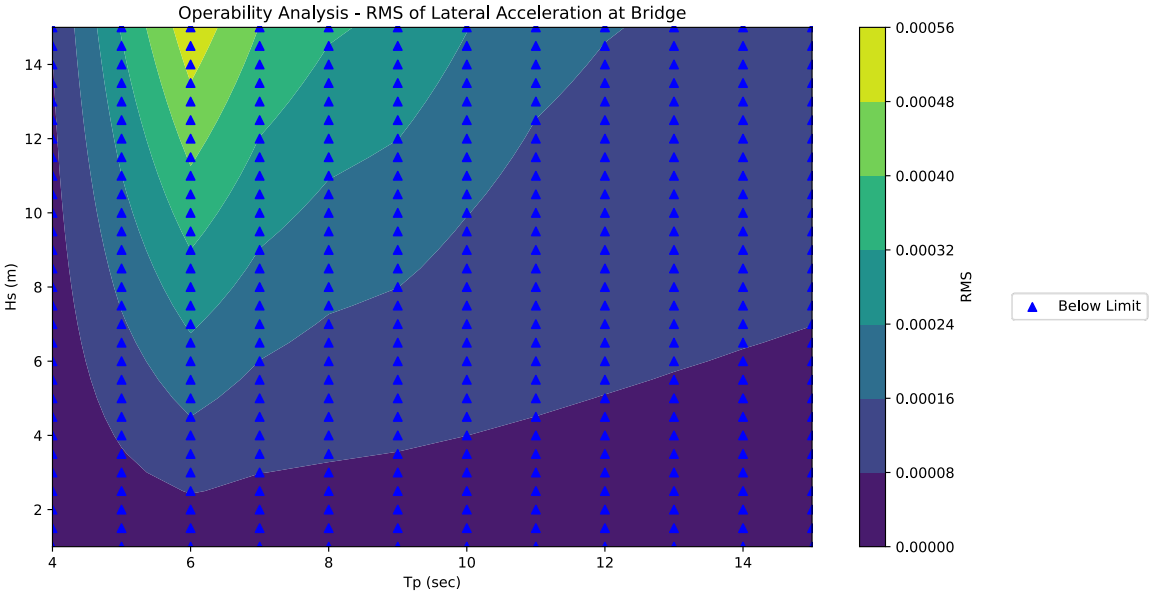

Figure 7.11: Lateral acceleration at bridge criterion.

In the Figure 7.11, the operability analysis of lateral acceleration at the bridge is presented, with a threshold value of $RMS = 0.10g$ (NATO STANAG 4154, Table 1.1, Equation 2.56). The criterion is satisfied for all sea states, displaying minimal values. Similar to the roll amplitude criterion, in lateral acceleration as well, the responses are negligible due to the heading seas.

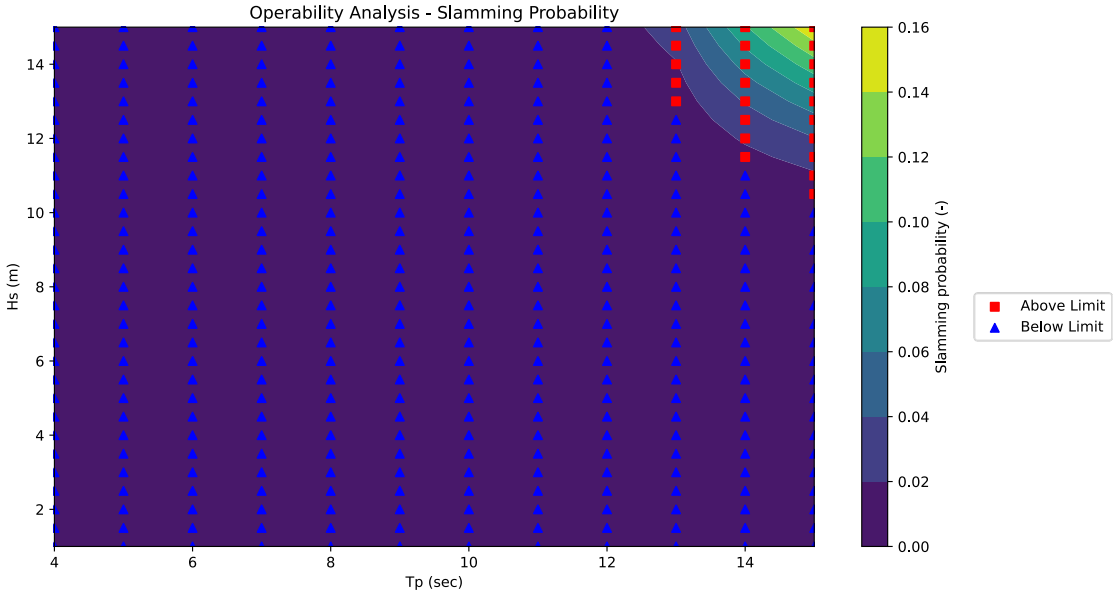

Figure 7.12: Slamming probability criterion.

In the Figure 7.12, the operability analysis of slamming probability is presented, with a threshold value of 0.01 (NORDFORSK 1987, Table 1.1, Equation 2.57). The criterion is not satisfied only for pairs with large significant wave height ($Hs > 10m$) and peak period ($Tp > 13\ sec$), indicating extreme and unfavorable wave conditions. Small errors may be involved in this criterion as well, due to the second moment of the vertical amplitude on the deck that needs to be calculated.

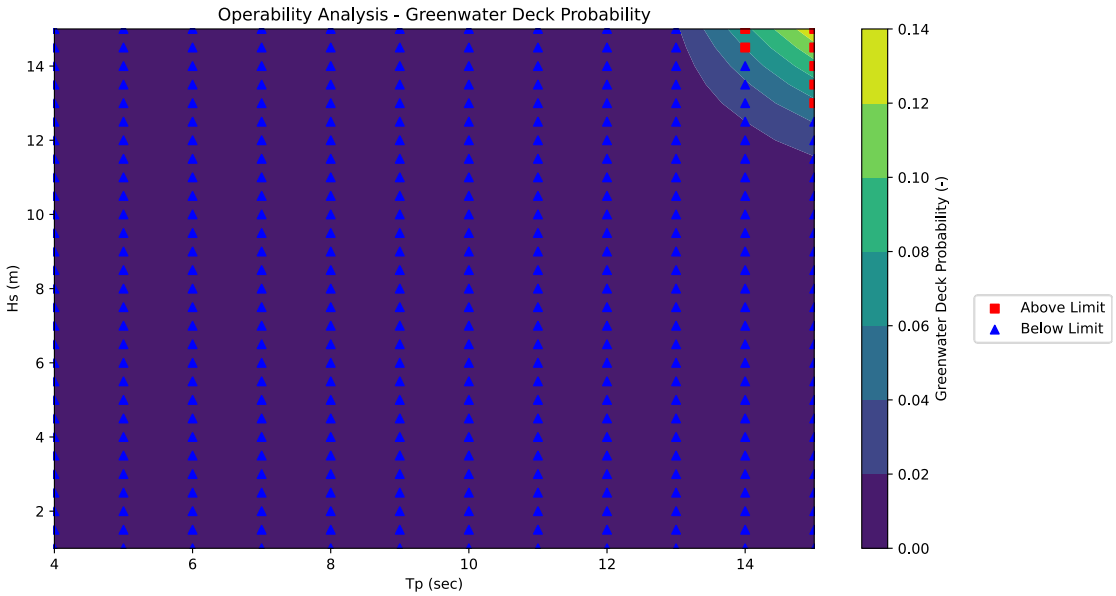

Figure 7.13: Green water deck probability criterion.

In the Figure 7.13, the operability analysis of green water on deck probability is presented, with a threshold value of 0.05 (NORDFORSK 1987, Table 1.1, Equation 2.58). Similar to slamming, this criterion is satisfied for all wave conditions except for certain extreme values of $Hs > 12m$ and $Tp > 14\,sec$. Calculating this criterion does not require the second or fourth moment, and therefore, it may not involve significant errors.

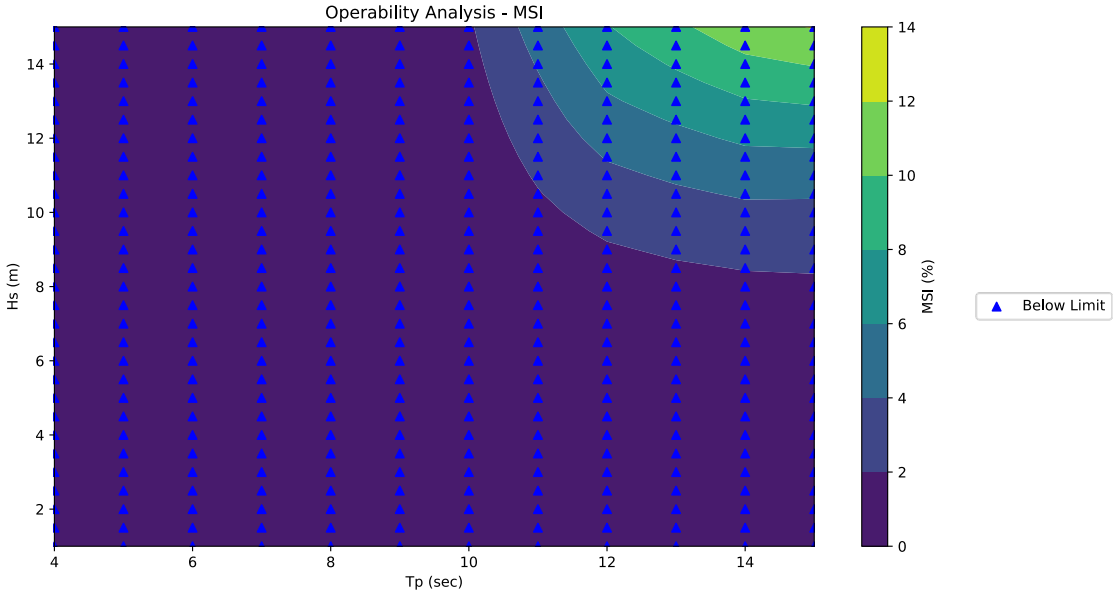

Figure 7.14: MSI criterion.

In the Figure 7.14, the operability analysis of the Motion Sickness Indicator (MSI) is presented, with a threshold value of $RMS = 20\%$ for every 4 hours of exposure (NATO STANAG 4154,

Table 1.1, Equation 2.59). Overall, the criterion is satisfied for all sea states, while it appears to increase significantly in more extreme wave conditions, as expected, primarily for $Hs > 9m$.

7.3 Method 2: Time domain

7.3.1 Response spectrums of the ship

The process of calculating and analyzing the response spectra of motions, velocities and accelerations at the ship's center of gravity (CG) or in any other point of interest, in irregular waves for each response of interest is the following:

- Initially, the time series of the response for the specific motion are plotted, along with the nominal position in meters or the nominal Euler angle in degrees at the CG along or around the axis in the earth-fixed coordinate system contextually, to visualize their difference. Then, to obtain the time series of the actual responses for the six degrees of freedom, the nominal positions time series are subtracted by the position ones. For velocities and accelerations of the responses, there is no nominal value, so this step is disregarded.

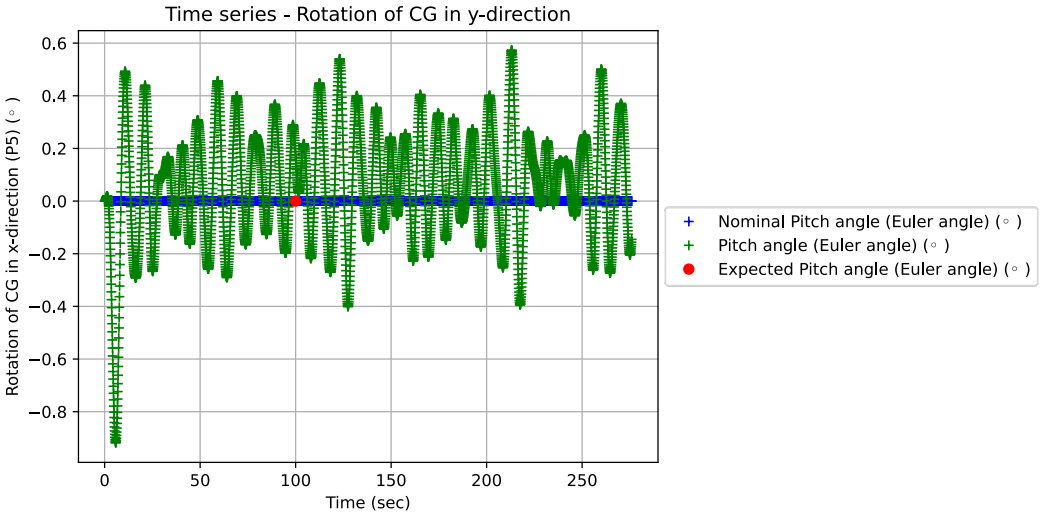

Figure 7.15:Time series of the response for the specific motion.

- Next, to eliminate the initial transitional period, which appears until the phenomenon stabilizes, the time series are taken into consideration after the 300th iteration, up to the 3200 iterations performed.

- In this sample, the mean value of the time series data is calculated, so as to subtract it and shift the time series around 0, where necessary, as the disturbance and the magnitude of the oscillation are of interest.

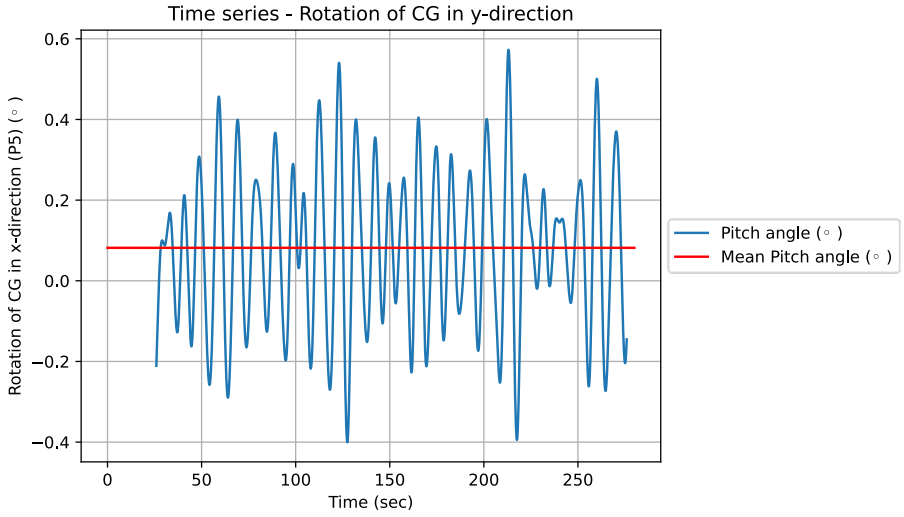

Figure 7.16: Calculation and visualization of time series mean value.

- Then, the Python library PyWafo was used to create the spectrum of each time series response. In this step, it is important to emphasize that the SHIPFLOW software, in order to generate and simulate the inputted irregular conditions based on the JONSWAP spectrum, arbitrarily selects 40 wave frequency values, the superposition of which constitutes the given sea state. This means that it uses both very small and very large wave frequencies to cover a wide range of them. The uncertainty of the response spectrum, especially in high frequencies, is significant, mainly for the calculation of the relative accelerations in the seakeeping criteria. However, for the completeness of the methodology, it was chosen to include the entire resulting response spectrum. To achieve this purpose, encounter frequencies were examined and found for each irregular sea state, which compose the result, including the "tails" and not only the frequencies that seemingly contribute dominantly to the phenomena, as well as discretize them for accuracy purposes.

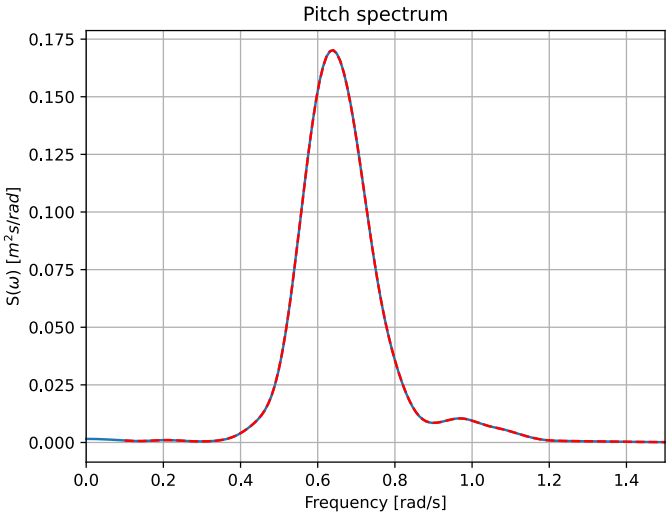

Figure 7.17: Visualization of response spectrum.

- Additionally, the introduction of the irregular wave characteristics (Hs, Tp), based on those of the simulation, in which JONSWAP spectrum, was implemented. Thus, for visualization purposes, the wave spectrums were also plotted and calculated with respect to the wave frequency and the encounter frequency respectively.

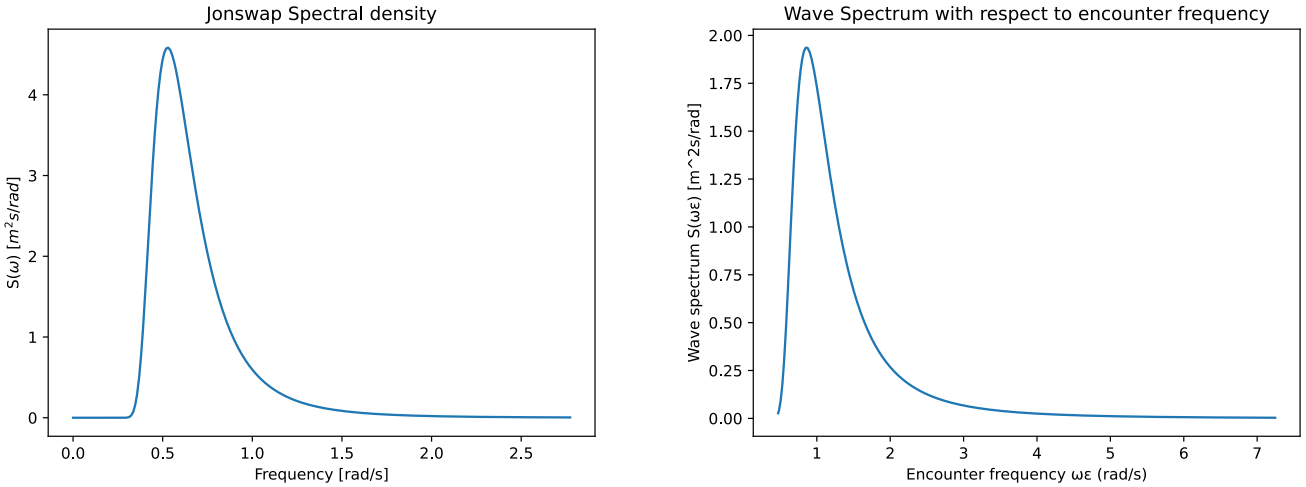

Figure 7.18: Visualizations of wave spectrums (Hs=5.2m and Tp=11.9sec).

- Utilizing the aforementioned results, comparison diagrams of wave spectrum and responses regarding amplitudes, velocities and accelerations are extracted and presented in this thesis.

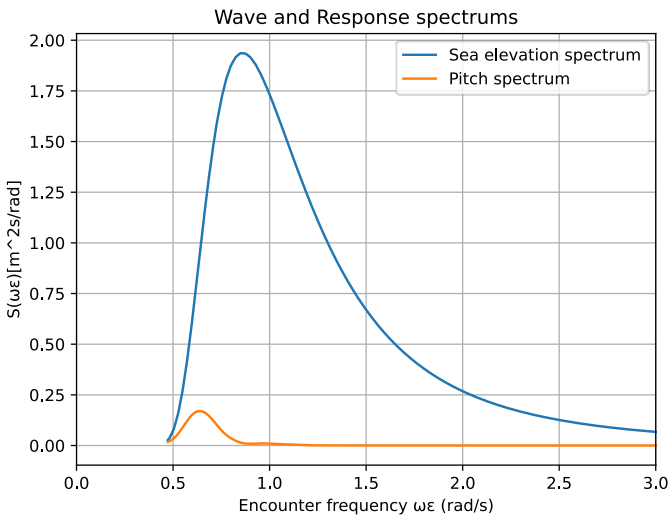

Figure 7.19: Wave and Response spectrums.

- In the next stage, the Response Amplitude Operators (RAOs) of responses, velocities and accelerations are calculated according to the theory and based on the respective wave and response spectrums.

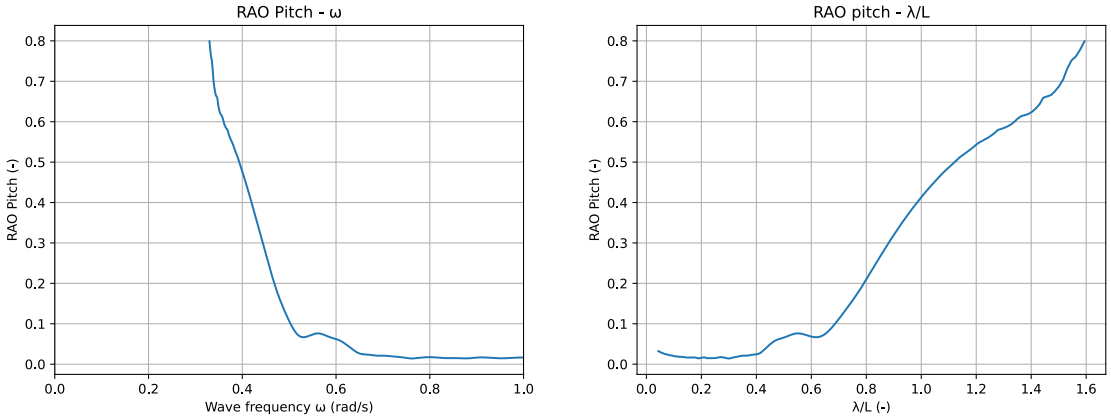

Figure 7.20: RAOs plots.

- Finally, having calculated the spectra of the responses of interest, the moments and rms values of these can be calculated, so as to check the seakeeping criteria satisfaction.

7.3.2 Relative response spectrums at the points of interest

The process of calculating and analyzing the response spectra of amplitudes, velocities and accelerations at the points of interest in Table 7.1, is the same with the one described in 7.3.1, with some additional steps.

- This time, both the time series of the positions of the points of interest in meters and those of the positions of the free surface elevation at these points are considered and analyzed.

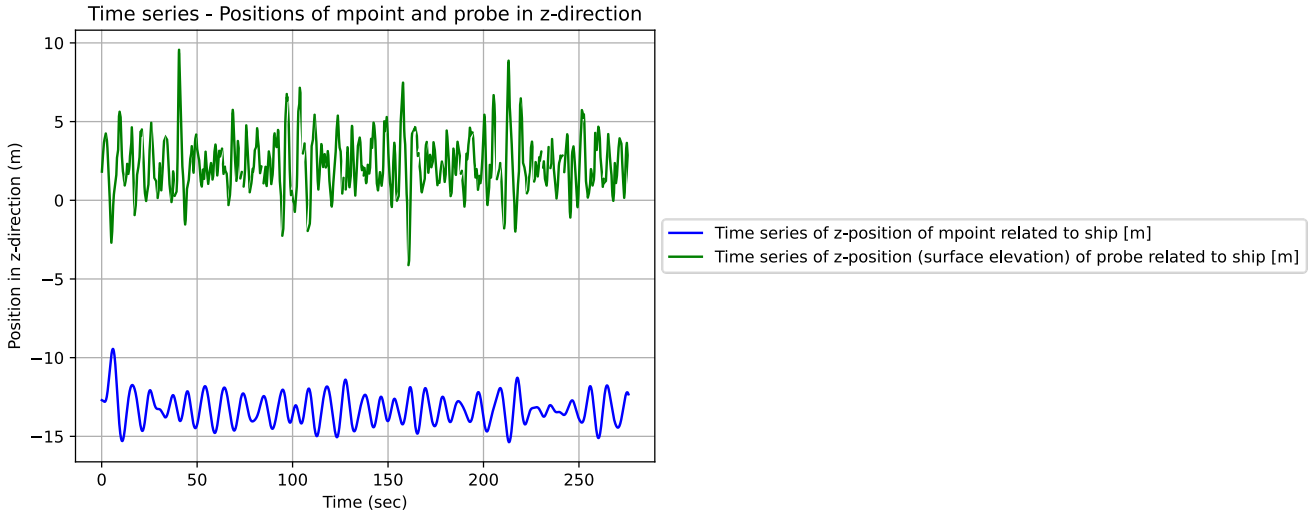

Figure 7.21: Time series of point of interest and probe amplitudes.

- In accordance with theory, subtracting the time series of the positions of the free surface elevation from those of the positions of the points of interest, generates the time series of the respective response.

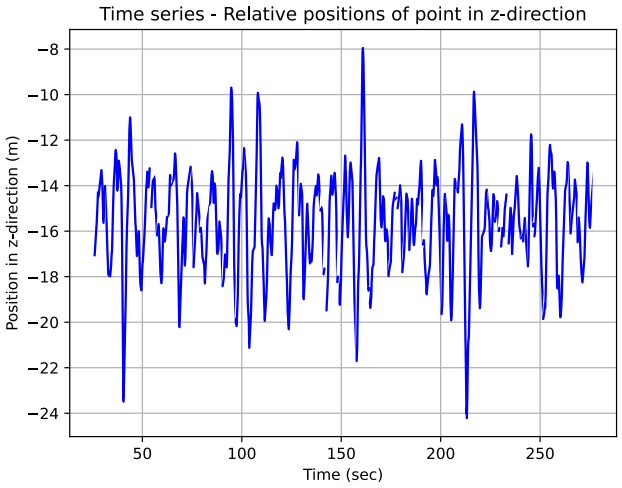

Figure 7.22: Time series of the respective response.

- Then, the same procedure is utilized, as explained in 7.3.1, with the difference that the response spectra of velocities and accelerations are indirectly calculated through the response spectrum of amplitude, as justified in the theory. This step may include significant errors, as the spectrum results are obtained indirectly and through

calculations. Specifically, it is worth pointing out that the segments of the response spectra referred to as "tails", are responsible for the errors that will emerge on the response spectra of velocities and accelerations, as they contain second and fourth-order moments, implementing forces of the second and fourth orders, thus significantly amplifying the existing errors of the response amplitude spectrum, from which the rest are calculated.

7.3.3 Seakeeping criteria results

Following the spectral analysis procedure described in 7.3.1 and 7.3.2 and using the sea states from Table 6.2, the fundamental seakeeping criteria were calculated at the points of interest, as presented below.

Table 7.3: Seakeeping criteria results (non-linear method).

Criteria	**C1** (RMS of Pitch Amplitude)	**C2** (RMS of Roll Amplitude)	**C3** (Vertical Acceleration at FP)	**C4** (Vertical Acceleration at Bridge)	**C5** (Lateral Acceleration at Bridge)	**C6** (Slamming Possibility)	**C7** (Green water deck Possibility)	**C8** (MSI)
Limit	**1.5°**	**4. 0°**	**0.05g**	**0.10g**	**0.10g**	**0.01**	**0.05**	**20%**
SS1 (Hs=5.2m, Tp=11.9sec)	0.196°	0.0377°	$0.042g$	0.021g	0.0005g	$8 \cdot 10^{-11}$	$2 \cdot 10^{-13}$	0.33%
SS2 (Hs=6.5m, Tp=12.4sec)	0.283°	0.06°	$\mathbf{0.057g}$	0.028g	0.0007g	$3 \cdot 10^{-6}$	$1 \cdot 10^{-7}$	0.80%
SS3 (Hs=6.5m, Tp=14.5sec)	0.578°	0.0395°	$\mathbf{0.097g}$	0.044g	0.0005g	0.0014	0.0005	1.74%
SS4 (Hs=7.5m, Tp=14.5sec)	0.656°	0.0757°	$\mathbf{0.111g}$	0.0502g	0.00086g	0.0073	0.0036	2.58%
SS5 (Hs=5m, Tp=15.5sec)	0.563°	0.027°	$\mathbf{0.085g}$	0.038g	0.0003g	0.00012	$4 \cdot 10^{-5}$	0.90%

Some significant observations are:

1. The RMS value for pitch amplitude (C1) seems to increase as the significant wave height increases, especially evident in sea states SS3 and SS4, which have the same

peak period. However, a greater increase is observed when, for a constant significant wave height, the peak period increases, as seen in SS2 and SS3, as well as SS1 and SS5. Therefore, an observation is that the peak period seems to significantly affect this criterion.

2. The RMS values of the roll amplitude (C2) are extremely small, almost negligible, due to heading waves.
3. The criterion for vertical acceleration at the FP (C3) is the only one that is not satisfied for the majority of the sea states. This can apply, considering that the simulated sea states are quite extreme ones, and thus it is reasonable. In fact, the chosen limit value of $0.05g\ RMS$ by NORDFORSK 1987 (as of Table 1.1) is strict compared to respective ones (i. e. $0.2g\ RMS$ by NATO STANAG 4154, in which all sea state criteria are satisfied).
4. The values for the criterion of vertical acceleration at the bridge (C4) are also small and acceptable. From the studied sea states, it appears that both the significant wave height and the peak period affect the results.
5. The criterion values for lateral acceleration at the bridge (C5) are zero and almost negligible, suggesting that the bridge is not affected laterally but more vertically.
6. The probability of slamming (C6) is equally negligible. From the result values, it seems that the peak period is decisive, indicating that the periodicity of waves in relation to the vessel's motion is significant.
7. Similarly, the probability of green water on deck (C7) is negligible. In this criterion, despite the small values, SS3 and SS4 stand out as the most adverse wave conditions compared to the others.
8. The MSI criterion (C8) is also satisfied. Indicatively, it appears that as the significant wave height and the peak period increase, so does the MSI percentage, a logical and expected phenomenon.

7.4 Comparison of results

In this subsection, the results of the operability analysis conducted using linear theory (regular heading waves) are compared with the corresponding results of the seakeeping criteria, from simulations of specific sea states (Table 6.2) (irregular heading waves).

The compared results are presented for each seakeeping criterion in the following Tables.

Table 7.4: Comparison results for C1 (RMS of pitch amplitude).

C1 (RMS of pitch amplitude)	**Method 2 (Time domain)**	**Method 1 (Frequency domain)**
Limit	**1.5°**	**1.5°**
SS1 ($Hs = 5.2m, Tp = 11.9sec$)	0.196°	0.211°
SS2 ($Hs = 6.5m, Tp = 12.4sec$)	0.283°	0.326°
SS3 ($Hs = 6.5m, Tp = 14.5sec$)	0.578°	0.63°
SS4 ($Hs = 7.5m, Tp = 14.5sec$)	0.656°	0.727°
SS5 ($Hs = 5m, Tp = 15.5sec$)	0.563°	0.589°

The results for the RMS values of pitch amplitude (Table 7.4) appear to almost agree with both methods. The percentage difference does not exceed 15%, and this occurs in extreme weather conditions, where the Method 2, of spectral analysis of irregular waves, seems to produce more accurate results. This is because it considers and implements many more frequencies (40) compared to the isolated frequencies (10) of the Method 1 of frequency domain, thus creating a more continuous and uniform spectrum as it contains more information.

Table 7.5: Comparison results for C2 (RMS of roll amplitude).

C2 (RMS of roll amplitude)	**Method 2 (Time domain)**	**Method 1 (Frequency domain)**
Limit	**4.0°**	**4.0°**
SS1 ($Hs = 5.2m, Tp = 11.9sec$)	0.0377°	0.0023°
SS2 ($Hs = 6.5m, Tp = 12.4sec$)	0.06°	0.0027°
SS3 ($Hs = 6.5m, Tp = 14.5sec$)	0.0395°	0.0029°
SS4 ($Hs = 7.5m, Tp = 14.5sec$)	0.0757°	0.0033°
SS5 ($Hs = 5m, Tp = 15.5sec$)	0.027°	0.0028°

The results for the RMS values of roll amplitude (Table 7.5) indicate a significant percentage difference. This occurs because the roll responses of the ship in heading seas are already negligible, making it even more challenging for the Method 1, which has limited information (few frequencies), to accurately approximate such small responses.

Table 7.6: Comparison results for C3 (Vertical acceleration at FP).

C3 (Vertical acceleration at FP)	Method 2 (Time domain)	Method 1 (Frequency domain)
Limit	$\mathbf{0.05g}$	$\mathbf{0.05g}$
SS1 ($Hs = 5.2m, Tp = 11.9sec$)	$0.042g$	$0.016g$
SS2 ($Hs = 6.5m, Tp = 12.4sec$)	$\mathbf{0.057g}$	$0.023g$
SS3 ($Hs = 6.5m, Tp = 14.5sec$)	$\mathbf{0.097g}$	$0.034g$
SS4 ($Hs = 7.5m, Tp = 14.5sec$)	$\mathbf{0.111g}$	$0.039g$
SS5 ($Hs = 5m, Tp = 15.5sec$)	$\mathbf{0.085g}$	$0.028g$

The results of the RMS values of vertical acceleration at FP (Table 7.6) also exhibit percentage differences between the two methods. Generally, as previously mentioned, calculating accelerations indirectly (without being directly computed by the solver) is challenging, as it involves many errors in the calculation of the 4th moment. Overall, the majority of the sea states criteria of time domain analysis are not satisfied, although it is considered to be more precise calculation method, with the highest RMS values appearing in the most extreme wave conditions.

Table 7.7: Comparison results for C4 (Vertical acceleration at Bridge).

C4 (Vertical acceleration at Bridge)	Method 2 (Time domain)	Method 1 (Frequency domain)
Limit	$\mathbf{0.10g}$	$\mathbf{0.10g}$
SS1 ($Hs = 5.2m, Tp = 11.9sec$)	$0.021g$	$0.019g$
SS2 ($Hs = 6.5m, Tp = 12.4sec$)	$0.028g$	$0.027g$
SS3 ($Hs = 6.5m, Tp = 14.5sec$)	$0.044g$	$0.036g$
SS4 ($Hs = 7.5m, Tp = 14.5sec$)	$0.0502g$	$0.042g$
SS5 ($Hs = 5m, Tp = 15.5sec$)	$0.038g$	$0.030g$

The results of the RMS values of vertical acceleration at the bridge (Table 7.7) for the two methods show an acceptable percentage difference, which increases to about 20% in extreme sea conditions. In this criterion, there is not as much risk in the calculation of accelerations because the software returns the time series of positions, velocities, and accelerations at specific

points other than the CG. Therefore, the discrepancy between the two methods may be limited to the amount of information each method possesses.

Table 7.8: Comparison results for C5 (Lateral acceleration at Bridge).

C5 (Lateral acceleration at Bridge)	**Method 2 (Time domain)**	**Method 1 (Frequency domain)**
Limit	$\mathbf{0.10g}$	$\mathbf{0.10g}$
SS1 ($Hs = 5.2m, Tp = 11.9sec$)	$0.0005g$	$8.3 \cdot 10^{-5}$g
SS2 ($Hs = 6.5m, Tp = 12.4sec$)	$0.0007g$	$9.6 \cdot 10^{-5}$g
SS3 ($Hs = 6.5m, Tp = 14.5sec$)	$0.0005g$	$7.8 \cdot 10^{-5}$g
SS4 ($Hs = 7.5m, Tp = 14.5sec$)	$0.00086g$	$9 \cdot 10^{-5}$g
SS5 ($Hs = 5m, Tp = 15.5sec$)	$0.0003g$	$5.5 \cdot 10^{-5}$g

The results of the RMS values of lateral acceleration at the bridge (Table 7.8) follow the pattern of the RMS values of roll amplitude, where due to heading seas, the lateral responses are negligible, especially the accelerations. Similarly, the same applies to the percentage difference between the two methods.

Table 7.9: Comparison results for C6 (Slamming possibility).

C6 (Slamming possibility)	**Method 2 (Time domain)**	**Method 1 (Frequency domain)**
Limit	$\mathbf{0.01}$	$\mathbf{0.01}$
SS1 ($Hs = 5.2m, Tp = 11.9sec$)	$8 \cdot 10^{-11}$	$3 \cdot 10^{-16}$
SS2 ($Hs = 6.5m, Tp = 12.4sec$)	$3 \cdot 10^{-6}$	$2 \cdot 10^{-9}$
SS3 ($Hs = 6.5m, Tp = 14.5sec$)	0.0014	$2 \cdot 10^{-6}$
SS4 ($Hs = 7.5m, Tp = 14.5sec$)	0.0073	$2 \cdot 10^{-5}$
SS5 ($Hs = 5m, Tp = 15.5sec$)	0.00012	$1.5 \cdot 10^{-9}$

The results of the slamming possibility (Table 7.9) values show a significant percentage difference between the two methods. These differences are reasonable, as the calculation of slamming probability requires the zeroth and second-order moments of the relative motion of the ship with respect to the sea surface. These calculations involve many intermediate steps, thereby increasing the occurrence of errors. Specifically, the Method 1 is considered a less

reliable approach, as, in addition to the moments, the RAOs of the relative vertical motion had to be calculated indirectly (as described in **Error! Reference source not found.**).

Table 7.10: Comparison results for C7 (Green water deck possibility).

C7 (Green water deck possibility)	Method 2 (Time domain)	Method 1 (Frequency domain)
Limit	**0.05**	**0.05**
SS1 ($Hs = 5.2m, Tp = 11.9sec$)	$2 \cdot 10^{-13}$	$2 \cdot 10^{-20}$
SS2 ($Hs = 6.5m, Tp = 12.4sec$)	$1 \cdot 10^{-7}$	$2 \cdot 10^{-11}$
SS3 ($Hs = 6.5m, Tp = 14.5sec$)	0.0005	$3 \cdot 10^{-7}$
SS4 ($Hs = 7.5m, Tp = 14.5sec$)	0.0036	$1 \cdot 10^{-5}$
SS5 ($Hs = 5m, Tp = 15.5sec$)	$4 \cdot 10^{-5}$	$2 \cdot 10^{-10}$

The results of the RMS values of green water on deck probability (Table 7.10) also exhibit significant percentage differences between the two methods, which are similarly explained as those of slamming probability, as the calculation steps are the same.

Table 7.11: Comparison results for C8 (MSI).

C8 (MSI)	Method 2 (Time domain)	Method 1 (Frequency domain)
Limit	**20%**	**20%**
SS1 ($Hs = 5.2m, Tp = 11.9sec$)	0.33%	0.194%
SS2 ($Hs = 6.5m, Tp = 12.4sec$)	0.80%	0.580%
SS3 ($Hs = 6.5m, Tp = 14.5sec$)	1.74%	0.91%
SS4 ($Hs = 7.5m, Tp = 14.5sec$)	2.58%	1.422%
SS5 ($Hs = 5m, Tp = 15.5sec$)	0.90%	0.377%

The results of the RMS values of MSI (Table 7.11) also exhibit significant percentage differences between the two methods. Even in this case, the non-linear method is considered more reliable as it involves direct calculations of the accelerations (time series), in addition to considering a greater number of wave frequencies. However, for the conditions under which the Method 1 is conducted (less wave frequencies, less computational time), the results obtained can be considered satisfactory.

Chapter 8 Conclusions and Recommendations

Conclusions

In this thesis, the seakeeping and operability analysis of the benchmark DTC hull was studied using the Boundary Element Method (BEM). Specifically, simulations were carried out using the specialized software SHIPFLOW, which is based on a fully non-linear unsteady potential flow solver with a time-dependent 3D panel method.

Initially, the DTC hull was simulated in regular waves, with 10 different wave frequency values (of constant steepness) and in 4 different wave directions. Through these experiments, time series of positions, velocities, and accelerations in 6 degrees of freedom (6DOF) were obtained, along with the RAOs of these responses. Additionally, resistance information was gathered for completeness.

These simulations demonstrated and confirmed that specific frequencies and directions significantly influence the 6DOF responses. It was observed that at low wave frequencies, the ship's responses are large because it moves together with the wave, whereas, at high frequencies, the responses are small, leaving the ship mostly unaffected. Furthermore, wave directions can excite different specific responses; for example, significant heave and pitch responses are seen in following and heading seas, while roll responses increase in quartering and beam seas.

In the second part of this thesis, the seakeeping of the DTC hull was simulated in irregular waves. To determine the irregular sea state conditions, weather data from the NOAA database and literature references on extreme wave conditions were used to reflect real-world data. Using the SHIPFLOW software and the JONSWAP spectral sea model, time series of the 6DOF responses were obtained, similar to the regular waves analysis.

The results from both parts, for regular and irregular waves, were used to assess the satisfaction of seakeeping criteria and to conduct the operability analysis. From the set of seakeeping criteria, eight key criteria were selected for study: pitch amplitude, roll amplitude, vertical acceleration at FP, vertical acceleration at the bridge, lateral acceleration at the bridge, slamming probability, green water on deck probability, and the Motion Sickness Indicator (MSI).

The operability analysis was conducted using two different methods: Method 1 (frequency domain) and Method 2 (time domain). For the frequency domain method, results from the

regular wave simulations were used. This involved calculating the RAOs of the responses of interest at the relevant points, followed by their spectra, and finally their RMS values to check the criteria for various combinations of sea states. In this method, an issue was identified in calculating the RMS values of relative velocities or accelerations in points of interest other than CG. These criteria are particularly complex as their calculation involves the relative motion of the ship and the sea surface, combined with the acceleration, which includes the fourth moment, and hence, a fourth-order, multiplying the errors.

On the other hand, for the time domain method, results from simulations in irregular waves were used, and the seakeeping criteria were calculated for the five defined sea states. Even in this method, there was a difficulty in calculating the criterion including relative responses in points of interest other than CG. This issue likely arises because the software does not produce results for the time series or RAOs of the relative accelerations between the ship and the free surface. Therefore, even in the time domain method, intermediate calculations of the fourth moment were necessary, in which there is significant uncertainty of the results, caused by "tails" in response's spectrum.

In summary, in this diploma thesis a significant part of seakeeping has been presented and analyzed, encompassing both the study of the hydrodynamic behavior of the vessel in regular waves and irregular waves, as well as operability analysis through comparison of linear and non-linear methods.

Recommendations

Some suggestions for future work are:

- Simulate more conditions with a wider range of wave frequencies and directions to study the responses and phenomena in greater detail.
- Conduct simulations of similar conditions using CFD software tools to compare these with BEM solvers and identify responses and discrepancies.
- Perform simulations of similar conditions in an experimental tank to validate the results obtained from the software, comparing experimental and numerical methodologies.
- Calculate seakeeping and added resistance due to waves based on data-driven models, in which data will be collected from sensors measuring the ship's responses, considering weather conditions at given times, as well as fuel consumption data.

Bibliography

ABS. (2006, March). *GUIDE FOR VESSEL MANEUVERABILITY*. https://ww2.eagle.org/content/dam/eagle/rules-and-guides/current/conventional_ocean_service/145_vesselmaneuverability/Vessel_Maneuverability_Guide_e-Feb17.pdf

ABS. (2014). *GUIDANCE NOTES ON WHIPPING ASSESSMENT FOR CONTAINER CARRIERS FEBRUARY 2014*. https://ww2.eagle.org/content/dam/eagle/rules-and-guides/current/design_and_analysis/173_whipping2014/container_whipping_gn_e.pdf

ABS. (2018, May). *Guide for "Safehull-Dynamic Loading Approach" For Vessels*. https://ww2.eagle.org/content/dam/eagle/rules-and-guides/current/design_and_analysis/140_safehulldlaforvessels/DLA-Vessels_Guide_e-May18.pdf

ABS. (2021, December). *Guide for Slamming Loads and Strength Assessment for Vessels*. https://ww2.eagle.org/content/dam/eagle/rules-and-guides/current/design_and_analysis/177_slamming_2021/177-slamming-guide-dec21.pdf

Arena, F., Guedes Soares, C., & Petrova, P. (2010). Theoretical Analysis of Average Wave Steepness Related to Peak Period or to Mean Period. *29th International Conference on Ocean, Offshore and Arctic Engineering: Volume 2*, 595–603. https://doi.org/10.1115/OMAE2010-20811

Ba, M. (1995). *A fast method of evaluation for the translating and pulsating Green's function*.

Baitis, A. E., Conwell, S. L., Crossland, P., Colwell, J., & Pattison, J. H. (1995). *Motion Induced Interruptions (MII) and Motion Induced Fatigue (MIF) Experiments at the Naval Biodynamics Laboratory* (CRDKNSWC-HD-1423-01).

Bertram, V. (2000). *Practical Ship Hydrodynamics*. Butterworth-Heinemann.

Bertram, V. (2012). *Practical Ship Hydrodynamics (Second Edition)* (Second Edition). Butterworth-Heinemann. http://www.sciencedirect.com/science/article/pii/B9780080971506100041

Bertram, V., & Yasukawa, H. (1996). *Rankine source methods for seakeeping problems*. 411–425.

Chirosca, A.-M., Medina, A., Pacuraru, F., Saettone, S., Rusu, L., & Pacuraru, S. (2023). Experimental and Numerical Investigation of the Added Resistance in Regular Head Waves for the DTC Hull. *Journal of Marine Science and Engineering*, *11*(4), 852. https://doi.org/10.3390/jmse11040852

Container ship. (2024). Wikipedia. https://en.wikipedia.org/wiki/Container_ship

Crighton, D. G. (1985). The Kutta Condition in Unsteady Flow. *Annual Review of Fluid Mechanics*, *17*(1), 411–445. https://doi.org/10.1146/annurev.fl.17.010185.002211

DNV-GL. (2018, January). *CLASS GUIDELINE, Wave Loads*. https://home.hvl.no/ansatte/tct/FTP/H2023%20Marinteknisk%20Analyse/Regelverk%20og%20standarder/DnV_documents/DNVGL-CG-0130.pdf

Evolution of Containerships | The Geography of Transport Systems. (2023, March). The Geography of Transport Systems | The Spatial Organization of Transportation and Mobility. https://transportgeography.org/contents/chapter5/maritime-transportation/evolution-containerships-classes/

Flowtech International AB. (n.d.). *SHIPFLOW 7.0 USERS MANUAL*.

Flowtech International AB. (2022, October 5). *SHIPFLOW MOTIONS 7.0 User's manual*.

Gerritsma, J., & Beukelman, W. (1972). *Analysis of the resistance increase in waves of a fast cargo ship*. *19*, 285–293. https://doi.org/10.3233/ISP-1972-1921701

Ghaemi, M. H., & Olszewski, H. (2017). Total Ship Operability –Review, Concept and Criteria. *Polish Maritime Research*, *24*(s1), 74–81. https://doi.org/10.1515/pomr-2017-0024

Heineke, D., & Verhagen, H. J. (2009). ON THE USE OF THE FICTITIOUS WAVE STEEPNESS AND RELATED SURF-SIMILARITY PARAMETER IN METHODS THAT DESCRIBE THE HYDRAULIC AND STRUCTURAL RESPONSE TO WAVES. *Coastal Structures 2007*, 1057–1066. https://doi.org/10.1142/9789814282024_0093

Hetland, M. L. (2017). *Beginning Python*. Apress. https://doi.org/10.1007/978-1-4842-0028-5

IACS. (2001). *Standard wave data* (Rec. No. 34). http://www.iacs.org.uk/publications/default.aspx

ISO. (1997). *ISO 2631-1 Mechanical Vibration and Shock—Evaluation of Human Exposure to Whole-Body Vibration—Part 1: General Requirements*. ISO (International Organization for Standardization).

ITTC. (2011). *ITTC – Recommended Procedures and Guidelines, Resistance Test* (7.5-02-02–01). https://ittc.info/media/1217/75-02-02-01.pdf

ITTC. (2021, June). *ITTC - Recommended Procedures and Guidelines. Benchmark Data for Validation of Manoeuvring Predictions*. https://www.ittc.info/media/9691/75-02-06-06.pdf

Iwashita, H. (1992). *Evaluation of the added-wave-resistance Green function distributing on a panel*. *11*, 21–39.

Journée, J. M. J. (1992). *Quick Strip Theory Calculations in Ship Design*. http://resolver.tudelft.nl/uuid:ceca89af-1ac5-4a5a-b211-764d7e6f3754

Judge, Dr. C. Q. (2019). *USNA EN455: Seakeeping and Maneuvering*. https://www.usna.edu/NAOE/academics/en455.php

Korvin-Kroukovsky, B. V., & Jacobs, W. R. (1957). *PITCHING AND HEAVING MOTIONS OF A SHIP IN REGULAR WAVES:* Defense Technical Information Center. https://doi.org/10.21236/AD0134053

Lagemann, B. (2019). *Efficient seakeeping performance predictions with CFD* [KTH ROYAL INSTITUTE OF TECHNOLOGY SCHOOL OF ENGINEERING SCIENCES]. https://www.diva-portal.org/smash/get/diva2:1359848/FULLTEXT01.pdf

Liu, S., Sprenger, F., Papanikolaou, A., Dafermos, G., & Zaraphonitis, G. (2021). Experimental and numerical studies on linear and nonlinear seakeeping phenomena of the DTC ship in regular waves. *Ship Technology Research*, *68*(1), 41–61. https://doi.org/10.1080/09377255.2020.1857007

Longuet-Higgins, & Selwyn, M. (1977, February 4). *The mean forces exerted by waves on floating or submerged bodies with applications to sand bars and wave power machines*. Royal Society.

MARIN. (2022). *Limiting sea state conditions for containerships: Seakeeping Analysis and Summary report* ((Report No. 33883-1-SEA); p. 96). MARIN. https://open.overheid.nl/documenten/ronl-680ab746ec3a1adfadc5a39ab2636a416df827d1/pdf

Maruo, H. (1960). *The drift of a body floating in waves*.

Mendes, D., & Oliveira, T. C. A. (2021). Deep-water spectral wave steepness offshore mainland Portugal. *Ocean Engineering*, *236*, 109548. https://doi.org/10.1016/j.oceaneng.2021.109548

Molland, A. F. (Ed.). (2008). *The maritime engineering reference book: A guide to ship design, construction and operation*. Butterworth-Heinemann. https://www.academia.edu/36843271/The_Maritime_Engineering_Reference_Book

NATO. (1997). *STANAG 4154: Common Procedures for Seakeeping in the Ship Design Process*.

NATO. (2018). *STANAG 4154: Common Procedures for Seakeeping in the Ship Design Process*.

Newman, J. (1985). *Algorithms for the free-surface Green function*. *19*, 57–67.

Newman, J. N. (1978). *The theory of ship motions*. *18*, 222–283.

Nordforsk. (1987). *Assessment of ship performance in a seaway*. Nordforsk.

O'Hanlon, J. F., & McCauley, M. E. (1974). *Motion sickness incidence as a function of the frequency and acceleration of vertical sinusoidal motion*. *45*(4), 366–369. https://doi.org/4821729

Pajankar, A. (2022). *Hands-on Matplotlib: Learn Plotting and Visualizations with Python 3*. Apress. https://doi.org/10.1007/978-1-4842-7410-1

Pennino, S., Gaglione, S., Innac, A., Piscopo, V., & Scamardella, A. (2020). Development of a New Ship Adaptive Weather Routing Model Based on Seakeeping Analysis and Optimization. *Journal of Marine Science and Engineering*, *8*(4), 270. https://doi.org/10.3390/jmse8040270

Pinkster, J. A., & Van Oortmerssen, G. (1977). *Computation of the first- and second-order wave forces on oscillating bodies in regular waves*. Proceedings of the Second International Conference on Numerical Ship Hydrodynamics.

Pipchenko, O. (2011). On the Method of Ship's Transoceanic Route Planning. In A. Weintrit & T. Neumann, *Methods and Algorithms in Navigation* (pp. 157–163). CRC Press. https://doi.org/10.1201/b11344-26

Rawson, K. J., & Tupper, E. C. (2001). Seakeeping. In *Basic Ship Theory* (pp. 457–522). Elsevier. https://doi.org/10.1016/B978-075065398-5/50015-7

RINA. (2024, January 20). William Froude: The father of hydrodynamics. *Royal Institution of Naval Architects - RINA*. https://rina.org.uk/industry-news/maritime-history-and-heritage/william-froude-the-father-of-hydrodynamics/

Salvesen, N., Tuck, O., & Faltisen. (1970). *Ship motions and sea loads*. *Transactions*.

Sclavounos. (2002). *SWAN2—User Manual*. Boston Marine Consulting Inc.

Sheinberg, R., Minnick, P. V., Beukema, T. G., Kauczynski, W., Silver, A. L., Cleary, C., Allan, R. G., Werenskiold, P., De Kat, J. O., Byers, D. W., & Lin, W. M. (2003). *Stern boat deployment systems and operability*. 1–32.

Shukui, L., Papanikolaou, A., & Zaraphonitis, G. (2014, July 7). *Time Domain Simulation of Nonlinear Ship Motions Using an Impulsive Responsive Function Method*. ICMT2014, Glasgow, UK. https://www.researchgate.net/publication/263657497_Time_Domain_Simulation_of_Nonlinear_Ship_Motions_Using_an_Impulsive_Responsive_Function_Method?enrichId=rgreq-101f86952bbf953ac688475891243305-XXX&enrichSource=Y292ZXJQYWdlOzI2MzY1NzQ5NztBUzoxMTc3MzIxMDAwMjIyNzNAMTQwNTA4MDkyODc1Ng%3D%3D&el=1_x_3&_esc=publicationCoverPdf

Söding, H. (2010). Boundary element methods for seakeeping. *ResearchGate*. https://www.researchgate.net/publication/260433070_Boundary_Element_Methods_for_Seakeeping

Stevens, S. C., & Parsons, M. G. (2002). Effects of Motion at Sea on Crew Performance: A Survey. *Marine Technology and SNAME News*, *39*(01), 29–47. https://doi.org/10.5957/mt1.2002.39.1.29

Svensen, T. (n.d.). *Seakeeping in Design*. Retrieved January 15, 2024, from http://resolver.tudelft.nl/uuid:dd1fc455-9696-4a92-9028-cf152bb06527

Tan, S. G. (1995). *Seakeeping considerations in ship design and operations* (Report 635001-Paper MARIN Report No. 635001; p. 31). MARIN, Wageningen. http://resolver.tudelft.nl/uuid:a7779757-73d0-4721-add6-4f501d20a0ce

Toffoli, A., Babanin, A., Onorato, M., & Waseda, T. (2010). Maximum steepness of oceanic waves: Field and laboratory experiments. *Geophysical Research Letters*, *37*(5), 2009GL041771. https://doi.org/10.1029/2009GL041771

WAFO. (2017). *WAFO – a Matlab Toolbox for Analysis of Random Waves and Loads, Tutorial for WAFO*. WAFO group.